ŽILINSKÁ UNIVERZITA V ŽILINE
Výskumné centrum UNIZA

Fakulta špeciálnej techniky
Trenčianska univerzita Alexandra Dubčeka v Trenčíne

STU MTF
SLOVENSKÁ TECHNICKÁ UNIVERZITA V BRATISLAVE
MATERIÁLOVOTECHNOLOGICKÁ FAKULTA SO SÍDLOM V TRNAVE

STROJNÍCKA FAKULTA
Katedra technológií, materiálov a počítačovej podpory výroby

TRUMPF

PRVÁ ZVÁRAČSKÁ, a. s.

NES

CENTRUM VEDECKO-TECHNICKÝCH INFORMÁCIÍ SR

PROCEEDINGS 2023

WELDING TECHNOLOGY 2023:

Industrial development technology of European Union

1st INTERNATIONAL SCIENTIFIC CONFERENCE

8th November 2023

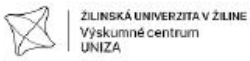

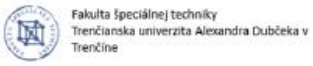

RECENZENTI / REVIEWERS:

Prof. Ing. Milan Marônek, PhD., *Slovak University of Technology in Bratislava, Faculty of Materials Science and Technology in Trnava, Slovakia (SK)*
Assoc. prof. Peter Polák, PhD., *The First Welding Company, Inc. in Bratislava, Slovakia (SK)*
Prof. Dr. József Sárosi, *University of Szeged, Hungary (HU)*
Prof. Dr. György Kovács, *University of Miskolc, Hungary (HU)*

WELDING TECHNOLOGY 2023
Industrial development technology of European Union

Vydavateľ / Publisher: Vydavateľstvo AlumniPress
J. Bottu 25
917 24 Trnava

Rok vydania / Year of publication: 2023
Vydanie / Issue : prvé / first

ISBN 978-80-8096-298-2
EAN 9788080962982

The organizers of the conference are:

PRVÁ ZVÁRAČSKÁ, a. s. in Bratislava,

STU Faculty of Materials Science and Technology in Trnave (within project APVV-21-0232),

Alexander Dubček University of Trenčín,
Faculty of Special Technology.

Vedecký výbor / Scientific Board

Predseda / Chairman:

Dr. h. c. Ing. Peter Fodrek, PhD., hosť. Prof., *The First Welding Company, Inc. in Bratislava, Slovakia (SK)*

Členovia / Members:

Ing. František Kolenič, PhD., *The First Welding Company, Inc. in Bratislava, Slovakia (SK)*

Prof. Petro Loboda, DrSc., *National Technical University of Ukraine "Igor Sikorsky Kiev Polytechnic Institute", Ukraine (UA)*

Prof. Ing. Milan Marônek, PhD., *Slovak University of Technology in Bratislava, Faculty of Materials Science and Technology in Trnava, Slovakia (SK)*

Prof. Dr. Ing. Steffen Keitel, *SLV Halle, Germany (DE)*

Ing. Beáta Šimeková, PhD., *Slovak University of Technology in Bratislava, Faculty of Materials Science and Technology in Trnava, Slovakia (SK)*

Prof. Volodimir Nesterenkov, DrSc.*, Institute of Electric Welding E.O.Patona (PWI) Kiev, Ukraine (UA)*

Assoc. prof. Ing. Pavel Kovačócy, *Slovak University of Technology in Bratislava, Faculty of Materials Science and Technology in Trnava, Slovakia (SK)*

Assoc. prof. Ing. Jozef Bárta, PhD., *Slovak University of Technology in Bratislava, Faculty of Materials Science and Technology in Trnava, Slovakia (SK)*

Ltc. Assoc. prof. Ing. Zbyněk Studený, Ph.D., *Department of Engineering Technology, Faculty of Military Technology, University of Defence, Brno, Czech Republic (CZ)*

Assoc. prof. Ing. Daniel Kottfer, PhD.*, Alexander Dubček University of Trenčín, Faculty of Special Technology, Slovakia (SK)*

Assoc. prof. Sergiu-Dan STAN, PhD, Eng., *Technical University of Cluj-Napoca, Romania (RO)*

Assoc. prof. Ing. Michal Krbaťa, PhD.*, Alexander Dubček University of Trenčín, Faculty of Special Technology (SK)*

Assoc. prof. Sandra Dedjier*, University of Novi Sad, Serbia (RS)*

Capt. Assoc. prof. Ing. David Dobrocký, Ph.D., *Department of Engineering Technology, Faculty of Military Technology, University of Defence, Brno, Czech Republic (CZ)*

Ing. Marcel Kohutiar, PhD., *Alexander Dubček University of Trenčín, Faculty of Special Technology (SK)*

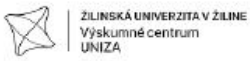

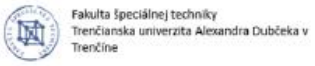

Ing. Ingrid Kovaříková, PhD., *Alexander Dubček University of Trenčín, Faculty of Special Technology, Slovakia (SK)*

Assoc. prof. Ing. Peter Košťál, PhD., *Slovak University of Technology in Bratislava, Faculty of Materials Science and Technology in Trnava, Slovakia (SK)*

Ing. Vanessa Prajová, PhD, *Slovak University of Technology in Bratislava, Faculty of Materials Science and Technology in Trnava, Slovakia (SK)*

Dr. Inž. Katarzyna Ciosk, *Politechnika Świętokrzyska, Kielce university of Technology, Poland (PL)*

Assoc. prof. Milan Rackov, *Faculty of Technical Sciences, University of Novi Sad, Serbia (RS)*

Assoc. prof. Remigiusz Labutsky, *University of Polytechnic Poznaň, Poland (PL)*

Dr. Róbert Sánta, *University of Dunaújváros, Hungary (HU)*

Prof. Dr. József Sárosi, *University of Szeged, Hungary (HU)*

Prof. Lubomir Dimitrov, PhD.*, Technical University of Sofia, Bulgaria (BG)*

Assoc. prof. Dr. Varga Gyula, *University of Miskolc, Hungary (HU)*

Prof. Dr. György Kovács, *University of Miskolc, Hungary (HU)*

Ing. Róbert Janík, PhD.*, Alexander Dubček University of Trenčín, Faculty of Industrial Technologies, Slovakia (SK)*

Assoc. Prof. Dr. M.Sc. Daniel Križan*, Research and Development Department, Business Unit Coil. Voestalpine Steel Division GmbH, 4020 Linz, (AU)*

Programový výbor / Organising Committee

Ing. Beáta Šimeková, PhD., *Slovak University of Technology in Bratislava, Faculty of Materials Science and Technology in Trnava, Slovakia (SK)*

Ing. Ingrid Kovaříková, PhD., *Alexander Dubček University of Trenčín, Faculty of Special Technology, Slovakia (SK)*

Ing. Michal Šimek, PhD., *The First Welding Company, Inc. in Bratislava, Slovakia (SK)*

Ing. Daniel Dřímal, PhD., *The First Welding Company, Inc. in Bratislava, Slovakia (SK)*

Ing. Tomáš Fodrek, *The First Welding Company, Inc. in Bratislava, Slovakia (SK)*

Ing. Slavomír Lipár, PhD., *The First Welding Company, Inc. in Bratislava, Slovakia (SK)*

Ing. Igor Kováčik, *The First Welding Company, Inc. in Bratislava, Slovakia (SK)*

Dr. Róbert Sánta, *University of Dunaújváros, Hungary (HU)*

1ST INTERNATIONAL SCIENTIFIC CONFERENCE
P R O G R A M

WELDING TECHNOLOGY 2023:
Industrial development technology of European Union

8th November 2023

12^{00} – 13^{00} Lunch

12^{30} – 13^{00} Visiting laboratories of PRVÁ ZVÁRAČSKÁ, a. s.

13^{00} Presentation of participants

13^{15} Opening of the scientific conference
Dr. h. c. Ing. Peter Fodrek, PhD., host. prof., general director of PZ, a. s. Bratislava

Section A: Welding technologies
Chairman: Ing. František Kolenič, PhD.

13^{20} Acquisition, recording and processing of analogue signals for monitoring selected electron beam parameters in mass production welding applications
Kováč Ľ., Dřímal D. (PRVÁ ZVÁRAČSKÁ, a. s. Bratislava)

13^{40} Selected thin film properties and possibilities of their alteration
Blanár J., Kottfer D. (Alexander Dubček University of Trenčín, Faculty of Special Technology)

14^{00} Weldability of stainless steel and copper by concentrated sources of energy
Hnilica M., Kovačócy P., Šimeková B., Bárta J., Kovaříková I. (MTF STU Trnava, Alexander Dubček University of Trenčín, Faculty of Special Technology)

14^{20} Mechanical and technological properties of composite pipe
Bilka M., Polášek M., Krbaťa M. (Alexander Dubček University of Trenčín, Faculty of Special Technology)

14^{40} Material degradation in the heat-affected zone during of welding high-strength steel hardox 500 and austenite steel 08CH18N10T
Macháček J., Kianicová M., Kovaříková I. (Alexander Dubček University of Trenčín, Faculty of Special Technology)

15^{00} Research of Joining of Stainless Steel and Copper by Laser Beam
Šimeková B., Kovaříková I., Kovačócy P., Hnilica M., Šimek M. (MTF STU Trnava, Alexander Dubček University of Trenčín, Faculty of Special Technology,PRVÁ ZVÁRAČSKÁ, a. s. Bratislava)

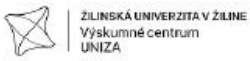

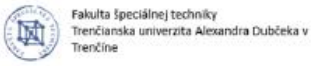

Coffee break

Section B: Innovations of welding equipment
Chairman: Ing. František Kolenič, PhD.

15^{20} **A new approach to welding current modulation in electron beam welding**
Darovec R., Kolenič F., Kunštek D., Koršňák P. (PRVÁ ZVÁRAČSKÁ, a. s. Bratislava)

15^{40} **Universal time course generator for use in electron beam welding**
Kunštek D., Sekerka R., Koršňák P., Kopecký M. (PRVÁ ZVÁRAČSKÁ, a. s. Bratislava, NES Nová Dubnica, s. r. o.)

16^{00} **Modular design of universal electron beam devices**
Sekerka R., Kolenič F., Koršňák P., Kováč Ľ. (PRVÁ ZVÁRAČSKÁ, a. s. Bratislava)

Coffee break

16^{20} **Welding current regulator in highly productive electron beam welding systems**
Koršňák P., Darovec R., Kunštek D., Sekerka R. (PRVÁ ZVÁRAČSKÁ, a. s. Bratislava)

16^{40} **Structural analysis and corrosion properties of materials used for constructions**
Válek L., Dománková M., Bárta J. (MTF STU Trnava)

17^{00} **The influence of the working position of the welder in assessing welding risks**
Marková P., Prajová V., Homokyová M., Horváthová M. (MTF STU Trnava)

17^{20} **Algorithm as a tool in programming and implementation of automated processes**
Matúšová M. (MTF STU Trnava)

17^{40} **Using the shewhart control charts by turning process evaluation**
Katarína Lestyánszka Škůrková, Filip Praj (MTF STU Trnava)

OBSAH / CONTENTS

ACQUISITION, RECORDING AND PROCESSING OF ANALOGUE SIGNALS FOR MONITORING SELECTED ELECTRON BEAM PARAMETERS IN MASS PRODUCTION WELDING APPLICATIONS

Ing. Daniel Dřímal, PhD.[1]
Ing. Ľuboš Kováč[2]
[1]ORCID: 0000-0003-2311-6228, PRVÁ ZVÁRAČSKÁ a. s., Bratislava, **Slovakia**
[2]ORCID: 0000-0003-2311-6228, PRVÁ ZVÁRAČSKÁ a. s., Bratislava, **Slovakia**

Abstract: The control and evaluation of the condition of the emission system and electron beam geometry characteristics in high production electron beam welding is important to prevent the production of scrap. The presented solution is based on the measurement of the transverse profile of the electron beam in two perpendicular axes. The problem involves the design of a complex technological tool (measuring probe, data acquisition module, processing software, analysis and visualization of the measured data), which will allow technologists to react promptly to the deterioration of the production quality. The technical solutions consisting of a DAQ analogue signal acquisition and recording module and a signal adaptation module which have been designed and tested. Experimental measurements were performed on the previously designed measurement probe. The measured signals were subsequently processed in order to remove undesired disturbed interferences. Two filters of different principles (Avg and Gaussian) were applied to suppress the interference and compensate for the lower resolution of the DA converter.

Keywords: electron beam welding, electron beam profile, beam quality

1 INTRODUCTION

Electron beam welding technologies have specific features compared to other technologies, which make them one of the most progressive welding technologies. The main advantages include in particular the high energy density in the electron beam, the high stability and reproducibility of the process parameters. This provides the advantage of high productivity, since high welding speeds can be (more than 100 mm/s) and perfect protection of the welded joint due to the high vacuum environment.
Less thermal impact of the material and better weld joint properties are achieved with this progressive welding technology. It allows to improve the quality and efficiency of production

in virtually all industries. The heart of the electron beam machine is the electron gun, which is used to generate and accelerate electrons. The electrons themselves are released by thermoemission from the cathode, which can most often be made of W or LaB6. The condition and quality of the cathode surface changes over its lifetime by evaporation, thermal stresses and, most importantly, by the back-bombardment of ions from the beam-welded material interaction process. This leads to a decrease in the cathode ability to emit electrons for welding or processing materials. The emission capability of the cathode can be restored by increasing its temperature in some cases. The decrease in cathode emissivity may not be directly reflected in a decrease of power of the electron beam.

It is reflected in the energy distribution in the beam (decrease of the energy density). Since the decrease of the cathode emissivity can be compensated by decreasing the control electrode voltage and thus increasing the cathode emissivity area in the case of triode electron guns. However, it may be noticeable in the weld itself, in particular by a decrease in the weld depth, which may result in the production of mismatched pieces. Evaluating the condition of the emission system and deciding whether the emission capability of the cathode can be restored by raising its temperature or whether replacement is necessary is critical, especially in the case of mass welding. Direct inspection of the condition and eventual replacement of the emission system is a time-consuming operation, shutting down production. It requires aerating the electron gun, opening it and, after intervention, pumping it back to working pressure (<9.10-2 Pa). This means interrupting production for more than an hour. Another option for checking the condition of the emission system is indirect inspection by welding and metallographic inspection of the weld itself. This method is relatively simple but time consuming also. In addition, it gives information on the ability of the emission system to produce identical welds, not on its condition and service life. Another possibility is to measure the power and geometrical characteristics of the electron beam itself.

The measurement of beam characteristics consists of measuring the total current or a portion of the current of an electron beam in most cases. The measurements are usually performed in the relevant part of the electron beam, i.e. the focal region. However, the high concentration of energy in the electron beam complicates its measurement and analysis capabilities. At the point where the electrons interact with the material, temperatures can reach several thousand °C, which is sufficient to melt any metallic material. Therefore, the use of refractory metals for the functional parts of the measuring probe is a necessary but not sufficient requirement. It is also necessary to reduce the exposure of the measuring probe as much as possible. The measuring and recording apparatus itself must also be adapted to this, as the measurement itself may take only a few microseconds. For inspection of the state of the emission system, we have chosen the concept of measuring the transverse electron beam profile by the linear slit measurement method with the help of a Faraday probe in two

mutually perpendicular axes. The design of the measuring probe itself as well as other elements of the measuring apparatus corresponds to the chosen concept.

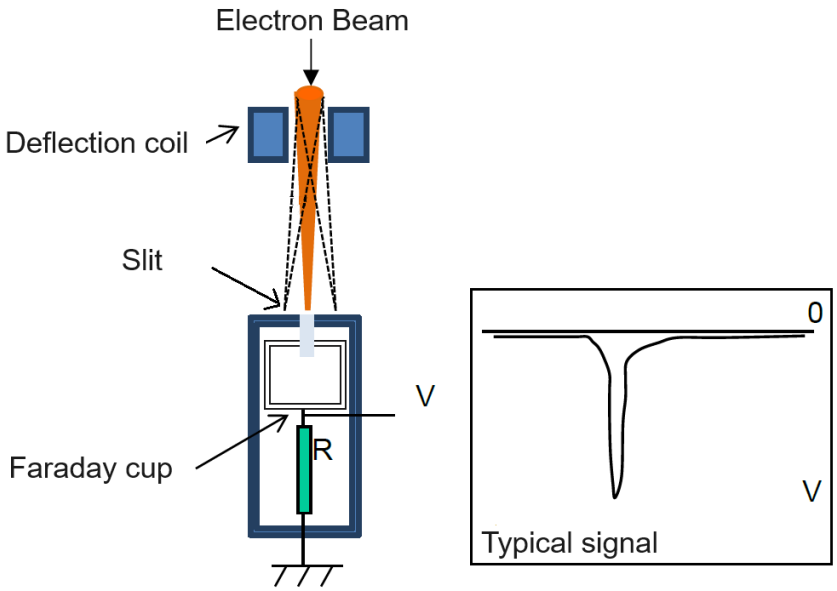

Fig. 1 Principle scheme for measuring beam parameters with a linear slit

The measurement of the electron beam profile by the slit method is based on the principle of detecting the time course of the beam current as it passes rapidly through the measuring slit. Part of the beam falls through the measuring slit into a Faraday cylinder which serves as a current measuring probe. The beam motion is realized by a magnetic deflection system due to the high speeds required. The width of the measuring slit should be smaller than the expected diameter of the measured beam. The time course of the current is recorded by the analogue signal acquisition and recording module DAQ.

2 ANALOGUE SIGNAL ACQUISITION AND RECORDING MODULE – DAQ

The initial parameters of the measurement system were determined based on the experience gained from the initial experiments. The proposed measurement slit width of 0.1 mm satisfies the basic requirement that it should be smaller than the diameter of the measured beam. A narrower slit can measure a more accurate representation of the actual electron beam profile, but at the same time the current signal obtained in this way has lower intensity and thus it is significantly more sensitive to interference. The measured analogue signal consists of several components. One of them is the useful signal, which is produced as a voltage drop

across the measuring resistor by the passage of an electric current from a portion of the electron beam cropped by the slit. The second component of the signal is from the unwanted current components arising predominantly by transmission from the pulse converters of the vn power supply and the servo converters of the positioning system of the welding machine. The useful signal will be lost in the interference if the slit is too narrow. The problems of a mechanical nature were encountered in experiments with narrower slit widths. The effect of wear on the edge of the tungsten slit by local melting of the passing beam during measurements was more pronounced when the slit width was set to less than 0.05 mm. Considering this knowledge, the width of the measuring slit was chosen to be 0.1 mm, which corresponds to the original estimates.

The electron beam switching on is a dynamic process influenced by several factors (welding current controller, etc.) and therefore the measurement itself should be performed after the transient events of the start have stabilized. The time required to stabilise the welding current depends on its absolute value and typically varies in tenths of a second. The time required to stabilize a welding current value of 100 mA was 0.2 s in oscilloscope measurements. A settling time with a sufficient margin of 0.5 s was used in the experiments.
In order to minimize the thermal exposure of the tungsten slit edge, it is advisable to start the electron beam outside its active part. The deflection amplitude of the electron beam should meet the requirement that in the extreme deflection position the electron beam is directed to the thermal absorber. The absorber must have sufficient thermal capacity to absorb the heat received without thermally affecting the geometry of the measuring slit. It is therefore appropriate to choose a pitch between 20 and 40 mm in the proposed slit design. The voltage of the deflection generator voltage spread is chosen with respect to the distance of the measuring probe from the electron gun. The output voltage of the generator is directly proportional to the deflection angle, not the length.

The duration of the beam deflection cycle (the deflection speed) is subject to similar considerations of useful signal strength with respect to the effect of the surrounding environment with electromagnetic interference as in determining the slit width. High speed deflection gives a low intensity current signal with significant noise and interference effects. Slow beam deflection across the slit can cause local melting and degradation of the tungsten slit edge, especially at higher current values. A compromise solution appears to be to choose a 1 ms oscillation duration, i.e. the distance determined by the amplitude is covered by the beam in 0.5 ms. The chosen pulse type is a linear ramp with a phase shift adjustment of 270° to ensure that the electron beam is at rest at the extreme deflected position (on the absorber).
The analogue signal acquisition and recording module DAQ requirements:
- 2 input measurement channels,

- external trigger capability,
- voltage input range ±10 Vpp or ±20 Vpp,
- measurement input resolution min. 8 bit (ideally 12),
- sampling rate min. 100 MS/s (10 ns period),
- control and transfer of measured data via Ethernet or USB communication bus,
- market availability.

Fig. 2 Analogue signal acquisition and recording module DAQ, PC oscilloscope PicoScope 3204D

3 SIGNAL PROTECTION AND ADAPTATION MODULE

Measured analogue signals comes from the welding chamber, where undesirable HV discharges can occur. This HV discharges are a source of interference of significant intensity in a wide range of frequencies. For this reason, in particular, the input signals are routed through coaxial wires and are protected with a three-stage overvoltage protection consisting of a lightning arrester, a varistor, a transistor and series resistors. This protection ensures that the voltage on the input of the PC oscilloscope does not exceed ±34 V.

To suppress noise and higher frequency interference, a low inductance capacitor was connected in parallel to the measurement resistor. This capacitance, together with the resistors, forms a low-pass filter with a time constant of less than 80 ns. The filter itself has negligible effect on the distortion of the useful component of the signal.

The electron beam is deflected perpendicularly to the measurement slit. The electron current is captured at the Faraday cylinder collection electrode below the slit, and it produces a voltage signal on the measuring resistor. The measuring resistor can be placed directly in the Faraday cylinder and the voltage signal is routed outside the chamber, or the resistor can be placed outside the chamber near the DAQ module. Both options have advantages and disadvantages, so a compromise solution was chosen. Part of the resistor is located directly at the electrode in the Faraday cylinder and other resistors (series and parallel) are located at the analogue signal acquisition and recording unit and some are part of the overvoltage protection and low-pass filter. The three-stage overvoltage protection together with the low-pass filter and the measurement resistor for both measurement channels are located in the signal protection and adaptation module.

Fig. 3 Signal Protection and Adaptation Module Box

4 EXPERIMENTAL MEASUREMENT SYSTEM FOR MONITORING ELECTRON BEAM PARAMETERS

The DAQ analogue signal acquisition and recording module, PicoScope 3204D PC oscilloscope, which meets the requirements specified above, was used in the experimental measurement system setup. Furthermore, a signal protection and adaptation module was designed and fabricated to replace the experimentally designed overvoltage protection, input RC filter and signal Adaptation for the new solution.

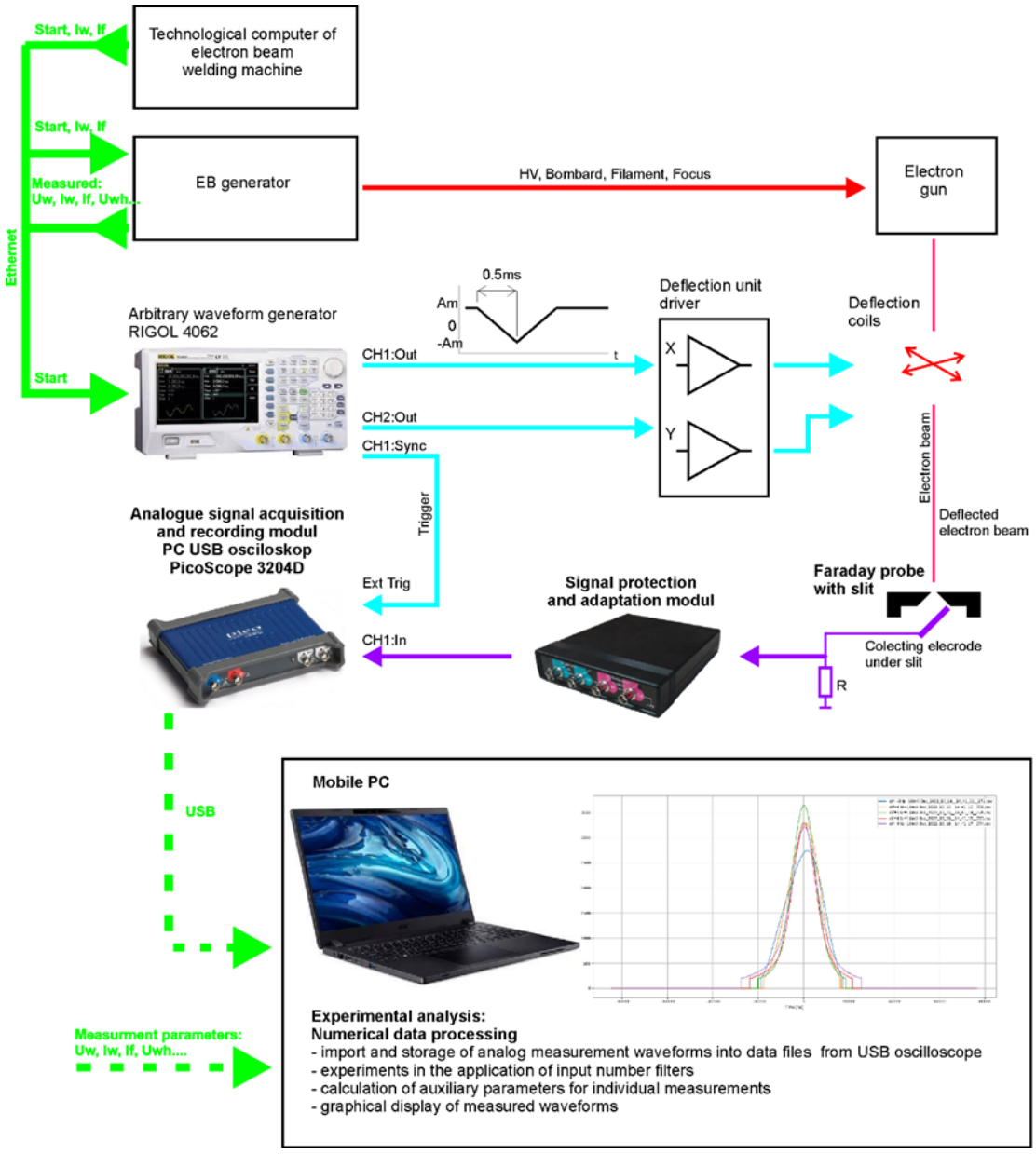

Fig. 4 Block diagram of the measurement system for monitoring electron beam parameters

5 FUNCTIONAL TESTS OF MEASURING APPARATUS

The tests were carried out to verify the functionality of the individual modules and the communication between the oscilloscope and the portable PC after assembling the measuring apparatus. The test programme was carried out on the experimental universal

electron-beam technology complex PZ ELZA UNI. The wiring of the measuring apparatus was according to the block diagram shown in the above figure. The width of the linear slit was set to 0.1 mm. The measuring probe was placed so that the slit was aligned with the undeflected electron beam. The working distance was 370 mm. The deflection amplitude of the beam was 32 mm at a working distance of 370 mm, this was matched by the generated signal with a voltage of 10 Vpp. The total measurement time was 0.5 ms. For this time the time period during which the electron beam passes over the measuring slit is relevant, i.e., approximately 50 to 150 μs. This has to be adapted to the start delay of the analogue signal recording with respect to the synchronization pulse from the deflection generator. The proper setup of recording delay reduces the amount of data to be sensed, transmitted, recorded and processed.
In the beginning of the measurements, the influence of the multi-stage overvoltage protection on the measured analogue signal was verified. The measurements showed that the resulting proposed configuration of the three-stage surge protector had no significant effect on the shape and magnitude of the measured analogue signal, the signal distortion was less than 1%. The same procedure was followed to verify the characteristics of the low-pass filter for suppressing unwanted interference from the industrial environment.

A program was created in the technological computer. The program setup the relevant parameters of the deflection system and the electron beam parameters (welding current - Iw, focal current If). The program performed the cyclic start of the measurement sequence, which consisted of setting and settling the desired value of If, starting the electron beam and settling at the desired value of Iw, and starting the deflection pulse and switching off the beam after initializing the deflection generator. The selected parameter is changed by the default step in the following sequence. The number of cycles is defined in the program and can be changed as needed, as well as the step of change for selected parameter.
Displaying a multiple measured waveforms from one cycle in one graph, a mutual time offset of the measured signals was observed. The times corresponding to the peaks of the individual waveforms (i.e., the position of the maximum expressed by the time sample in the record) were not aligned, nor did they follow a trend with respect to the change in the variable parameter. Further investigation of this anomalous phenomenon clarified the mechanism causing these shifts. The remanet magnetism of the deflection coils that originates from the DC saturation of the ferrite core during the steady-state period of the electron beam, affects the dynamics of the deflection of the beam when the measurement pulse is executed. This phenomenon is not deterministically repeatable and therefore the individual measured signal waveforms exhibited stochastic time shifts in the record, corresponding to a linear position shift. The amplitude of the deflection in the measurement is large enough to keep the velocity value constant during linear motion at the measurement slit location.

It was necessary to align the individual signals in the time axis to align the measurements. The position and number of maxima of the individual signals may vary depending on the beam quality. Therefore, the alignment of the signals to the position of the centre of gravity of the electron beam energy was performed.

6 PROCESSING OF MEASURED SIGNALS

The measured analogue signal, formed by the current of electrons passing through the measuring slit, and passing through the measuring resistor generates a voltage signal, which is routed through the protection circuits to the voltage input of the DAQ module. At a properly selected input range (in our case ±10 V), the DAQ converts the input signal into a data file, which is then transferred via the communication bus to the PC, where it is stored in a text file for further processing.

A certain non-zero level of the analogue signal can be observed throughout the measurement chain, even when the welding current is switched off. This analogue signal corresponds to interference from the measuring system and interference coming from the industrial environment (in particular, the inverter of the HV power supply, the inverter of the motion mechanisms, fluctuations in the power supply system of the production hall.

The influence of the direct current (DC) component of the disturbance signal originating from the measurement chain can be evaluated and eliminated from the measured signal by subtracting the DC component from all samples of the measured record. Determination of the DC component of the interfering signal was solved by summing the mean of the first and last 10% of the samples that are safely outside the signal obtained from the electron beam passing over the measurement slit.

The measured signal also contains noise and random disturbances from the industrial environment, which in calculations (e.g., integration of values - for determining the area under the curve) results in a bias of the result (right or left), especially if the centre of the measured pulse is not exactly in the middle of the record. That is, the integral of the noise from the beginning of the recording to the measured pulse is not the same as the integral of the noise from the measured signal to the end of the recording. This is because the length of the recording is determined so that there are a sufficient number of useful samples even in the case of a larger diameter electron beam measurement. As a solution to this problem, replacing the samples with a value lower than the chosen decision level (in our case, 200 mV at an input range of ±10 V), and replacing these values with 0, has proven to be a good solution. So, the results of further calculations are not affected.

The centre of gravity of the transverse electron beam profile is, in our understanding, the point corresponding to the power centre, i.e., the imaginary centre of the beam which is characterized by 50% of the total energy being both on the left and on the right. The position

of the centre of gravity can be determined as the ratio of the sum of the moments and the sum of the measured values (Eq. 1).

$$Centre\ of\ gravity = \frac{\sum t_i . U_i}{\sum U_i} \tag{1}$$

Where t_i is the time coordinate of the i^{th} sample of the signal recording, U_i is the voltage value of the i^{th} sample.

It was necessary for further processing of the measured signals to synchronize the measured waveforms with each other by aligning the time coordinates of the centres of gravity of the individual signal. The alignment of individual signals was necessary due to the above considerations about the influence of the remanent magnetism of the deflection coils on the shift in the time axis of the individual measurements. An example of a set of measured signals where the variable parameter was the variation of focal current intensity (focal position) is shown in the following figure.

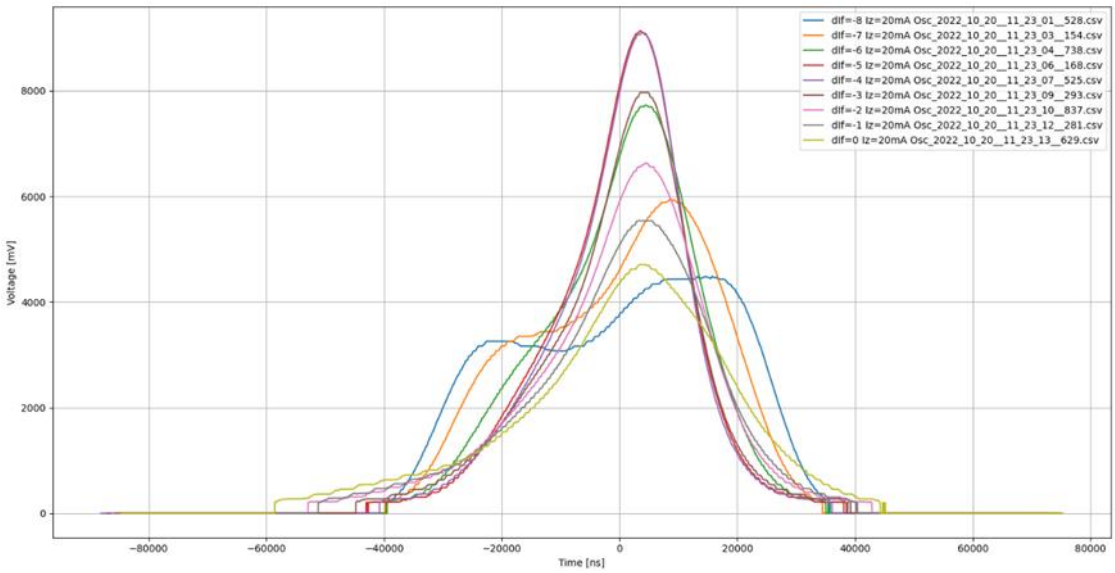

Fig. 5 Block diagram of the measurement system for monitoring electron beam parameters

We can conclude the beam section profile changes with changing focusing current from displayed signals. At the same time, it can be determined which focusing current corresponds to the highest and narrowest profile, corresponding to the optimum focus on the surface of the measuring slit. Specifically, the narrowest and highest profiles were recorded

at defocus currents ΔI_f = -5 and ΔI_f = -4 mA relatively the base value of I_f = 793 mA at a welding current value of I_w = 20 mA, (the red and purple lines, respectively). At defocus ΔI_f = -7 and ΔI_f = -8 mA, the obvious existence of profile asymmetry can be observed (orange and blue line). If such a visible asymmetry were observed close to the optimum focus, such a beam would be evaluated as unsuitable for welding and replacement of the LaB_6 emission cathode or other intervention in the emission system would be necessary. The next figures display an example of one recording of the beam passing over the measuring slit along with the various evaluation steps.

Shown are:

Orig - recorded unmodified signal,

D1 - remDC - signal with suppressed DC component,

D2 Avg15 Th5 - applied filter of the average value from the interval of 15 samples and suppression of values less than 5% of the maximum amplitude,

D6 Avg25 Th5 - applied filter of the average value from the interval of 25 samples and suppression of values less than 5 % of the maximum amplitude,

D7 Gauss7 Th5 - applied Gaussian filter of 7th order and suppression of values less than 5 % of the maximum amplitude,

D8 Gauss5 Th5 - Gaussian filter of 5th order applied and suppression of values less than 5 % of the maximum amplitude.

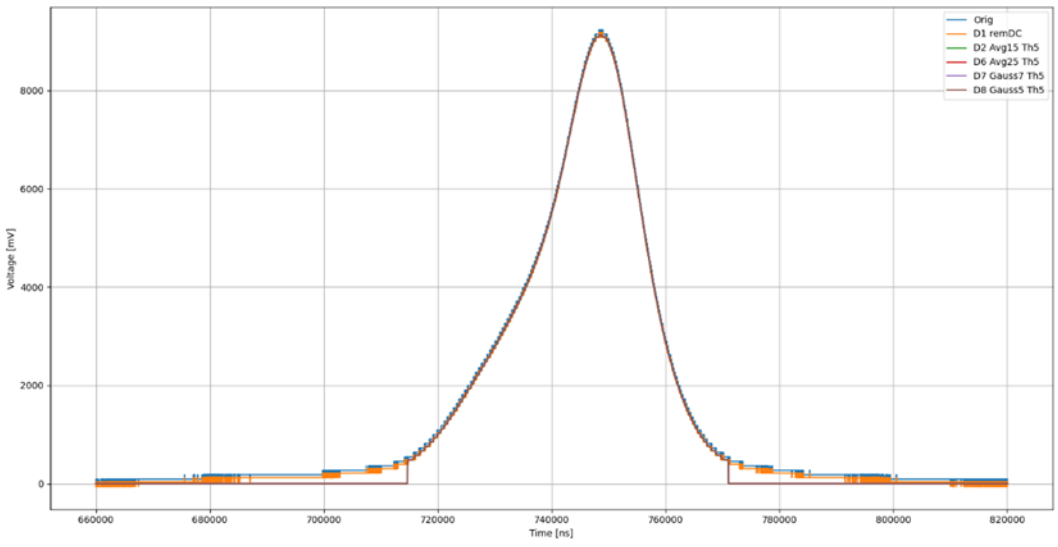

Fig. 6 One measured waveform at different stages of evaluation

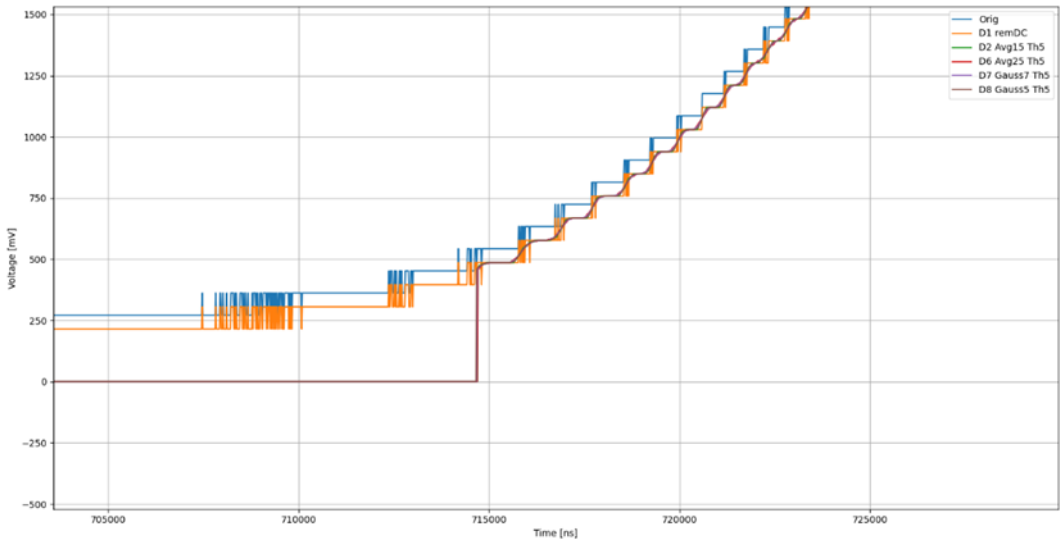

Fig. 7 Detail of the foot of the pulse course

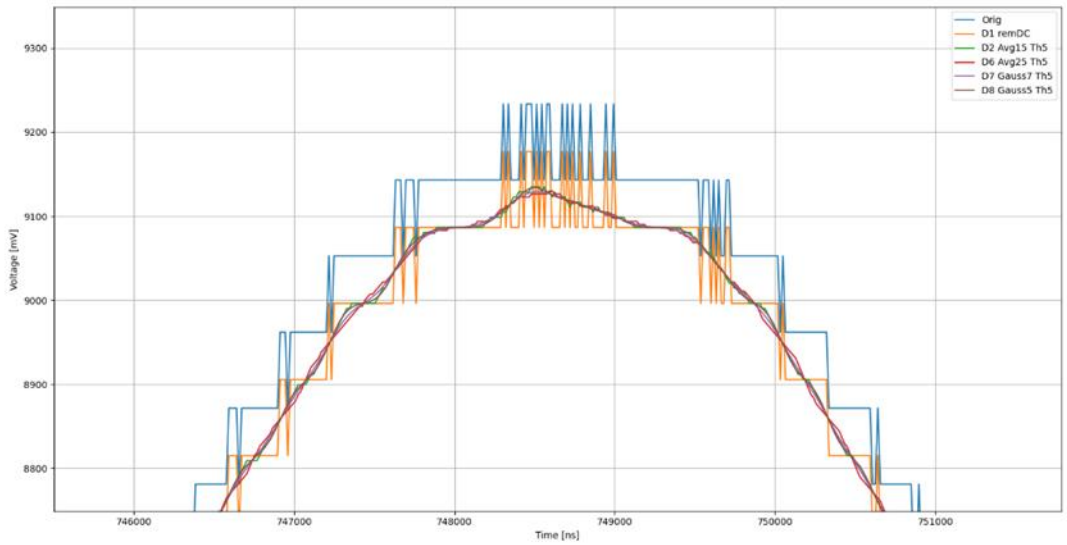

Fig. 8 Detail on the peak of the pulse waveform

It can be concluded that the entire profile is located asymmetrically over the entire length of the record by inspection of fig. 6. Therefore, it is reasonable to replace all samples smaller than the chosen 5% of the maximum with zero in the manner of the previous considerations. The areas under the curve will not enter into the calculation when calculating the centre of gravity. Some asymmetry with respect to the maximum can be seen from the shape of the

profile. The different positions of the maximum and the centre of gravity will be observed after the calculation. This is indicative of some measurable asymmetry.
The voltage inputs of the PicoScope 3204D PC oscilloscope used have a resolution of 8 bits for symmetrical voltage input ranges of ±20 mVpp to ±20 Vpp. For our measurements, we use ranges of ±5 Vpp, ±10 Vpp, or ±20 Vpp. The measured signal is of single polarity, so we will use only ½ of the 255 voltage levels of the converter, i.e., 127 levels. Since the measured signal does not reach the maximum of the used range in its amplitude, but only about 2/3. So, the effective sensitivity of the voltage range is about 100 levels of the analogue-to-digital converter. This fact is reflected in a significant signal gradation in discrete levels, especially in the shallow rise, peak and foot regions. It can be seen in Fig. 7 and Fig. 8 for the blue (Orig) and orange (D1 - remDC) signals. By using a higher resolution transducer, 10 to 16 bits, this phenomenon can be eliminated, but the acquisition cost is several times higher and at the time of acquisition they were only available with very long delivery times.

We tried to suppress the low resolution of the AD converter voltage inputs to an acceptable level by using various digital filters applied to the measured signals in our solution. Digital filter requirements for analogue signals:

- Suppression of interference from the servo converters and the inverter HV power supply,
- smoothing of steps in the signal caused by the low resolution of the AD converter,
- preserving time position, i.e., not shifting the signal in time after filter application,
- acceptably low impact on signal amplitude.

We selected the Avg average method and the Gaussian filter among the tested filters. We computed the Avg filter as the average value from a symmetrically chosen interval around each point with aim to do not affected time position of the sample. The ambient interval was chosen as a parameter with respect to the sampling period. The Gaussian filter favours the mean value of the near interval over the more distant samples in the calculation. Also, the filtering order was chosen as a parameter. The filters were applied to the signal with the DC component removed and samples with value less than the chosen 5% of the maximum were replaced by zero.
We evaluated the effect on the amplitude in the peak and the level of smoothing stages from the AD converter after application of the different filters. We assessed the smoothing by counting the local extremes of the signal. The ideal signal has only one maximum in the peak. If the measured beam cross section is a distorted significantly, it may contain multiple local extrema, e.g., two peaks and one local minimum. For a correct evaluation of the beam profile, the filters used should not suppress such a fact.
We consider the filtered signals D2 Avg15 Th5, D6 Avg25 Th5, D7 Gauss7 Th5, D8 Gauss5 Th5 shown in Fig. 6 to Fig. 8 to be satisfactory for further mathematical treatment.

7 CONCLUSION

The tests were carried out to verify the functionality of the individual modules and the communication between the oscilloscope and the portable PC after build up the measuring apparatus. The chosen hardware solution for measuring and recording signals from the measuring probe appears to be fully satisfactory and suitable for further development procedure. The measuring oscilloscope (DAQ module) is fully controllable from a portable PC and can be used in the proposed system for monitoring selected electron beam parameters for high-cadence welding processes. The recorded and digitized signal could not be analytically evaluated without further processing, as it exhibited a significant step-like signals. Filters were applied to suppress the stepping and smooth the signals. The filters of the average value from the sample interval - Avg (n samples before and after the current value) and the Gaussian filter were tested and evaluated. The applied filter order (number of samples in the case of averaging and order in the case of Gaussian filter) represents a compromise between signal smoothing and signal distortion. Optimal results were obtained when averaging 15 to 25 values in the interval of the filtered value and in the case of the Gaussian filter applying a filter of 5^{th} to 7^{th} order. At lower filter orders, the stepping was still significant, making it difficult to identify local extremes explicitly. On the other hand, there was a decrease in amplitude and distortion of the signal when higher order filters were applied. The use of filters made it possible to reasonably suppress the interference from the servo converters and the HV converter of the power-block source and to smooth out the steps in the signal caused by the low resolution of the AD converter. The chosen filters Avg (15 and 25) and Gauss (5 and 7) did not shift the time position of the signal and the effect on the signal amplitude was at an acceptable level.

ACKNOWLEDGEMENT:

This work was supported by the Slovak Research and Development Agency under the contract No. APVV-20-0103.

REFERENCES

Ahmed, N.: (2005). New developments in advanced welding. Cambridge: Woodhead Publishing Ltd.

Dilthey, U., Goumeniouk, A., Böhm, S., Welters. (2001). Electron beam diagnostics: a new release of the diabeam system. Vacuum, Vol. 62, Issue: 2-3, 77-85 pp.

Dilthey, U. and Weiser, J. (1997). Investigations of EB characteristics and their influences on the weld shape. Weld world 39(2), pp. 89-98.

Elmer, J. W. and Teruya, A. T. (1998). Fast method of measuring power density distribution of non-circular and irregular electron beams. Science and Technology of Welding and Joining.

Kaur, A., Ribton, C. and Balachandran, W. (2015). Electron beam characterisation methods and devices for welding equipment. Journal of materials processing technology, volume 221, pp. 225-232.

Koleva, E., Mladenov, G., Kardjiev, M. and Todorov, D. (2014). Electron beam characterization at changes of EBW process parameters. In: Proceedings of the 11th International Conference on Electron Beam Technologies, 8-12 June, Varna, Bulgaria.

Menhard, C. G., (2006). Fast Measurements of important electron beam parameters by variation of beam focusing. In: Proceedings of the 8th International Conference on Electron Beam Technologies, 5-10 June 2006, Varna, Bulgaria, pp. 11-12.

Meleka, A. H.: (1971). Electron beam welding: Principles and Practice. London: McGRAW-HILL.

Schultz, H.: (1993). Electron beam welding. England: Abington Publishing House.

SELECTED THIN FILM PROPERTIES AND POSSIBILITIES OF THEIR ALTERATION

Ing. Mgr. Jakub Blanár[1]
Asssoc. prof. Ing. Daniel Kottfer, PhD.[2]
[1]ORCID: 0009-0009-9673-3754, Alexander Dubček University of Trenčín, Faculty of Special Technology, Department of Mechanical Technologies and Materials, Ku Kyselke 469, 911 06 Trenčín, **Slovakia**
[2]ORCID: 0000-0003-3662-7641, Alexander Dubček University of Trenčín, Faculty of Special Technology, Department of Mechanical Technologies and Materials, Ku Kyselke 469, 911 06 Trenčín, **Slovakia**

Abstract: The article presents directions of the research in thin film properties and their alteration. The main goal is to bring a summary of published results on topics including the improvement of hardness and toughness of hard coatings and also enhancing the growth rate of films prepared by HiPIMS deposition method. The discussed novel approaches include employing variable positioning of the substrate with relation to the target, introducing an auxiliary anode, producing nano-composite material coatings, influencing the properties through changes in the layer deposition time, chemical elements doping or bombardment by heavy particles without heating the substrate.

Keywords: HiPIMS, toughness, hardness, modulus of elasticity

1 INTRODUCTION

The lifespan of machines and tools is closely related to properties of their surfaces, which are subject to mutual physical contact during tool operation. The mutual contact and relative movement of the parts cause wear. The most important factors contributing to wear resistance are mechanical properties of the tools, like hardness, modulus of elasticity but also tribological properties like coefficient of friction.
To minimize tool wear it is key that the tool surface has hight hardness and the coefficient of friction of the tool – machined part couple is kept at minimum. If feasible, tools are heat treated to achieve higher hardness. Surface properties and wear resistance can be further improved by coating the tool with thin film. Appropriate selection of the coating material, type of the thin film, deposition technology and process parameters can lead to obtaining a tool surface with optimal properties.

Vacuum film deposition technologies can be divided into two main groups, depending on the dominant mechanism: physical vapour deposition (PVD) and chemical vapour deposition (CVD) (Baptista et al., 2018). Further classification of PVD methods is shown in Fig. 1.
Hight Power Impulse Magnetron Sputtering (HiPIMS) represents the most advanced deposition technology to the current day. It provides films of high hardness, low roughness and porosity, however, at the cost of low growth rates of the coatings. This article focuses on summarising recent findings of possibilities how to improve the speed of the film growth as well as how to increase hardness and toughness of composite coatings.

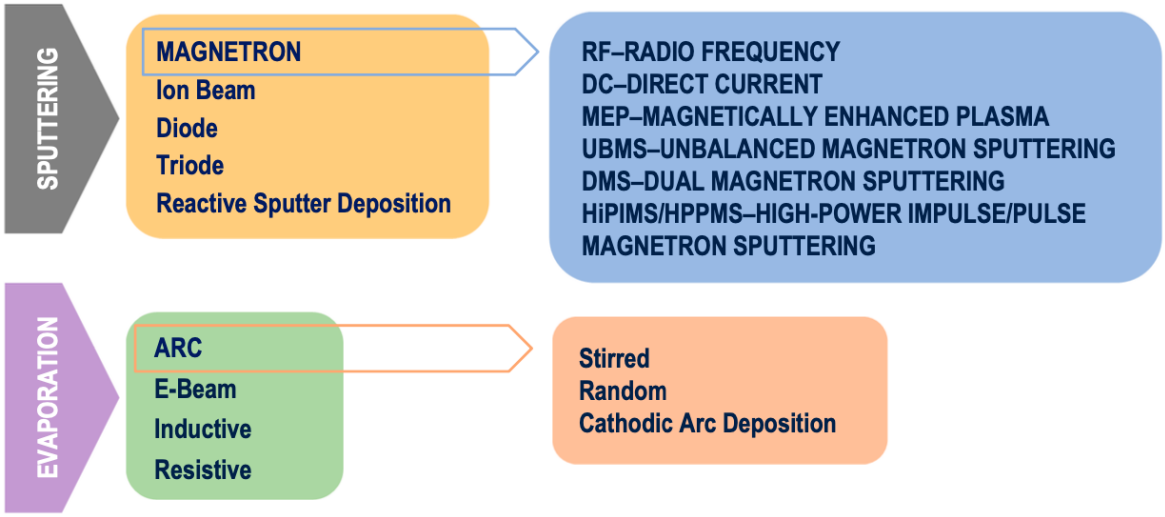

Fig. 1 Classification of PVD thin film deposition methods (Baptista et al. 2018)

2 INCREASING DEPOSITION RATES IN HIPIMS BY SAMPLE POSITIONING AND UTILIZING AN AUXILIARY ANODE

Published research articles show eminent interest in the HiPIMS technology due to its advantages in PVD films production. Nevertheless, the main disadvantage of this process remains the film growth rate, which is significantly lower when compared with conventional DC sputtering. Li et al. (2016, 2017) studied two different approaches to enhance the deposition rates using HiPIMS. They tested five different substrate orientations with regards to the target, namely 0°, 45°, 90°, 135° a 180°. Scheme of the layout in the vacuum chamber is depicted in the Fig. 2. The first study (Li et al., 2016, Fig. 2a) employed unbalanced magnetic field during the deposition process.

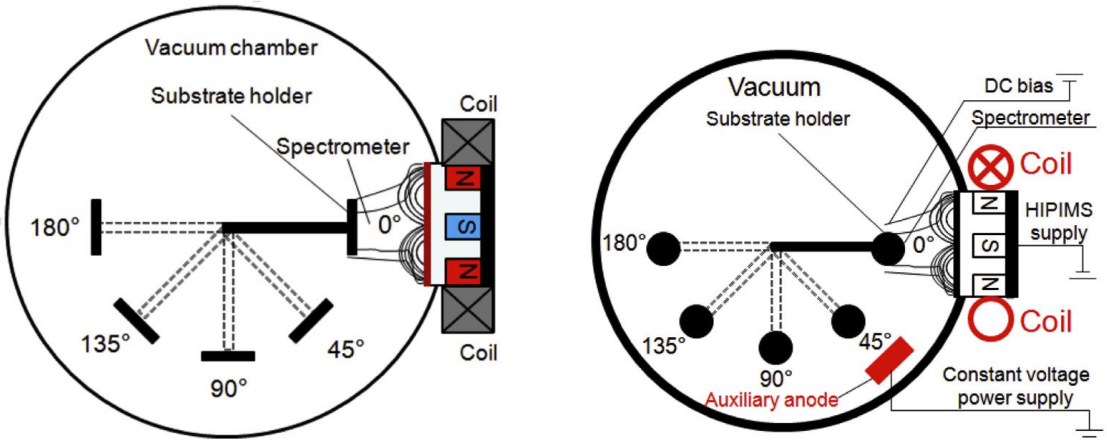

Fig. 2 Layout of the vacuum magnetron sputtering system: a) using external unbalanced magnetic field (Li et al., 2016), b) using external electric and magnetic fields (Li et al., 2017)

It has been observed that a much stronger ion current was present on the substrate in the 0° position when compared with all the other orientations. The plasma density was increased in the vicinity of the substrate. The second article focused on creating a more simplified and efficient ion discharge with the assistance of external electric and magnetic fields using an auxiliary anode (Li et al., 2017, Fig. 2b). Coaxial electromagnetic coil was used to produce optimal distribution of the magnetic field. This approach allowed for a more uniform distribution of the electric field and electric potential within the reactor, more intensive plasma and directionality. The amplitude of plasma was five times higher in all substrate positions when compared with discharging without the external fields (Li et al. 2017).

3 INCREASING HARDNESS AND TOUGHNESS OF HARD COMPOSITE FILMS

The main sources of film hardness are (Vepřek and Reiprich, 1995):

- Intrinsically hard materials, like diamond, DLC, c-BN
- High residual pressure stresses in the film – may cause decohesion or decomposition of the coating at elevated temperatures
- Nanocrystalline structure of the film, e.g. nanoparticles of TiN in Si_3N_4 matrix

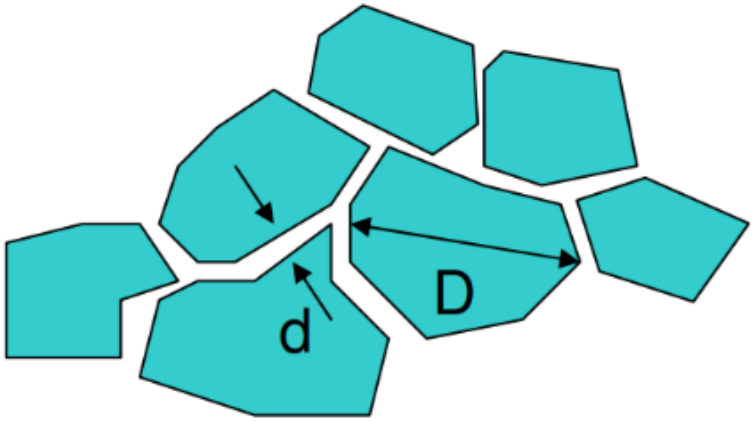

Fig. 3 Vepřek's model of super hard films: D~5 nm: no dislocation movement possible; d~1 nm: continuous amorphous skeleton (Vepřek and Reiprich, 1995)

According to Mishra (2020) there are two ways how to increase hardness of nanocomposite thin films:

- By nanocomposite monolayer deposition (Fig. 3)
- By multilayer microstructure of the film (Fig. 4)

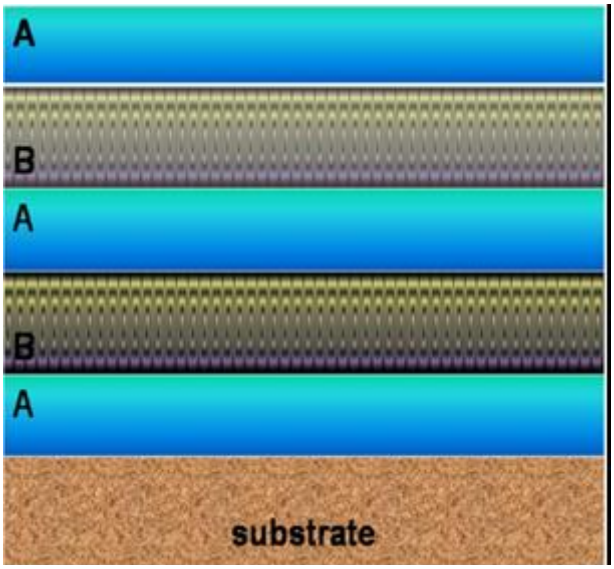

Fig. 4 Scheme of a multilayer film composition (Mishra, 2020)

Multilayer coatings with a reduced layer thickness (order of nm) and alternating high and low elasticity modulus layers lead to films with high strength. As a result of this design, the dislocations created in the low modulus layer are prevented from further movement at the interface with the high modulus layer. This is caused by the presence of repulsive force and high stresses at the layer interface. If one of the layers is amorphous, also the stresses are eliminated. Deposition of multilayer films on 3D objects and keeping the correct thickness of the layers proved to be demanding, so oftentimes these films manifest imperfections and defects (Mishra, 2020).

Musil (2012) described high hardness nanocomposite films which, at the same time, have sufficient strength. According to Andres et al. (1989) hard nanocomposite coatings may have:

- Nano size bi-layers (Fig. 5a)
- Nanocolumnar microstructure (Fig. 5b)
- Dense globular microstructure, with nanograins surrounded by amorphous phase (Fig. 5c)
- Nanostructure consisting of grains of different crystallographic orientations (Fig. 5d).

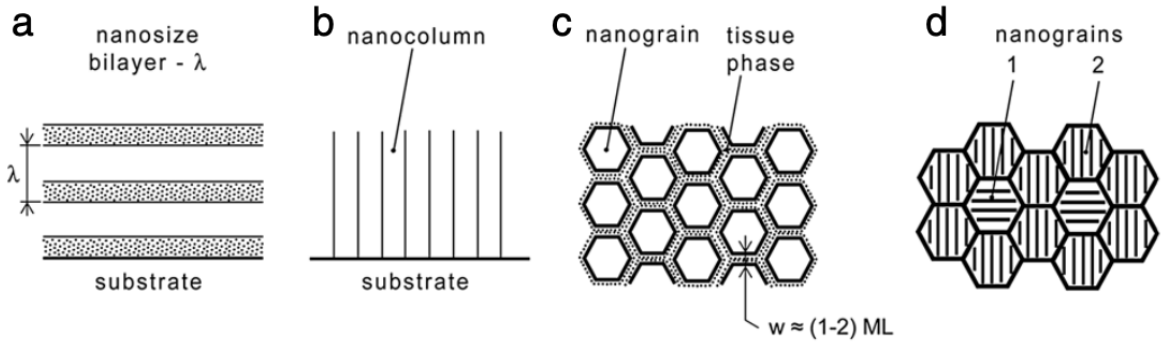

Fig. 5 Nanocomposite materials with high hardness: a) nano size bi-layer; b) nanocolumns; c) nanograins surrounded by amorphous phase, d) nanograins with different crystallographic orientation (Musil, 2012).

3.1 HARD AND RESISTANT NANOCOMPOSITE COATINGS DESIGN

One of the possible ways to increase hardness is through grain boundaries. The increase is highest when the grain size is around 10 nm (Fig. 6) (Musil et al., 2005; Voevodin and Zabinski, 2005).

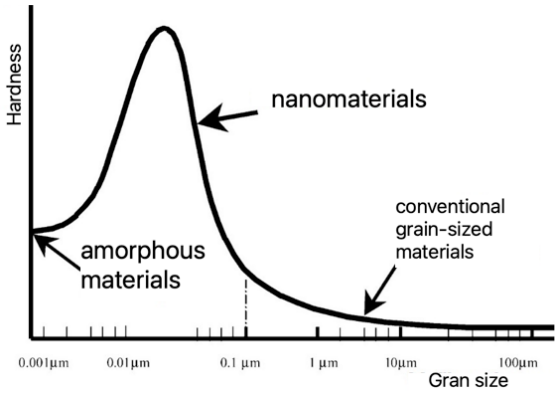

Fig. 6 Hardness of material as a function of grain size (Musil et al., 2005; Voevodin and Zabinski, 2005).

High fracture toughness of nanocomposite films can be achieved through nano-sized grain structure, deflection of the fracture by secondary phase and by stopping the fracture on grain boundaries. Grain boundary properties, such as their structure or the angle between grains, play important role in dislocation movement and as a result determine mechanical properties of nanocomposites. Improvement of nanocomposite films toughness requires only little diffusion and sliding at the grain boundaries. Design of nanocomposite films can incorporate materials with different levels of hardness.

Ternary, quaternary or even more complex systems containing amorphous phase that is harder than the matrix together with the nanocrystalline phase enhance strength at the grain boundary. Chemical bond in the composite too determines how hard and tough the film is. The Fig. 7 shows a triangle of properties change that is dependent on the chemical bond type.

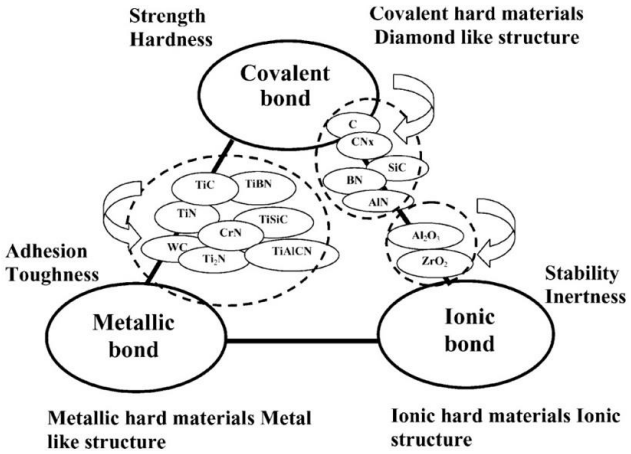

Fig. 7 Hard materials in the chemical bond triange – influence of the chemical bond type on nanocomposite film properties (Holleck and Schier, 1995)

3.2 INFLUENCING HARDNESS AND TOUGHNESS OF HARD COMPOSITE COATINGS THROUGH CHANGES IN DEPOSITION TIMES

Postolnyi et al. (2017) deposited CrN/MoN film by alternating electric arc evaporation of CrN and MoN layers from two sources (Fig. 8).

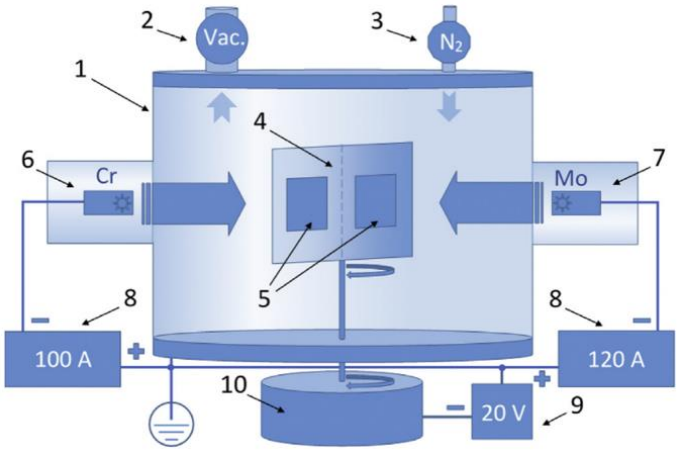

Fig. 8 Electric arc vacuum evaporation device: 1- vacuum chamber, 2 – vacuum system, 3 – N2 inlet, 4 – substrate holder, 5 – substrates, 6 – Cr evaporator, 7 – Mo evaporator, 8 – electric arc power supply, - 9 – substrate voltage bias, 10 – rotating system of substrate holder (Postolnyi et al., 2017)

The authors (Postolnyi et al., 2017) performed 6 deposition sessions. The deposition parameters remained constant across all sessions: electric arc current for Mo and Cr evaporation were 120 A and 100 A, respectively. Bias voltage on substrate was -20 V, pressure in the vacuum chamber 0,4 Pa. They varied the deposition time of a single layer, ranging from 300 s to 10 s. Final films consisted of different number of layers from 12 to 354 (Fig. 9).

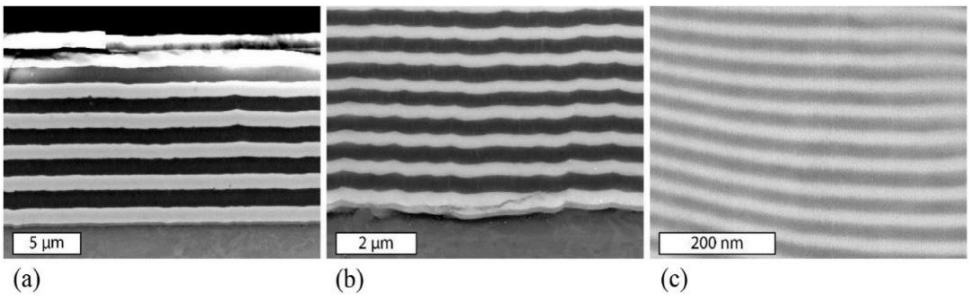

Fig. 9 Cross-sectional SEM view of CrN/MoN multilayer film: a) deposition time 300 s, bilayer thickness 2,26 µm, total 12 layers; b) deposition time 80 s, bi-layer thickness 0,6 µm, total 45 layers; c) deposition time 10 s, bi-layer thickness 0,044 µm, total 354 layers (Postolnyi et al., 2017)

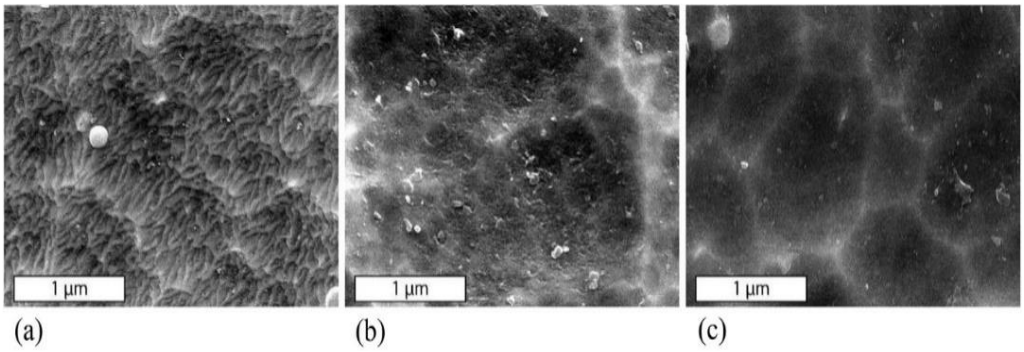

Fig. 10 SEM view of the CrN/MoN film surface: a) deposition time 300 s, bi-layer thickness 2,26 µm, total 12 layers; b) deposition time 80 s, bi-layer thickness 0,6 µm, total 45 layers; c) deposition time 10 s, bi-layer thickness 0,044 µm, total 354 layers (Postolnyi et al., 2017)

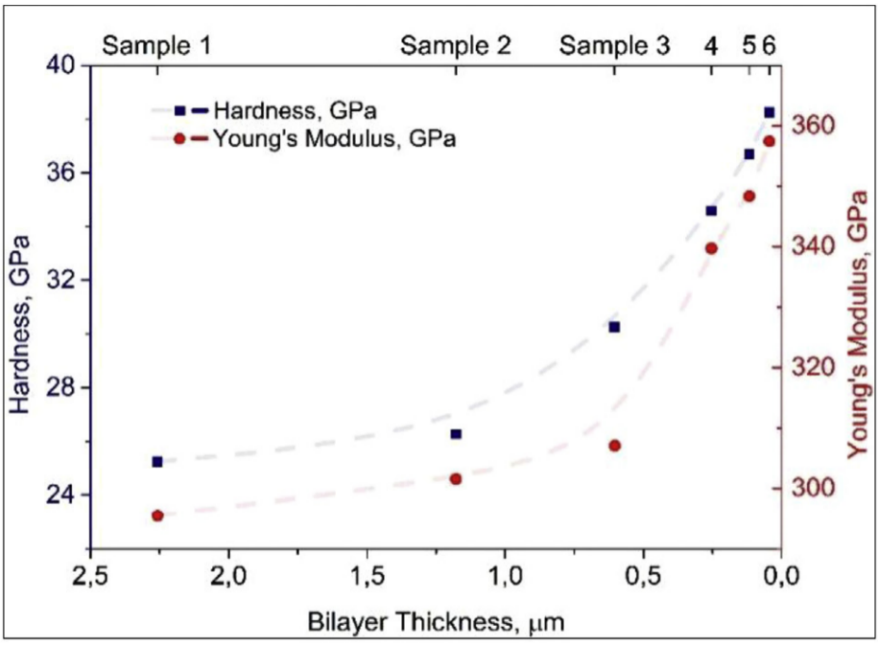

Fig. 11 Influence of the CrN/MoN bi-layer thickness on hardness and modulus of elasticity (Postolnyi et al., 2017)

Parameters of the deposition remained constant with deposition time being the only variable that was changing.

Films prepared using different deposition times manifested similar phase and chemical composition. However, what varied was the film microstructure (Fig. 10). The grain size decreased along with the overall thickness of the film. This led to volume increase of the

interfaces in the CrN/MoN coatings. On the other hand, as a result of the reduced single layer thickness, the number of interlayer interfaces arose. These effects contribute to Hall-Petch strengthening of the film and to reduced movement possibilities for dislocations in the multi-layered coatings. The film with the lowest bi-layer thickness of 0,044 μm showed the maximum hardness measured at 42,3 GPa (Fig. 11).

3.3 INFLUENCING THE HARDNESS AND TOUGHNESS OF HARD COMPOSITE FILMS BY CHEMICAL ELEMENTS ADDITION

Addition of elements like aluminium or silicon can change the film microstructure and thus also their hardness and toughness. Nanocomposites consisting of amorphous matrix and nanocrystalline grains improve toughness. It may be further enhanced employing multilayer structure with the presence of amorphous layers. The amorphous layers with thickness of several nanometers can participate in slowing down the creation and propagation of dislocations. TiAlSiN films are present as layered films with Ti-Al-N nano-composite layers which is alternated by Si_3N_4 layers (Fig. 12) (Yau et al., 2005).

Yau rt al. (2005) deposited TiAlSiN film through sputtering of two targets. One was TiAl (50:50%) using DCMS and Si using RFMS, temperature of the substrate was 300 °C. Sputtered atoms reacted with gaseous N2 which was introduced into the vacuum chamber (Fig. 13).

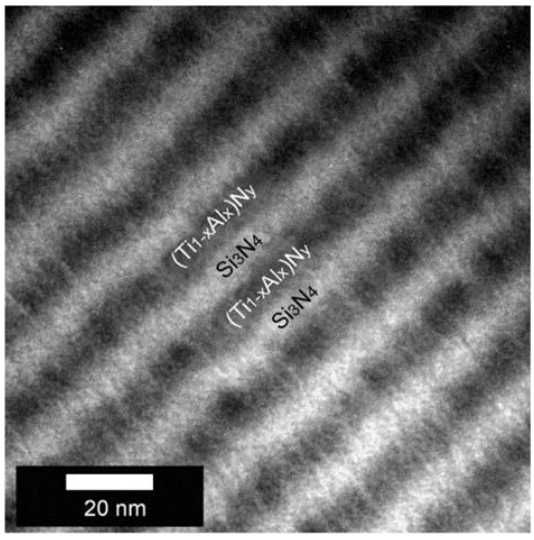

Fig. 12 Cross-section of the TiAlSiN film composed of alternating TiAlN and Si3N4 layers, TEM (Yau et al., 2005).

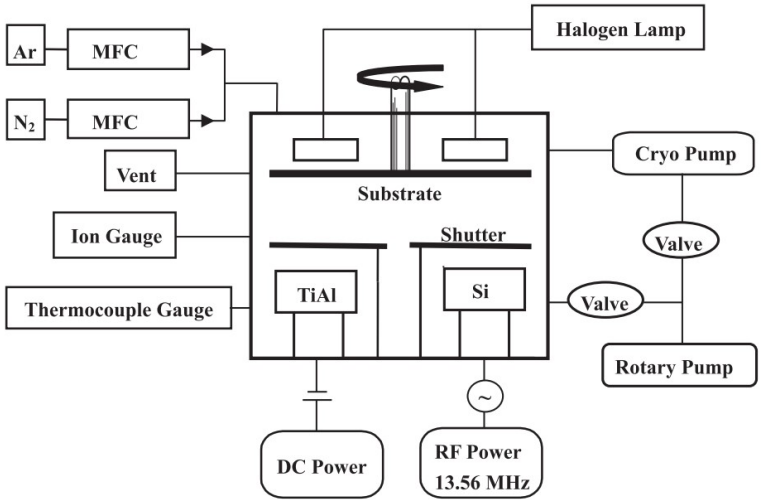

Fig. 13 Scheme of the device for deposition of the laminated TiAlSiN nanofilm (Yau et al.,2005).

The TiAlSiN films had thickness of 1 μm. The maximum measured hardness at 35 GPa (Fig. 14) was higher than hardness of TiAlN or Si_3N_4 monolayers. Dislocation movement was complicated by the presence of two alternating types of layers. The fracture mechanism changed from delamination to tensile cracking. Film with the bi-layer periodicity at 20 nm manifested nano-fracture deflection on the inner interface and its propagation on the interlayer interface (Fig. 15a, b), which suggests that such multilayers are significantly harder than a sole layer of TiAlSiN or TiAlN (Fig. 14). Fracture deflection between the layers and within the layers of nc-TiAlN/a-Si_3N_4 served as the dominant mechanism of material strengthening.

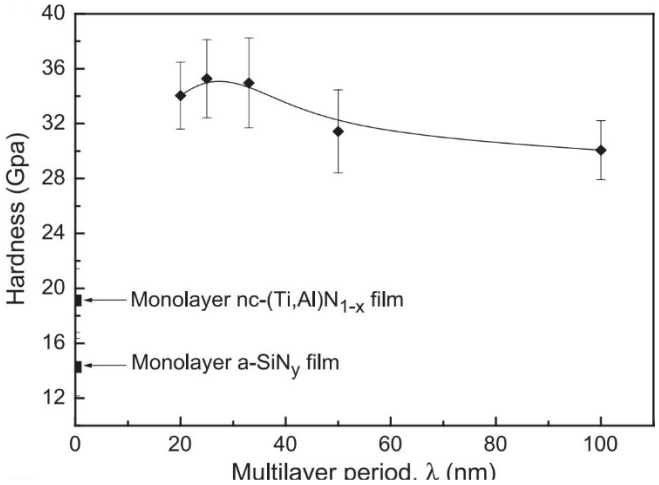

Fig. 14 Hardness of TiAlSiN film composed of ncTiAlN/a-Si_3N_4 nano-layers in dependence from the bi-layer thickness (Yau et al., 2005).

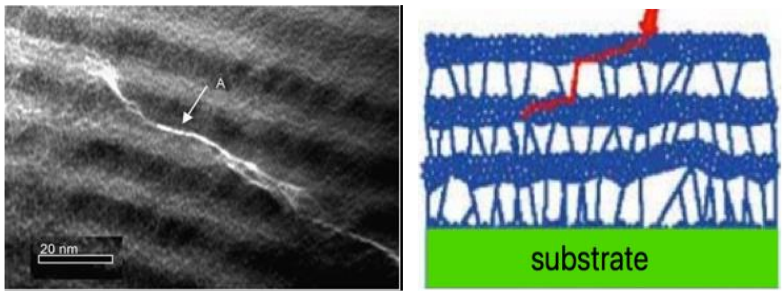

Fig. 15 a) TiAlSiN film composed of nc-TiAlN/a-Si_3N_4 nnano-layers showing fracture deflection on the interlayer interface and within the layers, TEM (Yau et al., 2005); b) scheme of the mechanism of fracture propagation in a multilayer film (Sosnová, Kříž et al. 2005)

3.4 INFLUENCING HARDNESS AND TOUGHNESS OF HARD COMPOSITE FILMS BY SPUTTERING WITH HEAVY TA PARTICLES WITHOUT SUBSTRATE HEATING

Greczynski et al (2014) introduced a new way of depositing dense refraktory ceramic films without heating the substrate. Bombardment with heavy Ta ions was used to obtain $Ti_{(1-x)}Ta_xN$ layers with high hardness, high modulus of elasticity and reduced residual stresses. $Ti_{0.92}Ta_{0.08}N$ film was deposited using HiPIMS (for Ta) and DCMS (for Ti) at substrate temperature below 120 °C and bias voltage of 160 V.

As a result of the target bombardment with heavy atoms of the sputtered metals, the intercolumnar and intracolumnar porosity (so typical for growth of refractory ceramic films at low temperatures) was eliminated due to effective mixture of the sputtered atoms present above the film surface (Fig. 16b). On the other hand, voids are visible between the Ti DCMS columns and sides of the columns manifest microstructure that corresponds with nano-porosity in the intercolumnar spaces (Fig 16a). Surface of the Ta(HiPIMS)/Ti(DCMS) films are significantly smoother and hardness is at 330% higher when compared with TiN(DCMS, V_s = 10 V) coatings, while the residual stresses are kept at minimum (Fig. 19).

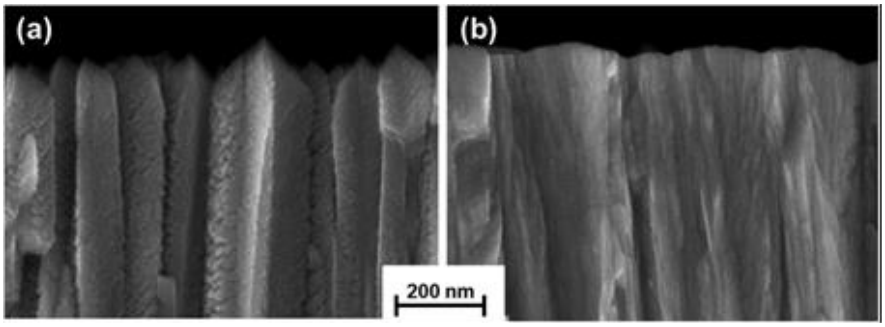

Fig. 16 SEM cross-sectional view on the film near the surface: a) DCMS TiN film with conical column ending, Vs =10 V; b) Ta(HiPIM)/ Ti(DCMS) TiN film deposited with synchronized substrate bias at 20 V and 280 V without substrate heating (Greczynski et al., 2014)

In the Fig. 17, 18 and 19 is shown the dependency of hardness, modulus of elasticity and residual stresses on the bias voltage. The graphs also show results of four sets of referential films deposited on Si substrates, for comparison: (1) DCMS TiN with V_s = 10V, (2) DCMS TiN at T_s = 500 °C and V_s = 60 V, (3) Ta(HiPIMS)/Ti(DCMS) TiN deposited with synchronized bias voltage 20 V and 280 V, (4) alloys of $Ti_{0,92}Ta_{0,08}N$ deposited at T_s < 120 °C and V_s=10 V. Except for the film (2) all films were deposited with T_s < 120 °C (Greczynski et al., 2014).

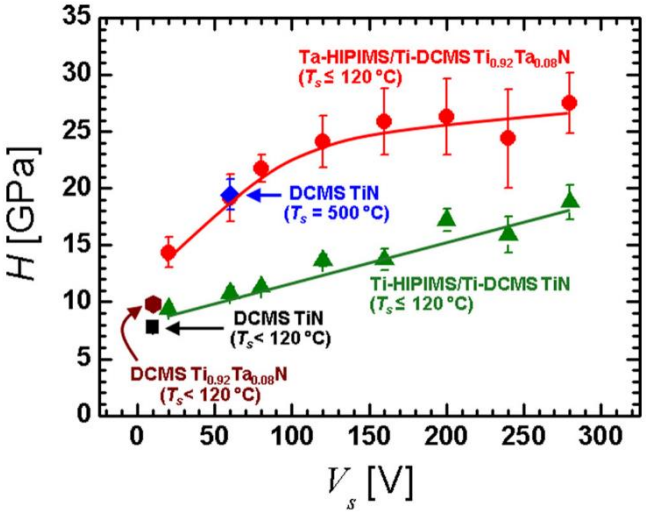

Fig. 17 The effect of substrate bias voltage on hardness of the Ta(HiPIMS)/Ti(DCMS) film (Greczynski et al., 2014).

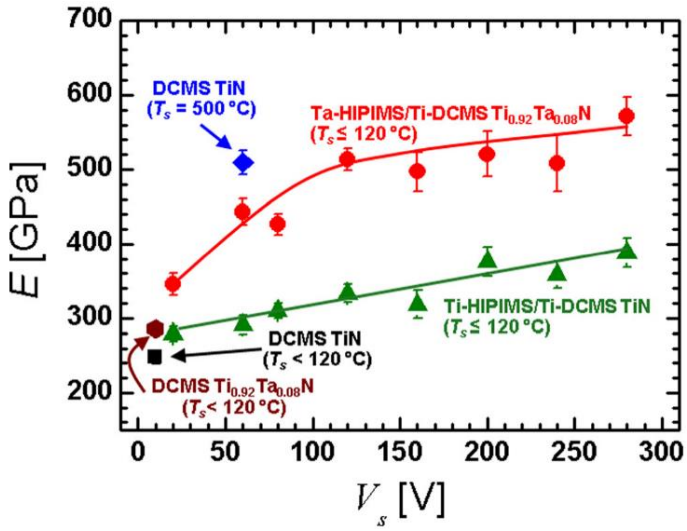

Fig. 18 The effect of substrate bias voltage on modulus of elasticity of the Ta(HiPMS)/Ti(DCMS) film (Greczynski et al., 2014).

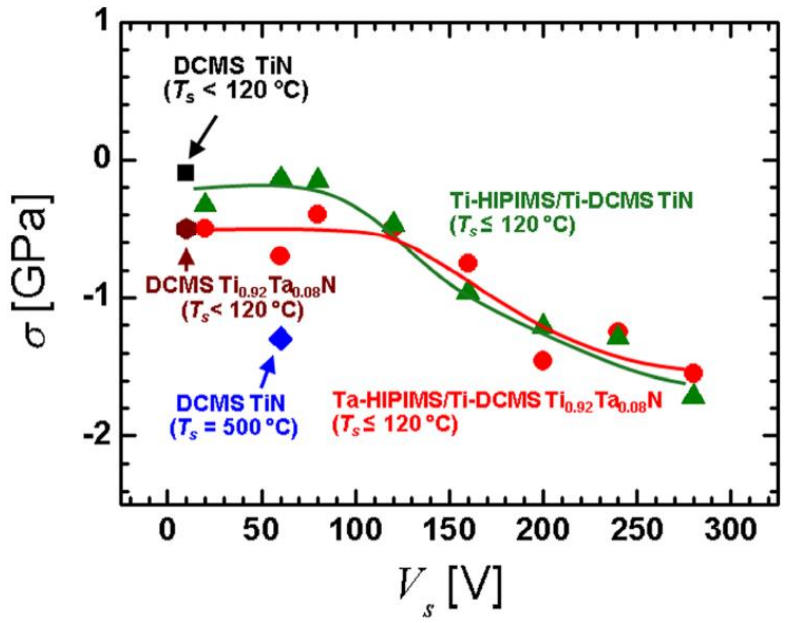

Fig 19 The effect of substrate bias voltage on residual stresses of the Ta(HiPIMS)/Ti(DCMS) film (Greczynski et al., 2014).

Grzeczynski et al. (2014) has shown that utilisation of synchronized bias voltage on the substrate to produce an ion flux that is rich on the metal particles, provides new possibilities for film growth. The flux can be tuned by proper selection of the metal ions in the hybrid co-sputtering configuration. Residual stresses can be reduced or completely eliminated based on the film growth conditions, as the metal ions are part of the film. Increase in the bias voltage is connected with higher hardness and modulus of elasticity and with residual stresses approaching zero. Increasing bias comes together with slightly increasing compressive stresses, which, in return, contribute to higher hardness and modulus. Measured levels of these two parameters were H = 25,9 GPa and E = 497 GPa, respectively, which represents 100% increase in hardness and 60% increase in modulus, in comparison with sputtering Ti using the same methods.

4 CONCLUSION

Even though thin coatings and their properties have been under research and investigation for decades, it is relevant also today. There is a perpetual need for higher machining speeds, more pieces to be machined in shorter time, harder and more advanced materials are being used. This puts higher requirements on the tools, their properties and, in the end, on the quality of the tool surface. There are various ways of enhancing the tool surface properties and its longevity to be still investigated. One of the promising directions is addition of other elements into a known chemical composition (e.g. WC) during the HiPIMS sputtering

process. It is possible to find the optimal process parameters – like the frequency, pulse length, substrate temperature and others – to obtain the appropriate coating. Further research efforts will presumably bring more data and possibly enable more applications (for example higher thermal stability of the film during machining operation).

REFERENCES

Andres, R. P., Averback, R. S., Brown, W. L., Brus, L. E., Goddard, W. A., Kaldor A. et al. (1989). Research opportunities on clusters and cluster-assembled materials. Journal of Materials Research, Vol. 4, No. 3, pp. 704–736.

Baptista A., Silva F. F., Porteiro J., Míguez J., Pinto G. (2018). Sputtering Physical Vapour Deposition (PVD) Coatings: A Critical Review on Process Improvement and Market Trend Demands. Coatings, 8, 402, 22 p.

Greczynski G., Lu J., Bolz S., Koelker W., Schiffers Ch., Lemmer O., Petrov I., Greene J. E., Hulman L. (2014). Novel strategy for low-temperature, high-rate growth of dense, hard, and stress-free refractory ceramic thin films. Journal of Vacuum Science & Technology A - Vacuum, Surfaces, and Films, 32, 4, 12 p.

Holleck, H. and Schier V. (1995). Multilayer PVD coatings for wear protection. Surface and Coatings Technology, Vol. 76–77, pp. 328–336.

Li, C., Tian, X., Gong, C., Xu, J. (2016). The improvement of high power impulse magnetron sputtering performance by an external unbalanced magnetic field. Vacuum, 133, pp. 98–104.

Li, C., Tian, X., Gong, C., Xu, J., Liu, S. (2017). Synergistic enhancement effect between external electric and magnetic fields during high power impulse magnetron sputtering discharge. Vacuum, 143, pp. 119–128.

Mishra, S. K. (2020). Toughening of nanocomposite hard coatings. Rev. Adv. Mater. Sci., 59, pp. 553–585.

Musil, J. (2012). Hard nanocomposite coatings: Thermal stability, oxidation resistance and toughness. Surface and Coatings Technology, Vol. 207, pp. 50–65.

Musil J., Baroch P., Vlček J., Nam K. H. and Han J. G. (2005). Reactive magnetron sputtering of thin films: present status and trends. Thin Solid Films, 475, pp. 208-218.

Postolnyi B. O., Beresnev V. M., Abadias G., Bondar O. V., Rebouta L., Araujo J. P. and Pogrebnjak A. D. (2017). Multilayer design of CrN/MoN protective coatings for enhanced hardness and toughness. Journal of Alloys and Compounds, 725, pp. 1188-1198.

Sosnová, M., Kříž, A. et al. (2005). Aplikace tenkých vrstev v strojírenství [online] A team materiálový výzkum, Západočeská universita v Plzni. Available at: https://www.opi.zcu.cz/tz_prednaska.pdf. [Accessed: 01 Mar 2022]

Vepřek S. and Reiprich S. (1995). A concept for the design of novel superhard coatings. Thin Solid Films, Vol. 268, No. 1-2, pp. 64–71.

Voevodin A. A. and Zabinski J. S. (2005). Nanocomposite and nanostructured tribological materials for space applications. Compites Science and Technology, Vol. 65, No. 5, pp. 741–748.

Yau, B. S., Huang J. L., Lu H. H., Sajgalik P. (2005). Investigation of nanocrystal-(Ti1- xAlx) Ny/amorphous-Si3N4 nanolaminate films. Surface and Coatings Technology, Vol.194, No. 1, pp. 119– 127.

WELDABILITY OF STAINLESS STEEL AND COPPER BY CONCENTRATED SOURCES OF ENERGY

Ing. Martin Hnilica[1]
Assoc. prof. Dr. Ing. Pavel Kovačócy[2]
Ing. Beáta Šimeková, PhD.[3]
Assoc. prof. Ing. Jozef Bárta, PhD.[4]
Ing. Ingrid Kovaříková, PhD.[5]

[1]ORCID: , Department of Welding and Joining of Materials, Institute of Production Technologies, Faculty of Materials Science and Technology in Trnava, Slovak University of Technology in Bratislava, **Slovakia**

[2]ORCID: 0000-0002-4377-7659, Department of Welding and Joining of Materials, Institute of Production Technologies, Faculty of Materials Science and Technology in Trnava, Slovak University of Technology in Bratislava, **Slovakia**

[3]ORCID: 0000-0002-6499-0096, Department of Welding and Joining of Materials, Institute of Production Technologies, Faculty of Materials Science and Technology in Trnava, Slovak University of Technology in Bratislava, **Slovakia**

[4]ORCID: 0000-0003-0607-4433, Department of Welding and Joining of Materials, Institute of Production Technologies, Faculty of Materials Science and Technology in Trnava, Slovak University of Technology in Bratislava, **Slovakia**

[5]ORCID: 0000-0002-0063-8210, Department of Engineering Technologies and Materials, Faculty of Special Technology, Alexander Dubček University of Trenčín, **Slovakia**

Abstract: Aim of the paper is to design experiment of butt weld made of stainless steel and elctrothough pitching copper by laser beam. This experiment should be used for approximate prediction of ultimate strenght with changing of the observed parameters. The effect of three welding parameters were investigated in this study by Taguchi Design of Experiments. The parameters of interest were welding power, velocity of welding beam and offset. Those parametres were examined on 3 levels. Analysis of Variance was used to determine statistical influence of welding parameters. Our response was tensille strenght and it was performed via STN EN ISO 6892-1. The value measured in results is response average from 3 samples. Result is to create regression equation to approximatly predict ultimate strenght when different welding parameters are used.

Keywords: Taguchi, DOE, Laser Welding, Tensile strength

1 INTRDUCTION

Welded joints of dissimilar materials are widely used in the automotive, oil, aerospace and nuclear power industries. In this research work, two materials were chosen, stainless steel 304 and pure copper. This combination of materials was mostly used in past as pipes or copper stave coolers, where are used combination of their properties like corrosion resistance and thermal conduction [1]. In last decade combinations of welded thin sheets undoubted industrial interest due to its implications in e-mobility fields. In the automotive industry prevails application when cylindrical cells needs to be connected to any elements constituting the battery, such as printed circuit boards or busbars [2]. Many reaserchers have performed optimalisation of welding process with DOE. Seung Gu Kang et al 2021 [3] created design of experiment of laser beam welding, where was used tensile strength as response. Acharjee et al 2012 [4] did a reasearch for prediction and finding, the parameters have positive and negative effects on the weld pool in the case of a lap weld. Ascari et al 2022 [5] investigated the ideal heat input to achieve a weld joint without pores and cracks and at the same time achieve an ideal weld shape. Hijazi et al 2020 [6] tested the setting of laser welding parameters when focusing into copper experimentally using the Taguchi method. Nisar et al 2023 [7] studied parametric effects of laser welding speed on peak temperatures. His results show positive correlation between laser power and temperatures and negative correlation between welding speed and temperature. Yang et al 2012 [8] tried optimalisation of weld bead geometry by Taguchi method. Their choosen parameters were laser power, welding speed, and wire feed rate.

2 METHODOLOGY OF RESEARCH

The dissimilar welding of stainless steel and copper presents a series of problems. First, there are large differences between their physical properties, including melting point, thermal conductivity, and thermal expansivity. With experimental method based on design of experiment of welding process of dissimilar materials with laser beam welding is possible to predict normaly measured responses based only on parameters. The main problem is to find a general solution of regression equation for prediction value of ultimate stress for laser welding of two dissimilar materials – stainless steel AISI 304 and eletropitching copper [9].

Materials

The AISI 304 stainless steel (SS) is being widely used in different industrial applications and is accounted for approximately 50% of the world's SS production [10,11]. It has been reported that because of AISI 304 SS superior aesthetic, mechanical, physical properties, weldability, chemical and corrosion resistance, it is one of the most preferred structural materials. The chemical composition of SS304 is listed in table 1. [12-14].

Table 1. Chemical composition of AISI 304

C	Si	Mn	P	S	N	Cr	Ni	Fe
≤ 0,07	≤1,00	≤2,00	≤0,045	≤0,03	≤0,11	17,00-19,5	8,00-10,5	Balance

Cu ETP is the most common copper. It is universal for electrical applications. Cu ETP has a minimum conductivity rating of 100% IACS and is required to be 99.9% pure. It has 0.02% to 0.04% oxygen content. Most common Cu ETP - C11000C is an electrolytic refined copper widely used for electrical and electronic applications. Cu ETP has the properties required in all applications with a hydrogen-free atmosphere. In the presence of H_2 and heat, all oxygen-bearing coppers suffer from so-called hydrogen embrittlement. This is a chemical reduction of copper oxide by diffusing hydrogen leading to the formation of H_2O within the microstructure, resulting in embrittlement of the grain boundaries. The phosphorus of our copper content is very low, so electrical conductivity is comparable to the best performing materials. C1100 is an oxygen-containing copper which has a very high electrical and thermal conductivity. It has excellent forming properties. Due to its oxygen content soldering and welding properties are limited. Chemical composition of Cu ETP is listed in table 2. [15-18].

Table 1. Chemical composition of Cu ETP

Cu	O	Bi	Pb
Balance	≤0.04	≤0.0005	≤0.005

Set up the DOE

Different values for each design variable are selected to cover wide range of welding conditions. Three parameters were selected for Design of experiment and put on three different levels that are continuosly adjustable. These parameter combinations were choosen to maintain a heat imput range between 60-110 J/mm^2. The offset in the table indicates, that focused laser beam was moved to copper, stays on the edge between materials or to stainless steel.

Table 3. Examined parameters with values

Power [W]	Velocity [mm/s]	Offset [mm]
1800	20	-0.15
2000	25	0
2200	30	0.15

Welding was performed with Trudisk 4002 disk laser with wavelength of 1030 nm. As shielding gas was used argon and material thickness was 1 mm. During laser beam welding with focusation to copper was laser beam not focused directly from topside. but because of reflection. small angle of 4° was used for safety reasons.

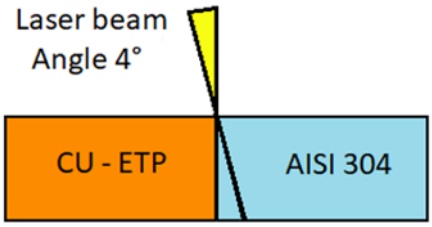

Fig 1. Illustration of laser beam deflection

Results

There are 27 possible parameter combinations fore the experiment design that can be created using the parameters in table 3.

Table 4. Combinations of welding parameters with measured respose

Sample No.	Power [W]	Velocity [mm/s]	Offset (-copper; +SS) [mm]	Ultimate Stress [MPa]
1	1800	20	-0.15	244.00
2	1800	25	-0.15	245.67
3	1800	30	-0.15	263.00
4	1800	20	0	240.67
5	1800	25	0	250.33
6	1800	30	0	198.73
7	1800	20	0.15	99..63
8	1800	25	0.15	91.03
9	1800	30	0.15	224.8
10	2000	20	-0.15	245.00
11	2000	25	-0.15	243.33
12	2000	30	-0.15	246.67
13	2000	20	0	254.00
14	2000	25	0	243.33
15	2000	30	0	222.67
16	2000	20	0.15	171.00
17	2000	25	0.15	144.33
18	2000	30	0.15	177.67
19	2200	20	-0.15	241.67
20	2200	25	-0.15	242.67
21	2200	30	-0.15	243.00
22	2200	20	0	244.33
23	2200	25	0	245.00
24	2200	30	0	243.67

25	2200	20	0.15	221.67
26	2200	25	0.15	200.33
27	2200	30	0.15	152.67

Table 4. displays also collum with ultimate stress. This value is measured response from DOE. It was achieved after combination of welding parameters and subsequent cutting 3 samples from same weld, performed tensile strenght test and by averaging these values. Test sample dimensions are in figure 2.

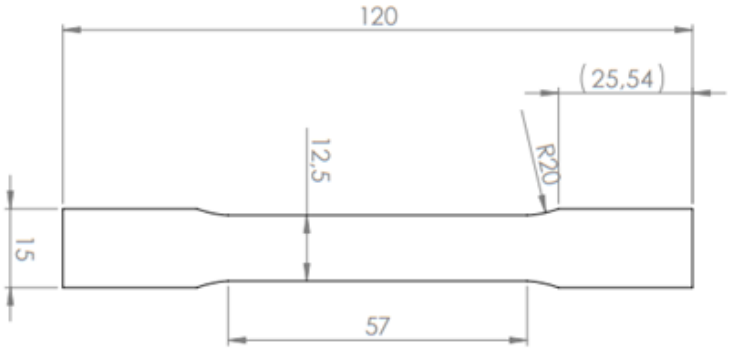

Fig 2. Schematic of the sample used for measuring ultimate strength

Analysis of Variance

ANOVA was used to determine the statistical significance of the parameters based on DOE. Table 5. has F and P values that are of importance. The bigger is F-value and the smaller is P-value means, that the null hypothesis is discredited and it is possible to assert, that there is a general relationship between the response and predictors. If there will be small F-value and big P-value in ANOVA, it will suggest there is no associations.

Table 5. Analysis of Variance

Source	DF	Adj SS	Adj MS	F-Value	P-Value
Power	2	1717.9	859.0	0.57	0.575
Velocity	2	126.1	63.1	0.04	0.959
Offset	2	23014.7	11507.4	7.62	0.003
Error	20	30196.1	1509.8		
Total	26	55054.9			

Dependency graphs illustrating how parameters affect the measured response should be made based on table 5. It can be shown by graphs and the ANOVA, that offset had the most impact, subsequently power and velocity is last.

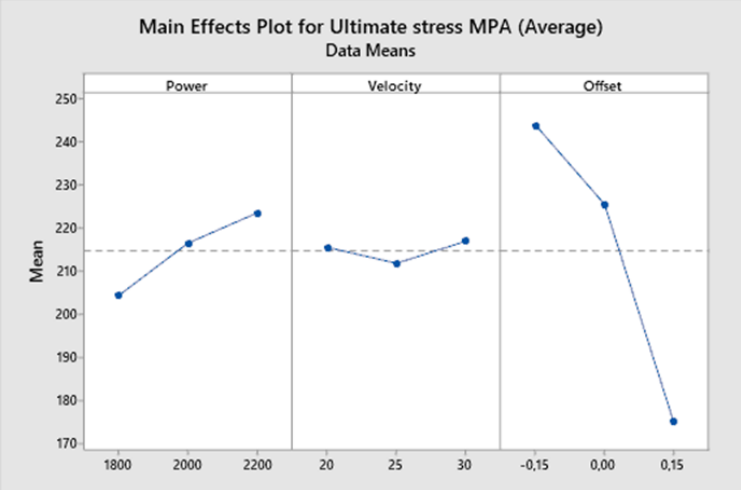

Fig 3. Main effects plot for ultimate stress

From results can be created general regression equation 1. Regression equation is the algebraic expression of the regression lines. It is used to predict the values of the dependent variable from the given values of independent variables. Based on knowledge, that there are 3 parameters on 3 levels, general equation is displayed as equation number 1.

$$R_m = d + x_1 * A_1 + x_2 * A_2 + x_3 * A_3 + y_1 * B_1 + y_2 * B_2 + y_3 * B_3 + z_1 ** C_1 + z_2 * C_2 + z_3 * C_3 \quad (1)$$

Where:

R_m	– ultimate stress	[MPa]
d	– constant	[-]
$x_1;x_2;x_3$	– influence of 1st parameter	[-]
$y_1;y_2;y_3$	– influence of 2nd parameter	[-]
$z_1;z_2;z_3$	– influence of 3rd parameter	[-]
$A_1;A_2;A_3$	– level of parameter 1	[W]
$B_1;B_2;B_3$	– level of parameter 2	[mm*s^{-1}]
$C_1;C_2;C_3$	– level of parameter 3	[mm]

Based on general regression equation and results from ANOVA is possible to create specific equation (2), which includes values for influence of chosen parameters.

$$R_m = 214.72 - 10.5 * \text{Power}_{1800} + 1.7 * \text{Power}_{2000} + 8.8 * \text{Power}_{2200} + \\ +0.8 * \text{Velocity}_{20} + 2.9 * \text{Velocity}_{25} + 2.2 * \text{Velocity}_{30} + +29.2 * \\ * \text{Offset}_{-0.15} + 10.7 * \text{Offset}_{0.00} - 39.92 * \text{Offset}_{0.15} \quad (2)$$

This regression equation is more accurate but impractical for standard use, because it also takes into account combinations of paramteres with a very low influence on the resulting measured response. For subsequent adjustment and simplification. it is advisable to use the backward regression method. Since it would be appropriate to keep all parameters in the regression equation, the alpha statistical significance level should be set to such a level, that also the welding speed parameter has an influence. For this purpose Pareto Chart of Standardized Effects is used.

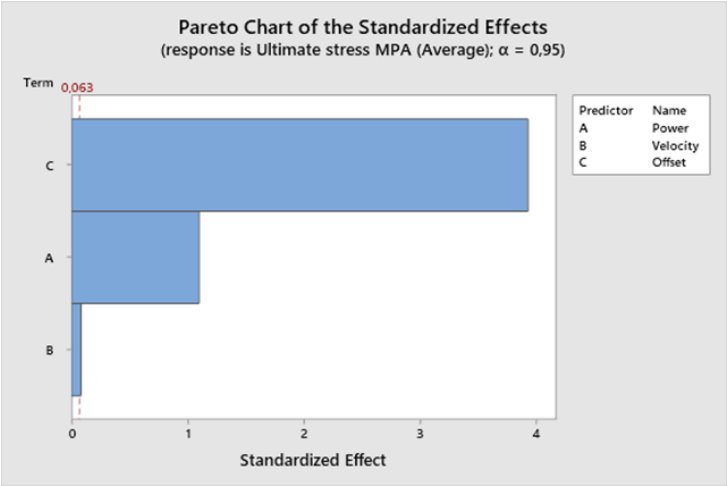

Fig 4. Pareto Chart of Standardized Effects

From Pareto chart in figure 4 can be determined that everything over 6.3% statistical significance could not be removed. Based on this knowledge, it is possible to eliminate everything below 5% statistical significance. In equation 2 was applied backward elimination of terms with α to remove 0.95. Result of general equation after backward elimination is listed as number 3.

$$R_m = d + x * A + y * B + z * C \quad (3)$$

Where:

R_m	– ultimate stress	[MPa]
d	– constant	[-]
x	– influence of 1st parameter	[-]
y	– influence of 2nd parameter	[-]
z	– influence of 3rd parameter	[-]
A	– level of parameter 1	[W]
B	– level of parameter 2	[mm*s^{-1}]
C	– level of parameter 3	[mm]

Equation 3 was supplemented with values representing corrected influence on result.

$$R_m = 114.6 + 0.0483 * \text{Power} + 0.14 * \text{Velocity} - 230.2 * \text{Offset} \quad (4)$$

After backward elimination final regression equation can predict ultimate stress value on intervals given with 60.95% accuracy. This accuracy is lowered by combinations of parameters where weld was weaker than material it joins together. Part of the results are contour graphs in the figure 5 which shows influence of parameters on response.

From contour graphs in figure 5 can be observed, where the highest value of ultimate stress was measured. When the laser beam was focused to copper, it melts him and by the high thermal conductivity it melts also stainless steel.

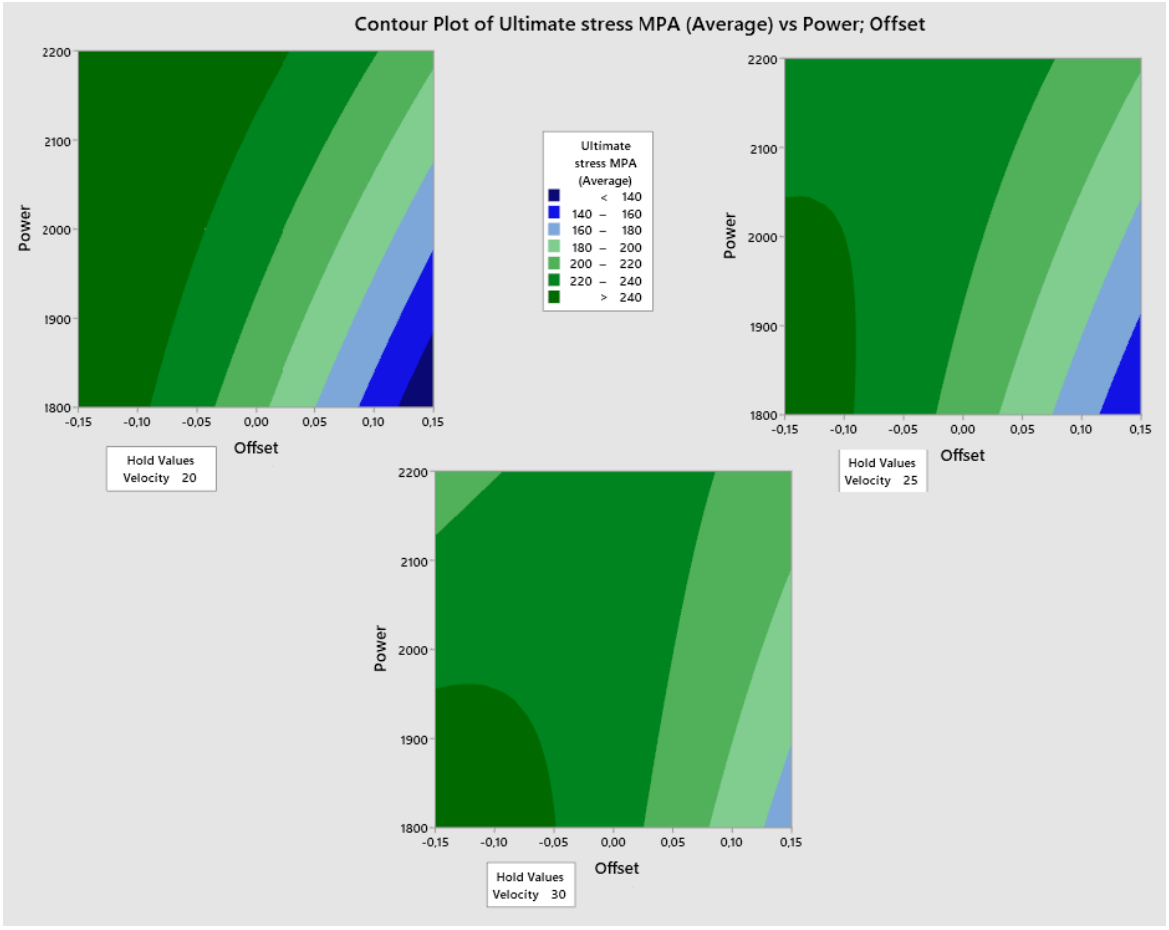

***Fig 5**. Contour graphs for ultimate stress*

3 DISCUSSION

The research paper's findings demonstrated the need to eliminate exceptionally low values, indicating that the weld was subpar and overly affected the regression equation which was created. Also is necessary to design it so that the final projection is valid throughout the whole range of values. There was an attempt to solve it by measuring several tensile strength tests, so severe responses could be partially eliminated. It would most likely be beneficial to look into how heat input affects the strength limit and attempt to modify the welding conditions accordingly. Although the experiment would be more complicated, the results might be more accurate.

4 CONCLUSION

This study investigated possibilities of prediction of ultimate strength based on the design of experiment by using Taguchi method. The results obtained from the experimental tests provide an objective picture of the behavior of different base materials under the influence of the laser beam. Thermal conductivity and specific heat have a significant effect on the results of ultimate stress test. Based on it is possible to optimize welding parameters, welding conditions and predict response parameters with significant level of accuracy.

ACKNOWLEDGEMENT

The research was carried out under the support by the Vedecká grantová agentúra VEGA grant agency of the Ministry of Education. Science. Research and Sport of the Slovak Republic, project No. 1/0499/21 and by the Slovak Research and Development Agency under the contract No. APVV-18-0116.

REFERENCES

[1] X. Zhang. T. Pan. A. Flood. Y. Chen. Y. Zhang. and F. Liou. “Investigation of copper/stainless steel multi-metallic materials fabricated by laser metal deposition.” Mater. Sci. Eng. A. vol. 811. 2021. doi: 10.1016/j.msea.2021.141071.

[2] A. Sadeghian and N. Iqbal. “A review on dissimilar laser welding of steel-copper. steel-aluminum. aluminum-copper. and steel-nickel for electric vehicle battery manufacturing.” Optics and Laser Technology. vol. 146. 2022. doi: 10.1016/j.optlastec.2021.107595.

[3] S. G. Kang and J. Shin. “Laser beam oscillation welding of aluminum alloy using the spatially modulated beam by diffractive optical element (DOE).” J. Manuf. Process.. vol. 66. 2021. doi: 10.1016/j.jmapro.2021.04.029.10.1016/j.procir.2022.08.125.

[4] B. Acherjee. A. S. Kuar. S. Mitra. and D. Misra. “Modeling of laser transmission contour welding process using FEA and DoE.” Opt. Laser Technol.. vol. 44. no. 5. 2012. doi: 10.1016/j.optlastec.2011.12.049.

[5] A. Ascari. E. P. Zapico. V. Dimatteo. and A. Fortunato. “Dissimilar laser welding of copper and stainless-steel thin sheets for e-mobility applications.” in Procedia CIRP. 2022. vol. 111. doi:

[6] L. Hijazi. E. Kaiser. and S. Altarazi. “Pulsed green laser welding of copper materials: A statistical-based methodology for parameters setting.” in Procedia Manufacturing. 2020. vol. 51. doi: 10.1016/j.promfg.2020.10.125.

[7] S. Nisar. A. Noor. A. Shah. U. Siddiqui. and S. Zia Khan. “Optimization of process

parameters for laser welding of A5083 aluminium alloy.” Opt. Laser Technol.. vol. 163. 2023. doi: 10.1016/j.optlastec.2023.109435.

[8] D. Yang. X. Li. D. He. Z. Nie. and H. Huang. “Optimization of weld bead geometry in laser welding with filler wire process using Taguchi’s approach.” Opt. Laser Technol.. vol. 44. no. 7. 2012. doi: 10.1016/j.optlastec.2012.03.033.

[9] Agrawal H. Sharma P. Tiwari P. Taiwade R v.. Dayal RK. Evaluation of Self-Healing Behaviour of AISI 304 Stainless Steel. Transactions of the Indian Institute of Metals. 2015;68(4). doi:10.1007/s12666-014-0467-7

[10] Mascaraque-Ramirez C. Franco P. Experimental Study of Surface Finish during Electro-Discharge Machining of Stainless Steel. In: Procedia Engineering. Vol 132. ; 2015. doi:10.1016/j.proeng.2015.12.547

[11] H. C. Chen. G. Bi. M. L. S. Nai. and J. Wei. “Enhanced welding efficiency in laser welding of highly reflective pure copper.” J. Mater. Process. Technol.. vol. 216. 2015. doi: 10.1016/j.jmatprotec.2014.09.020.

[12] N. N. Khobragade. M. I. Khan. and A. P. Patil. “Corrosion behaviour of chrome-manganese austenitic stainless steels and AISI 304 stainless steel in chloride environment.” Trans. Indian Inst. Met.. vol. 67. no. 2. 2014. doi: 10.1007/s12666-013-0345-8.

[13] T. Balusamy. S. Kumar. and T. S. N. Sankara Narayanan. “Electrochemical behaviour of surface modified AISI 304 grade stainless steel in ringer’s solution.” Trans. Indian Inst. Met.. vol. 64. no. 4–5. 2011. doi: 10.1007/s12666-011-0076-7.

[14] G. Chandrasekar. C. Kailasanathan. D. K. Verma. and K. Nandagopal. “Optimization of Welding Parameters. Influence of Activating Flux and Investigation on the Mechanical and Metallurgical Properties of Activated TIG Weldments of AISI 316 L Stainless Steel.” Trans. Indian Inst. Met.. vol. 70. no. 3. 2017. doi: 10.1007/s12666-017-1046-5.

[15] European copper institute. “Properties of Cu-ETP.” 2012. .

[16] Tadeusz Antoni Knych. Beata Smyrak. and Monika Walkowicz. “Selected aspects of evolution properties of oxygen free copper for high-advanced electrotechnical application.” https://www.researchgate.net/publication/267411152_Selected_aspects_of_evolution_properties_of_oxygen_free_copper_for_high-advanced_electrotechnical_application. 2011.

[17] J. Freudenberger and H. Warlimont. “Copper and copper alloys.” in Springer Handbooks. 2018.

[18] P. Segl’a. D. Miklos. and Milan Melnik. Structures. Physico-chemical Properties and Biological Activities of Copper II Pyridinecarboxylates. 10th ed. 2007.

MECHANICAL AND TECHNOLOGICAL PROPERTIES OF COMPOSITE PIPE

Ing. Martin Bilka[1]
Ing. Miroslav Polášek[2]
Assoc. prof. Ing. Michal Krbaťa, PhD.[3]
[1]ORCID: 0009-0009-9673-3754, Alexander Dubček University of Trenčín, Faculty of Special Technology, Department of Mechanical Technologies and Materials, Ku Kyselke 469, 911 06 Trenčín, **Slovakia**
[2]ORCID: 0000-0003-3662-7641, Alexander Dubček University of Trenčín, Faculty of Special Technology, Department of Mechanical Technologies and Materials, Ku Kyselke 469, 911 06 Trenčín, **Slovakia**
[3]ORCID: 0000-0003-3662-7641, Alexander Dubček University of Trenčín, Faculty of Special Technology, Department of Mechanical Technologies and Materials, Ku Kyselke 469, 911 06 Trenčín, **Slovakia**

Abstract
The goal of the production of the semi-finished product is to ensure resistance to high-temperature corrosion and at the same time it must meet the conditions of heat resistance. Corrosion resistance will be ensured by a protective layer consisting of AISI 347H, the heat resistance of the semi-finished product will be supported by a layer composed of 11CrMo9-10.

Key words: high-temperature corrosion, heat resistance, heat-resistant semi-finished product, spraying, intermediate material layer

1 INTRODUCTION

Refractory materials of low- and high-alloy CrMo steels in combustion chambers do not meet the requirements for increasing the thermal load of the evaporator, and in chambers designed for biomass combustion, they do not meet the conditions of corrosion resistance. The thermal energy of the future requires the application of innovative materials, the properties of which exceed the parameters of the materials used so far in evaporators. Development with the use of unique methods of technological processing and their experimental investigation will improve the properties of common materials, respectively, it

will make it possible to obtain new materials. An alternative is also the composition of materials, where by summarizing the complex properties of individual components, we obtain a completely new final product with properties derived from its components. In this area we can include composite materials and functionally graded materials (FGM).

2 PRODUCTION OF COMPOSITE SEMI-FINISHED PRODUCT

The goal of the production of the semi-finished product is to ensure resistance to high-temperature corrosion and at the same time it must meet the conditions of heat resistance. Corrosion resistance will be ensured by a protective layer consisting of AISI 347H, the heat resistance of the semi-finished product will be supported by a layer composed of 11CrMo9-10.

Preparation of semi-finished products by gravity casting technology

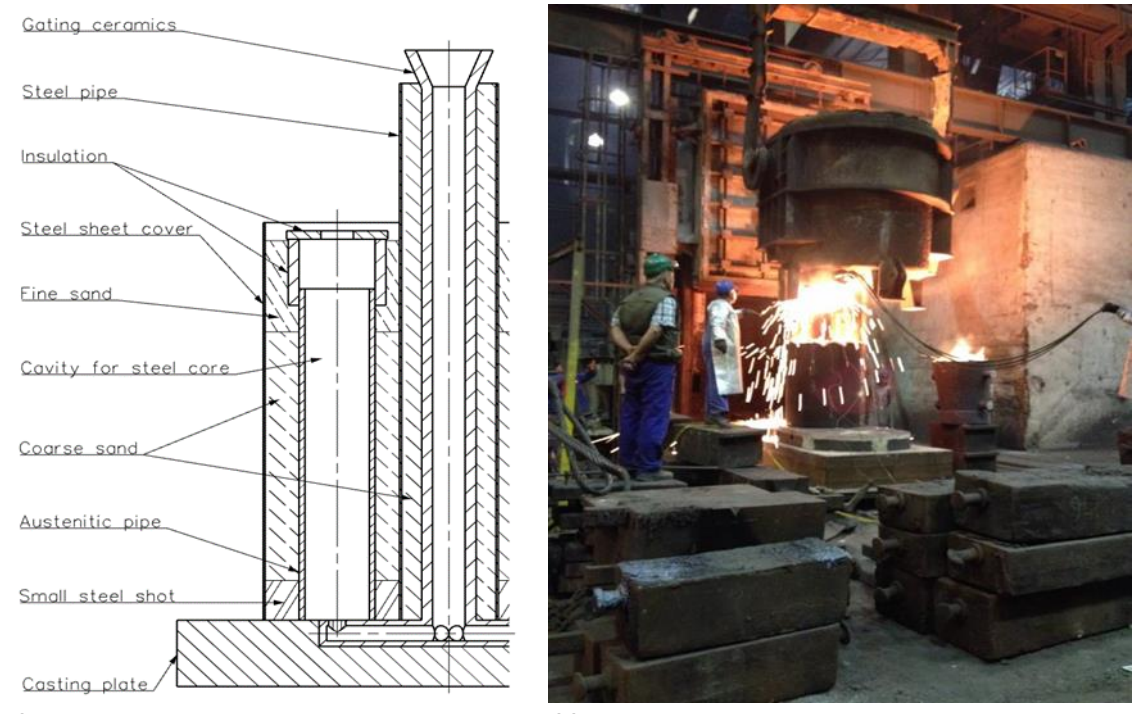

a) b)

Fig.1 Semi-finished 347H preparation: a) forming, b) casting CrMo

Processing of ingots: Hot rolling (Fig. 2), the resulting product is a tube with an outer diameter of ø38 [mm] and a wall thickness of 5 [mm], made of steel with the designation 11CrMo9-10 (core) 347H (sheath). The pipes were delivered in a condition after tempering according to EN 10216-2. Dimensional accuracy requirements in accordance with EN 10216-5:2013 and EN 10216-2:2002.

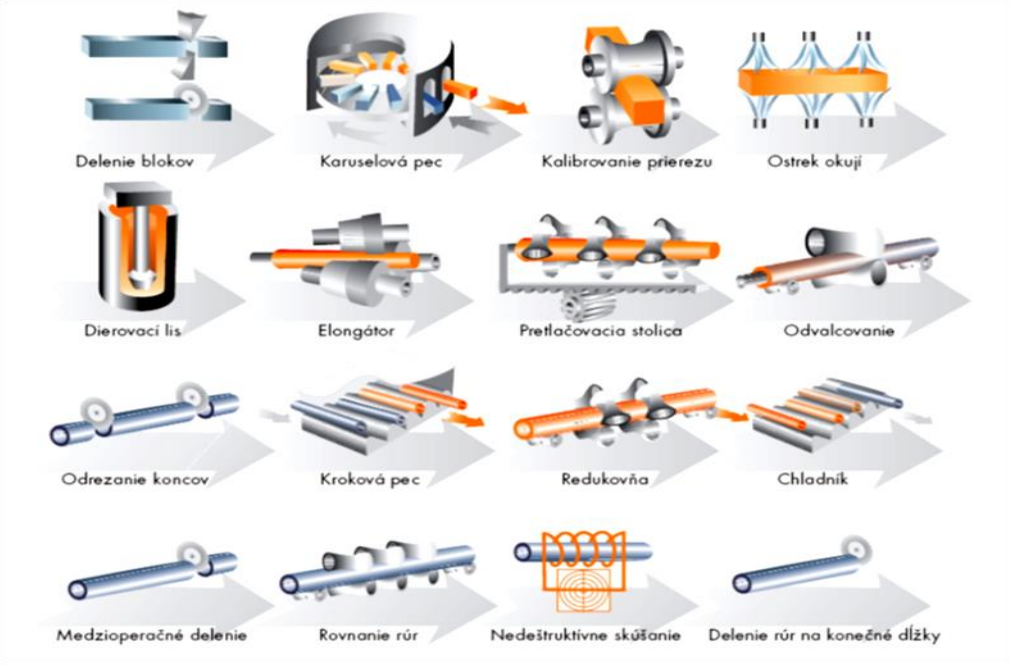

Fig. 2 Heat treatment process from ingot to product

The structure of the semi-finished product

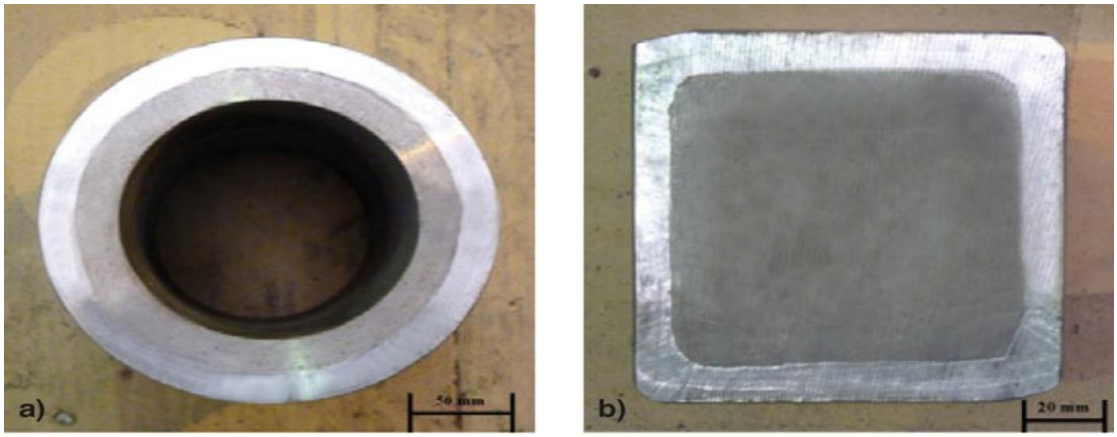

Fig. 3 a) After casting, b) After casting and subsequent reworking

3 COMPOSITE PIPE MECHANICAL AND TECHNOLOGICAL PROPERTIES

The following destructive tests were performed on a composite pipe with functionally graded material properties in cross section (austenitic outer shell AISI 347H (X7CrNiNb18-10), ferritic refractory core 11CrMo9-10) to determine mechanical and technological properties: measurement of shell thickness, chemical analysis, test tensile at 20 [°C] and at elevated temperatures of 450 [°C], metallographic analysis.

Microstructural analysis of the product cross section. Through the analysis, a deformed austenitic structure of the outer wall of the tube (347H) was observed on the longitudinal and transverse sections. The microstructure of the inner wall (11CrMo9 10) is formed by ferrite and bainite with a grain size of 8 and smaller. (Fig. 4).

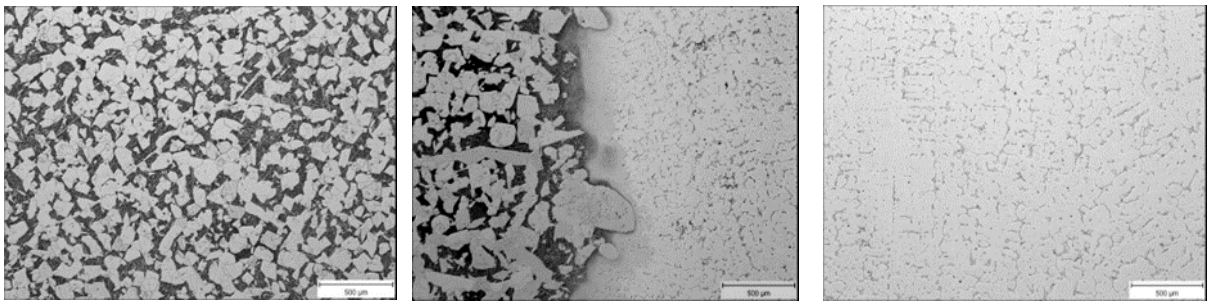

microstructure 11CrMo9 10 interface microstructure microstructure 347H

Fig. 4 The microstructure of the inner wall (11CrMo9 10) formed by ferrite and bainite with a grain size of 8 and smaller.

The thickness of the outer wall of the pipe with the length of the measurement at distances of one meter. The measurement distance was approximately 30 [mm], the measurement interval was every 60° along the pipe circumference. Values of austenitic layer thickness ranging from 0.6 to 1 [mm] were recorded. The chart documents; a) developed surface, b) measured values around the perimeter (Fig. 5).

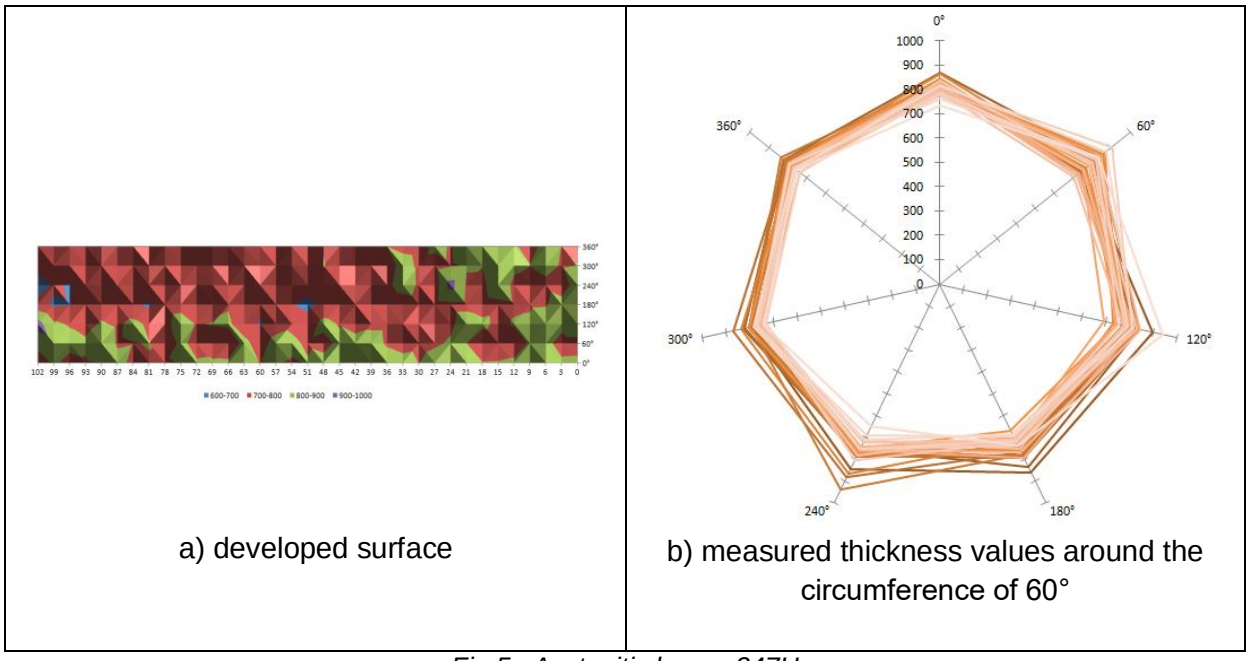

a) developed surface

b) measured thickness values around the circumference of 60°

Fig.5 Austenitic layer 347H

Material analysis of a composite pipe using an optical spectrometer - BELEC Compact port (Tab. 1).

Tab. 1 Material analysis of austenitic ferritic tube

materiál		C	Si	Mn	P	S		Cr	Ni	Nb	N
347H	produkt	0,074	0,43	1,56	0,025	<0,002		17,4	11,5	0,58	-
(obal)	odliatok	0,06	0,47	1,47	0,022	0,007		17,95	11,20	0,57	0,0118
11CrMo9		C	Si	Mn	P	S	Cr	Mo	Ni	Al	Cu
10	produkt	0,106	0,22	0,63	0,010	<0,002	2,29	0,83	0,21	0,006	0,11
(jadro)	odliatok	0,10	0,21	0,59	0,007	0,001	2,25	0,96	0,20	0,006	0,10

Tensile test at room temperature, the test was performed in accordance with STN EN ISO 6892-1: 2010 (Tab. 2). Tensile test at an elevated temperature of 450 [°C] (Tab. 3). The tests were performed at a temperature of 450 [°C] in accordance with STN EN ISO 6892-1: 2010, STN EN ISO 6892-2: 2011. The mechanical properties at room temperature of the oven as well as the mechanical properties at a temperature of 450 [°C] are in compliance with the requirements of the standards.

Tab. 2 The resulting values of the tensile test at room temperature

Steel	EN	Tensile test			
		$R_{p0,2}$ wall thickness Tmin. [MPa]	R_m [MPa]	A_{min}*[%]	
		T<16		l	t
11CrMo9-10 (core)	1.7383	355	540-680	20	18
347H (cover)	1.4912	345	510-710	40	30
Composite core 347H cover 11CrMo9-10		491	648	61	20

Tab. 3 The resulting values of the tensile test at elevated temperature 450[°C]

Steel	EN	Tensile test by temperature 450[°C]
		Minimum yield strength Rp0,2 [MPa]
11CrMo9-10 (core)	1.7383	257
347H (cover)	1.4912	283
Composite core 347H cover 11CrMo9-10		443

Metallographic analysis of the microstructure and macro were performed using an OLYMPUS 51GX optical microscope. The samples were prepared for analysis in longitudinal and transverse sections. Before analysis, the samples were ground and polished. The microstructure of the refractory matrix of the 11CrMo9-10 tube consists of ferrite and bainite, at the interface there is an austenite - ferritic region of decarburization (diameter 297 [µm]). The depth of decarburization (Fig. 7) was also confirmed by the Vickers hardness test (Fig. 6).

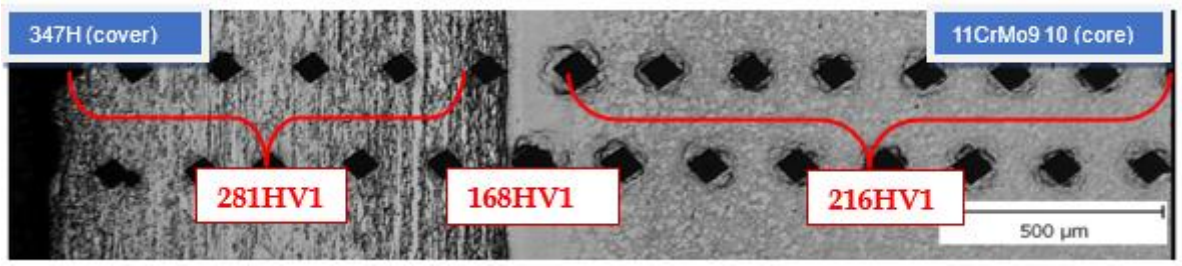

Fig.6 Measured hardness of both materials Vickers HV1

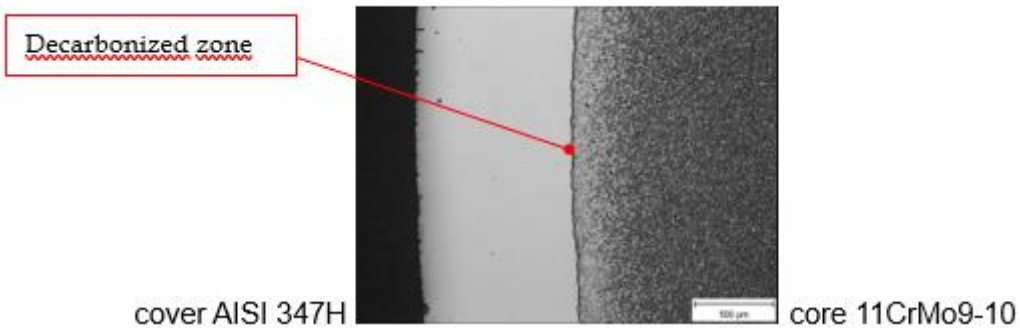

Fig. 7 The depth of decarburization

4 COMPOSITES AND FUNCTIONAL GRADED MATERIALS

A composite is a heterogeneous material that consists of two or more combinations of components that are at the macroscopic level. The components of the composite have a different chemical composition or different physical properties. The main material is called the matrix (reinforcement), to which a reinforcing composite component (reinforcement) is added (Fig. 8).

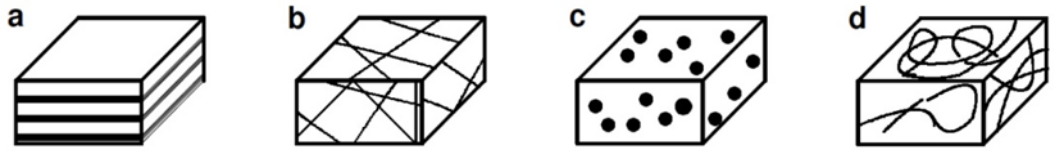

Fig. 8 Examples of composite materials a) layered structures, b) with an irregular structure c) reinforcing particles, d) continuous fiber reinforcement, (MURÍN, J., KUTIŠ, 2008)

We encounter composite as such in everyday life in combinations that can be divided into: Unnatural: the matrix material is generally continuous. An example is concrete reinforced with steel profiles or carbon fiber reinforced epoxy. Natural: wood where the lignin matrix (lianin) is reinforced by cellulose fibers, or bones in which calcium plates strengthen the soft collagen. Advanced: these composites have a high reinforcement performance, with the fibers having a thin diameter in a matrix that is reinforced from e.g. kevlar + epoxy matrix, boron + aluminum.

Composites with metal matrices, aluminum, magnesium, titanium (matrix), carbon, silicon carbide (fiber) by adding fibers to the metal matrix increases elastic stiffness and strength. It increases the coefficient of thermal expansion and electrical conductivity.

The production of this type of composites is dependent on diffusion bonding. With a suitable material combination, composites with metal matrices are widely used in space shuttles

(aluminum tubes reinforced with boron fibers), the military (aluminum matrices with silicon carbides), superheater systems for burning biomass. steel 347H.

Mixing rule for composite densities

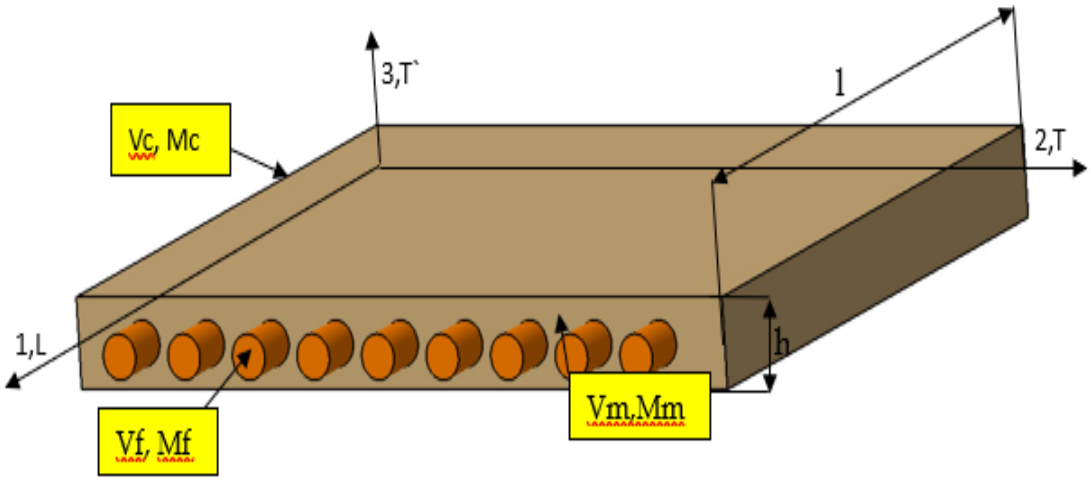

Fig. 9 Geometric calculation model of two-fiber composite

The coordinates L,T,T` represent the main material axes, 1,2,3 correspond to the main orthotropic axes (Fig. 9). The following calculation relations apply for an ideal void-free composite.

Vf is the total volume of fibers or of the strengthening phase, *Vm* is the total volume of the matrix, *Vc* is the total volume of the sample. We determine the mass fractions of fibers *Mf* and matrix Mm according to the following relations:

$$v_f = \frac{V_f}{V_c}$$

$$v_m = \frac{V_m}{V_c}$$

$$m_f = \frac{M_f}{M_c}$$

$$m_m = \frac{M_m}{M_c}$$

Conditions for conservation of volume and mass.

$$V_c = V_f + V_m = \frac{\sum_i V_i}{V_c}$$

$$1 = \frac{V_f}{V_c} + \frac{V_m}{V_c} = v_f + v_m = \sum_i v_i$$

$$M_c = M_f + M_m = m_f + m_m = \sum_i m_i$$

$$1 = \frac{M_f}{M_c} + \frac{M_m}{M_c} = m_f + m_m = \sum_i m_i$$

Relationships for volume and mass fractions through densityρ.

$$m_f = \frac{M_f}{M_c} = \frac{\rho_f V_f}{\rho_c V_c} = \frac{\rho_f}{\rho_c} v_f$$

$$m_m = \frac{M_m}{M_c} = \frac{\rho_m V_m}{\rho_c V_c} = \frac{\rho_m}{\rho_c} v_m$$

The relation for the density of the composite ρ_c, which is based on the total weight of the composite:

$$M_c = M_f + M_m$$

$$\rho_c V_C = \rho_f V_f + \frac{\rho_m V_m}{V_c}$$

$$\rho_c = \rho_f v_f + \rho_m v_m = \sum_i \rho_i v_i$$

The equations I mentioned are called the mixing rule for determining the density of the composite ρ_c.

The density of the composite ρ_c we also get using the previous relations as follows:

$$1 = v_f + v_m = \frac{\rho_c}{\rho_f} m_f + \frac{\rho_c}{\rho_m} m_m \Rightarrow \rho_c = \frac{1}{\frac{m_f}{\rho_f} + \frac{m_m}{\rho_m}} = \frac{1}{\sum_i \frac{m_i}{\rho_i}}$$

5 CONCLUSION

Functionally graded materials (FGM) appear as a new concept of composites, they are materials with spatially continuous variability of microstructures, variable mechanical and physical properties at different points of the material (MURÍN, J. et al. Multiphysics, 2010). The difference in their physical properties is due to the production process or technological processing. The field of material engineering (FGM) was established in 1984 in Japan (MURÍN, J., KUTIŠ, V. Thermo-elastic, 2006). Professional literature and scientific articles in which space is devoted to innovative methods and procedures, especially FGM simulations with structural systems and with a focus on classical structural analysis of shells (MURÍN, J., KUTIŠ, V. Electro-thermo-structural analysis ,2008), beams (MURÍN, J. et al. An effective multiphysical ,2008), planar elements (MURÍN, J., KUTIŠ, V. Electro-thermo-structural ,2008) and thermoelastic analysis. Publications with the application of numerical procedures (MURÍN, J. et al. An effective multiphysical ,2008), a combination of numerical and analytical methods, exclusively analytical methods [22].
In Slovakia, Prof. Murín and the team from the Institute of Applied Mechanics and Mechatronics, ÚEAE, Faculty of Electrical Engineering and Informatics, STU in Bratislava.

REFERENCES

MURÍN, J., KUTIŠ, V. Stability of a composite beam-column with transversal and longitudinal variation of material properties. In: Proceedings of the Ninth International Conference on Computational Structures Technology. Athens. September 2008. ISBN 978-1-905088-23-2

MURÍN, J. et al. Multiphysics analysis of a functionally graded material conductor with spatial variation of material properties. In: Proceedings of the Tenth International Conference on Computational Structures Technology. Valencia. September 2010. ISBN 978-1-905088-37-9

MURÍN, J., KUTIŠ, V. Thermo-elastic stress calculation in multilayered FGM sandwich beams. In: 70 rokov SvF STU. Bratislava. December 2008. ISBN 978-80-227- 2979-6

MURÍN, J., KUTIŠ, V. Electro-thermo-structural analysis of the multilayered sandwich bars. In: Acta Mechanica Slovaca. October 2008. Vol. 12. No. 3 p. 587-600. ISSN 1335-2393

MURÍN, J. et al. An effective multiphysical functionally graded material beam-link finite element with transversal sy[mm]etric and longitudinal continuous variation of material properties. In: Proceedings of the Ninth International Conference on Computational Structures Technology. Athens. September 2008. ISBN 978-1-905088-23-2

MURÍN, J., KUTIŠ, V. Electro-thermo-structural analysis of the multilayered sandwich bars. In: Acta Mechanica Slovaca. October 2008. Vol. 12. No. 3 p. 587-600. ISSN 1335-2393

MURÍN, J. et al. An effective multiphysical functionally graded material beam-link finite element with transversal sy[mm]etric and longitudinal continuous variation of material

properties. In: Proceedings of the Ninth International Conference on Computational Structures Technology. Athens. September 2008. ISBN 978-1-905088-23-2

URÍN, J., KUTIŠ, V. Electro-thermo-structural analysis of the multilayered sandwich bars. In: Acta Mechanica Slovaca. October 2008. Vol. 12. No. 3 p. 587-600. ISSN 1335-2393

MURÍN, J. et al. An effective multiphysical functionally graded material beam-link finite element with transversal symetric and longitudinal continuous variation of material properties. In: Proceedings of the Ninth International Conference on Computational Structures Technology. Athens. September 2008. ISBN 978-1-905088-23-2

MATERIAL DEGRADATION IN THE HEAT-AFFECTED ZONE WHEN WELDING HIGH-STRENGTH STEEL HARDOX 500 AND ASUTENITE STEEL 08CH18N10T

Ing. Jiří Macháček[1]
Assoc. prof. Ing. Marta Kianicová, PhD.[2]
Ing. Ingrid Kovaříková, PhD.[3]
[1]ORCID: Alexander Dubček University of Trenčín, Faculty of Special Technology, **Slovakia**
[2]ORCID: 0000-0001-9083-9552, Alexander Dubček University of Trenčín, Faculty of Special Technology, **Slovakia**
[3]ORCID: 0000-0002-0063-8210, Alexander Dubček University of Trenčín, Faculty of Special Technology, **Slovakia**

Abstract:
The austenitic stainless steel 08Ch18N10T is often used in nuclear power facilities due to its favorable properties. Many parts of the primary circuit of VVER 440 and VVER 1000 of the nuclear powerplants are manufactured of this steel. This material must possess very good resistance corrosion and thermal stability of the structure. The subject of research in the experimental program is the welding of high-strength steel HARDOX 500 and austenite (Stanley) steel 08CH18N10T. These two materials have a different property both in the area of material properties and in the requirements for welding and the design of the weld joint itself. By welding materials with different chemical and mechanical properties, a heterogeneous weld joint is created. When welding a heterogeneous weld joint, a large heat-affected zone is created, and its properties can significantly affect the resulting strength of the entire weld joint.
For this reason, it is important to choose suitable welding conditions and additional material. The result will be designed welded joint on these two different materials, verification of the mechanical properties of the welded joint and the properties of the heat-affected zone by tensile tests, bending impact test, hardness measurements in the heat-affected zone. Based on the results, we will check the method and suitability of welding materials (Jirkova et al., 2020).

Keywords: welding, austenite, high-strength steel, heat-affected zone (HAZ)

1 INTRODUCTION

Heterogeneous weld joints are a general problem in welding. Nuclear power is no exception. Here, however, much more emphasis is placed on the design and quality of the weld joint. As part of the welding of heterogeneous weld joints, the qualification of the welding procedure and verification tests of the weld joint and the heat-affected zone are carried out (Konat et al., 2017).

As part of our research, we will perform a heterogeneous weld joint of high-strength steel HARDOX 500 and austenitic steel 08Ch18N10T. The aim is to verify the weldability of these two steels and then verify the properties of the weld joint. The welding of these two steels will be carried out in order to increase the safety of reactors with the possibility of using high-strength materials and to reduce the costs of welding heterogeneous welds with an increase, or to maintain the requirements for their properties.

Heterogeneous welds are found in every nuclear power plant in the area of the primary ring, namely in the weld joint of the pressure vessel and the primary pipe, then the welded primary pipe and the heat exchanger (steam generator) and the weld lining of the pressure vessel, to increase the corrosion-resistant properties of the pressure vessel. The diagram of the primary circuit of the nuclear power plant is shown in Fig 1.

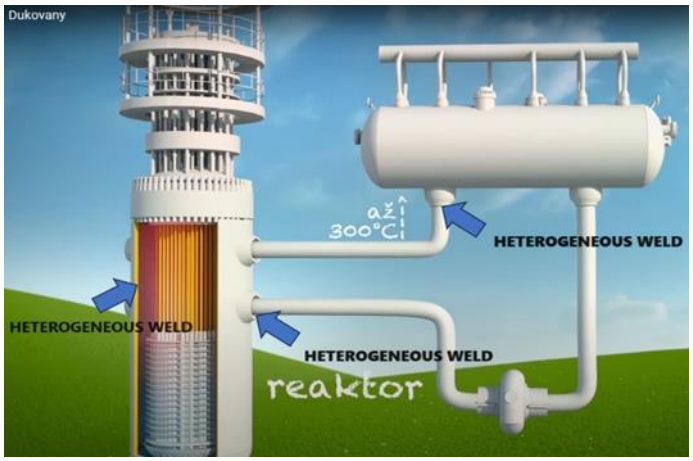

Fig. 1 The primary circuit diagram of a nuclear power plant

2 HEAT-AFFECTED ZONE (HAZ)

In the heat-affected zone, recrystallization and grain growth occur, i.e. strength, hardness and toughness decrease.

The size of the HAZ can be influenced in a suitable way by the welding speed and temperature. The temperature of the welding can be controlled directly with thermometers, or perhaps with thermo chalk. Figure 2 shows a diagram of the heat-affected zone created by welding.

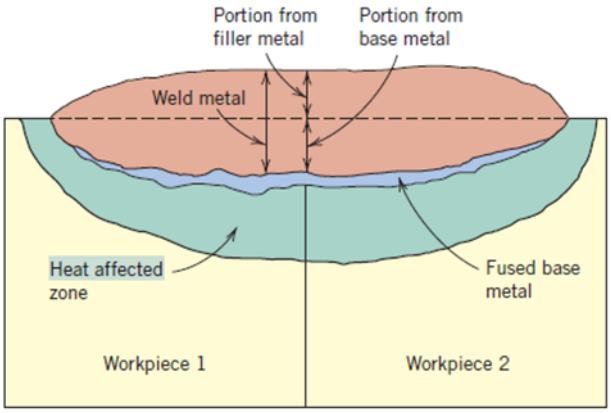

Fig. 2 Diagram of the heat-affected zone created by welding (Callister et al., 2007)

The influence of the size and structure of the HAZ after welding can be influenced by appropriate heat treatment, e.g. normalizing annealing to remove internal stress.

For welding of the heterogeneous weld joints, two basic materials will be used: high-strength steel HARDOX 500 and austenitic steel 08Ch18N10T. The filler welding material will be Inertrod 309L wire with a diameter of 2.4 and 3.2 mm.
TIG welding will be performed with a non-melting tungsten electrode with an inert Argon gas. The diagram of TIG welding is shown in Figure 3 (Shirsat, 2020).

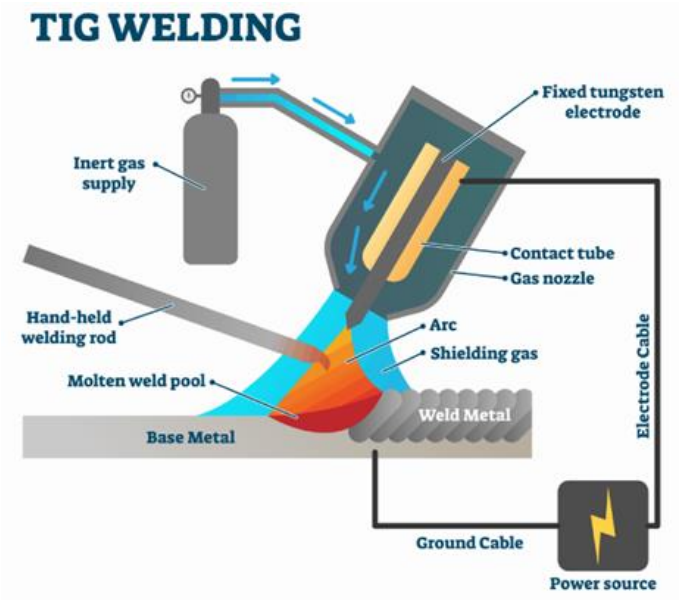

Fig. 3 Scheme of TIG welding (Shirsat, 2020)

3 EXPERIMENTAL MATERIALS AND THEIR PROPERTIES

In the experimental program, we designed basic materials and welding additive material. Basic material will be used high-strength steel and austenitic steel. The welding additive material will be used transition wire Inertrod 309L.

The welding additive material Inertrod 309L is used for heterogeneous weld joints, due to the high content of alloying elements, positively influencing the design of the weld joint and its subsequent mechanical properties. In Table 1, we have a comparison of the chemical composition of individual materials with the designation of elements that are different for individual materials and have a significant effect on their welding (ČSN EN ISO 3834-1, 2022).

Weldability and chemical composition of experimental materials

When creating a heterogeneous welded joint, it is necessary to thoroughly know the properties of individual materials, welding methods and the behavior of individual materials during welding.

Austenite 08Ch18N10T

We chose the steel on the basis of research and use in nuclear energy for its good properties against the chemical regime I.O, where there is a high content of boric acid H3BO3 with a concentration of up to 14% and at the same time it must withstand high temperatures up to 360°C and pressure up to 20MPa (Kudělka et al., 2021). The 08CH18N10T material is welded using the TIG method - Inert gas welding with a non-melting tungsten electrode. The

weldability of austenite 08CH18N10T is conditionally guaranteed, i.e. guarantees weldability in compliance with predetermined conditions specified in the steel quality standard (Weldability of materials – steels., 2015).

High-strength steel – Hardox 500

We designed the high-strength steel Hardox 500 for its excellent mechanical properties especially for forgings. The tensile strength limit for these materials ranges from 600 - 1300 MPa. The high strength will make it possible to reduce the thickness of the walls of the reactor pressure vessel, thereby ensuring or increasing nuclear safety. Reducing the weight of the pressure vessel, which will simplify handling and reduce the economic demands on the material. High-strength materials are welded by laser, plasma, as part of our experiment we will weld with the TIG method using preheating (Weldability of materials – steel., 2015).

Welding additive material – *Inertrod 309L*

Filler wire type ER 309L, for TIG welding of stainless steels with lower and medium strength steels. Ideal for creating intermediate layers before welding with stainless steel and also for welding clad steels with a working temperature of up to 300 °C.

The weld metal contains approximately 12% delta ferrite, which increases its resistance to hot cracking. Contains a low silicon content. The welding wire is designed for use with Ar shielding gas, which ensures a clean and safe welding process.

For a comparison of the chemical composition of individual materials, which affects the execution of the weld itself and subsequently the properties of the weld joint, see table.

Table. 1 Chemical elements affecting welding and weld properties

	C (max.), %	Cr, %	Ni, %
08Ch18N10T	0.150	17-19	8-10
Hardox 500	0.270	max. 1.200	max. 0.250
Inertrod 309L	0.020	24	13

The influence of individual elements on the weld joint:

- Carbon

Materials with a content above 0.25 wt.% must be preheated and heat treated to prevent the formation of cold cracks, i.e. that we will be welding two materials with different welding requirements.

- Chrome

After welding, the chromium content is depleted in the oxide layer by 3 – 5 wt.%, for this reason an additional material with a high chromium content of up to 24 wt. %.

- Nickel

Due to the low Ni content in Hardox 500 material, plasticity and toughness of the weld joint may be lost. For this reason, the additional material Inertrod L309 with a higher nickel content, up to 13 wt.%, will be used.

4 PROPOSAL FOR THE REALIZATION OF A HETEROGENEOUS WELD JOINT

In most cases, the construction of a welded joint consists of three basic parts:

Basic material - Weld metal - Basic material

As part of the designed experiment, heterogeneous weld joints will be created with two welding methods.

The first method uses TIG welding technology to create hardcladding surface with Inertrod 309L filler material on HARDOX 500 high-strength steel, which is subsequently processed by chip machining fig. 4.

Fig. 4 Schematic of the transitional weld joint

Subsequently, a weld joint will be made with 08Ch18N10T steel, where, due to the design of the weld, we are welding materials with similar chemical properties and welding requirements, see fig. 5.

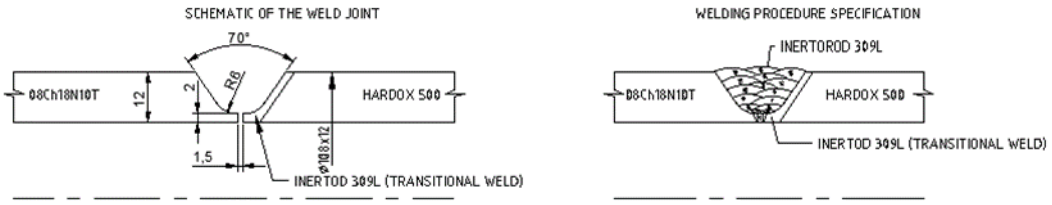

Fig. 5 Schematic of the weld joint

The proposed welding procedure is carried out for reasons of reducing tensile stresses and the formation of cracks in the weld joint. Due to the shrinkage effect in the weld area, the stress in the weld joint is redistributed and a compressive stress is created in the face area. At the same time, compressive or slightly tensile stress is created in the area of the root of the weld.

For welding, the designed additional material Inertrod 309L was used, which after welding achieves sufficient shrinkage values. The additional material Inertrod 309L was evaluated as the most suitable for the combination of materials of the designed heterogeneous weld joint.

The second method of creating a heterogeneous weld joint will be realized without creating a layer. The welding joint of both materials is performed directly with a combination of requirements for welding individual steels fig. 6.

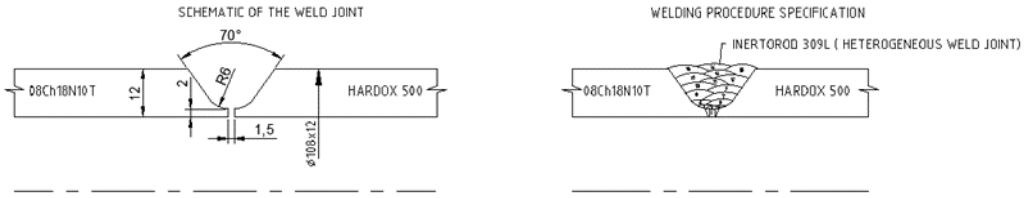

Fig. 6 Schematic of the weld joint without filler materials

In the case of a heterogeneous weld joint, the ferritic material is coated with an filler material with a high content of alloys that are deposited in the welded materials. This ensures at least partial homogeneity of the weld joint itself and the achievement of suitable mechanical properties of the weld.

5 CONCLUSION

The aim of the proposed experiment will be to verify the weldability of austenitic steel 08Ch18N10T and high-strength steel Hardox 500. The created experimental samples will be the subject of investigation structural properties of materials and mechanical properties of welded joints will be evaluated according to the proposed methodology. Verification of the mechanical properties of the welded joint and the properties of the heat-affected zone will by tensile tests, bending impact test and hardness measurements in the heat-affected zone. In case of positive test results, the proposed method using the filler welding material Inertrod 309L will be applied in the production of pressurized water reactors of nuclear power plants. By using them, we will ensure an increase in their safety, an extension of the life of pressure vessels and a reduction of the economic costs of their production.

REFERENCES

Jirková, H., Jand, T., Růžička, J., Mach, J. Effect of holding time at stabilization annealing on properties of 08ch18n10t austenitic stainless steel. METALS 2020 , May 20th - 22nd 2020, Brno, Czech Republic, EU

Konat, L., Bialobrzeska, B., Bialek, P. Effect of Welding Process on Microstructural and Mechanical Characteristics of Hardox 600 Steel. Metals 2017, 7, 349; doi:10.3390/met7090349

Callister, W.D Jr., Retwisch, D., G. Material Science and Engineering. (2007).

Seventh edition. ISBN-13: 978-0-471-73696-7 (cloth)

Shirsat, A., MIG vs TIG - Welding Types, Materials, and Applications - A Guide. Apríl, 2020, Available at: https://www.technoxmachine.com/blog/mig-vs-tig-welding/[Accessed 1 Nov. 2023]

ČSN EN ISO 3834-1 Požadavky na kvalitu při tavném svařování kovových materiálů: Část 1: Kritéria pro volbu odpovídajících požadavků na kvalitu. Květen 2022. Praha: Česká agentura pro standardizaci, 2022

Kudělka, V., Balej, Z., Opletal, J., Myšák, M., Vlhová, N. Korozivzdorné oceli, vlastnosti a rozdělení. Training material TESYDO, s.r.o. 2021, (121), Available at: https://www.cws-anb.cz/docu/texty/0000/000032_121-korozivzdorne-oceli-1.pdf [Accessed 1 Nov. 2023]

Weldability of materials – steels [online]. Mansfield Park: Mansfield Park, 2015, Jan 1, 2015 [cit. 2023-02-01]. Available at: https://welding.org.au/job-knowledge/weldability-materials-steels/[Accessed 4 Nov. 2023]

RESEARCH OF JOINING OF STAINLESS STEEL AND COPPER BY LASER BEAM

Ing. Beáta Šimeková, PhD.[1]
Ing. Kovaříková Ingrid, PhD.[2]
Assoc. prof. Dr. Ing. Pavel Kovačócy[3]
Ing. Martin Hnilica[4]
Ing. Michal Šimek, PhD.[5]

[1]ORCID: 0000-0002-6499-0096, Department of Welding and Joining of Materials, Institute of Production Technologies, Faculty of Materials Science and Technology in Trnava, Slovak University of Technology in Bratislava, **Slovakia**

[2]ORCID: 0000-0002-0063-8210, Department of Engineering Technologies and Materials, Faculty of Special Technology, Alexander Dubček University of Trenčín, **Slovakia**

[3]ORCID: 0000-0002-4377-7659, Department of Welding and Joining of Materials, Institute of Production Technologies, Faculty of Materials Science and Technology in Trnava, Slovak University of Technology in Bratislava, **Slovakia**

[4]ORCID: , Department of Welding and Joining of Materials, Institute of Production Technologies, Faculty of Materials Science and Technology in Trnava, Slovak University of Technology in Bratislava, **Slovakia**

[5]ORCID: 0000-0002-0920-9877, PRVÁ ZVÁRAČSKÁ, a.s, Bratislava, **Slovakia**

Abstract: The aim of the paper is focusing on the brazeability of stainless steel AISI 304 and copper Cu-ETP electrolytically tough pitch dissimilar materials by electron beam. The thickness of base materials was 1 mm. Ticusil eutectic brazing alloy highly active (68,8Ag26,7Cu4,5Ti) in the form of thin foil was used as filler material. Overlapped joints were manufactured using defocused vertical electron beam. The effect of beam current on braze appearance, microstructure, and microhardness of brazed joints was investigated. The scanning electron microscopy indicated the possibility of obtaining defect-free joints. The results show that the binary Ag-Fe equilibrium diagram is expectedly the microstructure even at the moderate cooling and solidification rates expected under the used electron beam brazing conditions and parameters. Beam current is the main brazing parameter influencing the joint quality. Optimum brazing parameters were as follows: beam current 10 mA, brazing speed of 5 mm/s, and 50 passes at constant accelerating voltage (U = 55 kV), focusing current (If = 990 mA) across the upper material length—Cu.

Keywords: brazing, electron beam brazing, brazing alloy, copper, stainless steel

1 INTRODUCTION

The aim of this work was to investigate the brazability of corrosion-resistant steel with copper using an electron beam as a heat source. The advantage of this method is the possibility to solder different materials with different melting temperatures [1-3].

This method is among the progressive methods of joining materials, which can be used in a wide range of industries. In today's modern era, it is mainly the automotive, space and nuclear industries, where it is possible to join together materials that cannot be welded or brazed using conventional methods.

Another very important advantage of this method is the possibility of achieving high-quality and strong joints even in the case of materials with a smaller thickness or in the case of more complex assemblies, especially in the case of joining alloys, when it is necessary that the base material does not deform during joining, or that undesirable fragile structures do not arise [3,4].

Electron beam brazing also brings great challenges in the future, where it is necessary to devote space to research and new knowledge. With growing technical progress, there are constantly new and stricter requirements, whether for the quality and reliability of materials and joints, or their safety of use, or economic efficiency and the very speed of making joints. And of course last but not least, especially nowadays, the lowest possible ecological load and pollution [5-7].

The brazing alloy microstructure (Fig. 1) consists of Cu (dark spots) and Ag+Cu eutectic (light spots). The presence of Ti in the brazing alloy causes the formation of the Ti3Cu4 phase.

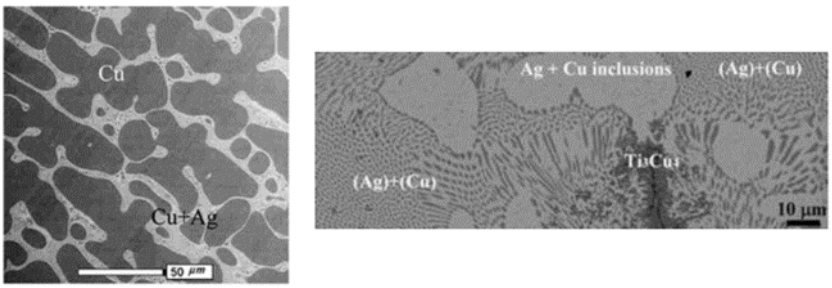

Fig. 1. Microstructure of Ticusil alloy

2 METHODOLOGY OF RESEARCH

Experimental samples of base materials AISI 304 and Cu-ETP were cut to dimensions: length 35 mm, width 15 mm and thickness 1 mm. The additional material was in the form of a foil with a thickness of 0.05 mm and cut into dimensions: length 15 mm and width 5 mm. The samples prepared in this way were placed in the form of a lapped joint, brazing alloy was placed on the bottom material AISI 304 steel and on top the top material copper Cu-ETP.

Subsequently, the samples were placed in a vacuum chamber and fixed on the welding table using clamps, then K-type thermocouples from the lower part of Cu 1 mm from the brazing alloy in the middle part of the sample were attached to the samples. Brazing parameters were adjusted to achieve integral joints. Five joints were made, with an accelerating voltage of 55 kV, a brazing speed of 5 mm/s, and an electron beam focusing current of 990 mA. These parameters remained constant for the production of all samples, while only the brazing current was changed (Tab. 1).

Table 1 Electron beam brazing parameters with Ticusil alloy

Samples	Acceleration voltage U [kV]	Brazing current I_s [mA]	Brazing speed [mm/s]	Number of cycles	Focusing current I_f [mA]	Heat input [J/mm]
1	55	10	5	8	990	110
2	55	11	5	8	990	121
3	55	12	5	8	990	132
4	55	13	5	8	990	143
5	55	14	5	8	990	154

3 RESULTS

The standard setting of the focusing current of the electron beam is 890 mA, while for brazing in this experiment the defocusing current el. beam 990 mA due to a change in the beam track. In this case, the beam footprint was enlarged to a diameter of 5 mm. Next, the movement of the beam along the surface of Cu in the place where the brazing alloy was deposited was set to a length of 15 mm, the beam trace had a diameter of 5 mm. The movement was set to the so-called multipass beam motion, where two beam passes (from one side of the sample to the other and back) formed one cycle. By evaluating the macrostructure of the brazed joints (Fig. 2), it was found that there was no complete flow of brazing alloy into the brazing gap and partial non-melting of the brazing foil, which may be caused by a low brazing current (10mA).

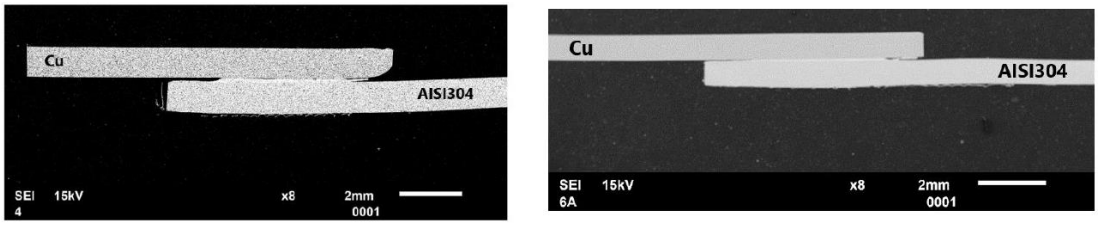

Fig. 2. Macrostructure of the sample produced at a) IS = 10 mA and b) IS = 14 mA

In addition to the set brazing parameters, especially the brazing current of electron beam, but above all the exact positioning of the materials before the actual brazing. All these attributes of the joint affect the mechanical properties, especially the shear strength.
Analysis of the microstructure and the distribution of elements at the interface of the brazed joint were performed by a scanning electron microscope. Brazed joint interface sample no. 1 produced at a brazing current of 10 mA is shown in fig. 3. The analysis found that the joint is intact without visible pores and cracks. Dark grey islands can be observed at the steel/brazing alloy interface. The steel/brazing alloy interface is clearly visible, at 800x magnification it is not possible to observe the formation of an intermetallic phase. There are also no visible cracks in the brazing alloy volume, there is a dendritic structure near the solder/Cu interface. The brazing alloy/Cu interface is indistinct, there are narrow and long islands of dark grey color near the interface.

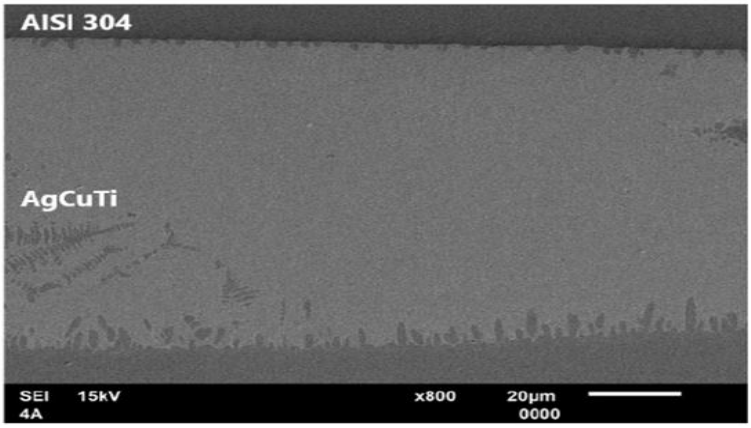

Fig. 3. Microstructure of the sample produced at IS = 10 mA

The distribution of the elements at the brazed joint interface of the sample was determined by performing an area EDX analysis shown in fig. 4.

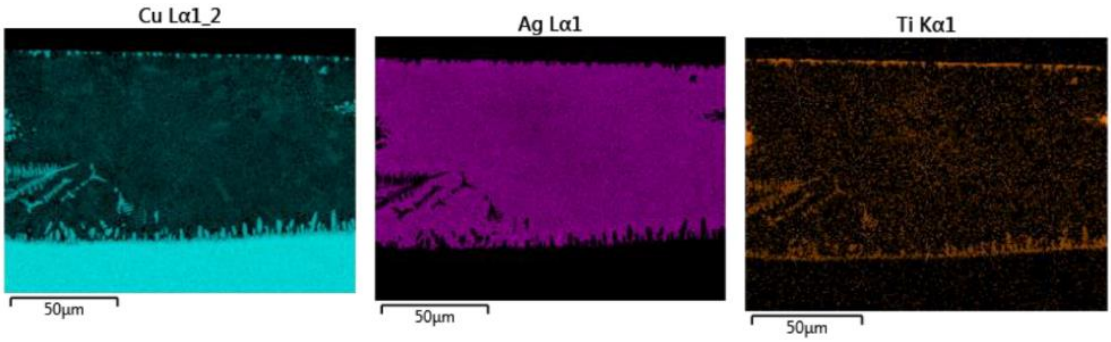

Fig. 4. Area EDX analysis of the sample interface element distribution

Based on the EDX area analysis, it is possible to confirm the formation of a continuous layer at the steel/brazing alloy interface consisting mainly of titanium. The dark gray islands located under the Ti layer are mainly made of Cu with a small amount of Ti. In the brazing alloy volume, it is found mainly with a small amount of Ti and trace elements of Cu. The dendritic structure near the brazing alloy/Cu interface is mainly made of copper with a small amount of Ti. Elongated white and dark grey islands at the brazing alloy/Cu interface contain Cu+Ti. The exact chemical composition of the individual phase can be identified using X-ray diffraction or point EDX analysis. The steel/brazing alloy interface is formed by a distinct continuous phase consisting mainly of Ti. The measurement of the phase thickness was carried out using the ImageJ program, three measurements were performed, while the measurement result was determined to be 1 μm (Fig. 5a).

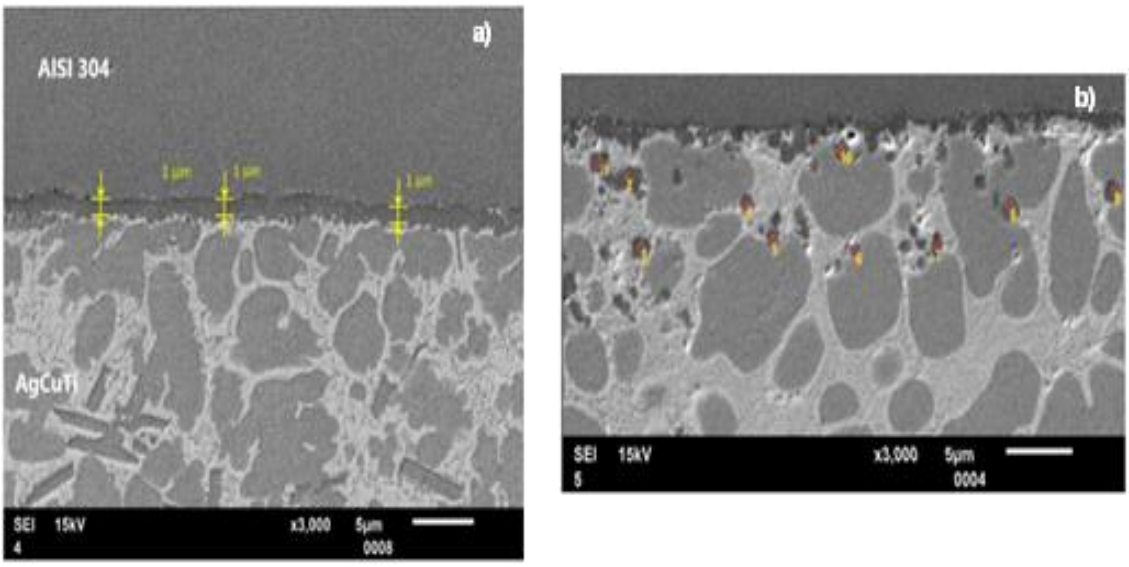

Fig. 5. a) Measurement of the brazed joint interface of steel-brazing alloy, b) significantly large number of pores at the interface and in the brazing alloy volume near the interface

Analysis of the sample made at IS = 12 mA showed the formation of a Ti layer at the steel/brazing alloy interface, while a significantly large number of pores are visible at the interface and in the brazing alloy volume near the interface (Fig. 5b). Pore size (diameter) was measured using ImageJ. The measured values were in the range of 0.7 - 3 μm while most were 1 μm in diameter.

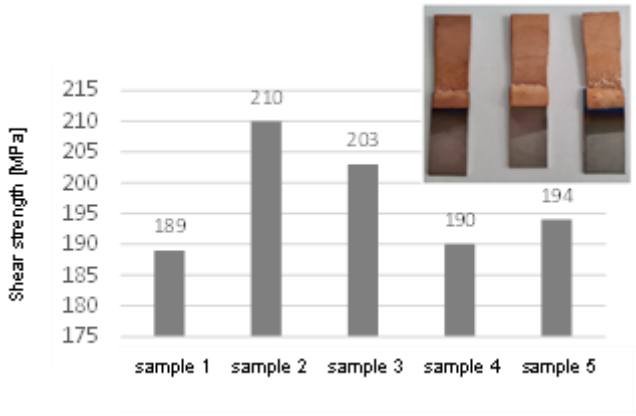

Fig. 6. Produced samples after the shear strength test and a graph with the achieved shear strength values

The samples for the shear strength test were made with the same parameters as the samples for macro and microstructural analysis, i.e. that all parameters were constant, the brazing current was varied in the range of 10-14 mA. The performed shear strength test showed that the values were in the range of 189-210 MPa. After the rupture, the brazed joints remained intact, the rupture occurred in the copper area close to the joint, it is assumed that the material was thermally affected and the grain thickened in this area. Fractographic analysis is necessary for a more precise definition.

4 RESULTS

The combination of the materials copper and corrosion-resistant steel is currently in great demand, despite the fact that they are very different, but it is by combining them that unique material properties are created. The mentioned combination of materials is mainly used in the aviation, automotive and energy industries, where high thermal and electrical conductivity (Cu) and corrosion resistance (steel) are required. For the combination of materials with different thermal conductivity, brazing in a vacuum is recommended in order to ensure a sufficient brazing gap so that the solder flows well into the brazing gap. The design of the experimental program consisted of the selection of suitable brazing parameters using electron beam, which served as a heat source. AISI 304 corrosion-resistant steel, Cu-ETP copper and Ticusil brazing alloy were the materials used to create the brazed joint. The connections were made using different brazing electron beam currents and were subjected to structural analysis and evaluation of mechanical properties. The obtained results can be summarized in the following points:

- The spreadability of the Ticusil brazing alloy on the Cu substrate was good (284.9 mm2), on the AISI 304 substrate the spreadability was satisfactory with a value of 100.92 mm2.

The wetting angle of the Ticusil brazing alloy on the Cu substrate was 18.53°, which is defined as very good wetting, in the case of corrosion-resistant steel, the wetting angle was measured as 21.92°, which represents good wetting. The spreadability and wettability of the solder is satisfactory in the case of both used substrates.

- Macrostructural analysis confirmed that the creation of a quality joint, which consists in the complete melting of the brazing alloy and its flow into the brazing gap, has an effect in addition to the set brazing parameters, especially the brazing current of electron beam, but above all the exact positioning of the materials before the actual brazing.
- Microstructural analysis showed the influence of the size of the brazing current on the integrity of the brazed joints. When using 12mA, pores are formed at the steel-brazing alloy interface, with increasing brazing current, the concentration of pores moves to the brazing alloy-Cu interface.
- Structural analysis of the brazed joint showed the formation of a CuTi layer at the steel-brazing alloy interface. The thickness of this layer was 1μm, while it did not change with increasing brazing current. Three phases were identified in the brazing alloy volume, namely a dark phase rich in Cu with a small content of Ti, a light phase rich in Ag. Within the light phase there are islands of the dark phase, which are rich in Ag+Cu. A continuous layer of Cu is formed at the Cu-brazing alloy interface. By determining the phase ratio in the brazing alloy volume, it is not possible to unequivocally confirm the influence of the size of the brazing current.
- From the measured average values, it follows that the microhardness of Cu coincides with the microhardness stated by the manufacturer, in the case of corrosion-resistant steel AISI 304, lower values were measured than stated by the manufacturer. The brazing alloy microhardness values ranged from 108 to 148 HV0.1.
- The shear strength test showed that the shear strength values were in the range of 189-210 MPa and the ductility values were in the range of 8.3-13.3%. After the rupture, the brazed joints remained intact, the rupture occurred in the copper area close to the joint.

The above results show the possibility of brazing corrosion-resistant steel with copper using electron beam. For a more accurate and detailed analysis, it is suggested to carry out additional tests, namely X-ray. Diffraction analysis to determine the exact composition of the formed phases at the interface of the brazed joint and in the volume of the brazing alloy, as well as fractographic analysis of the joint after performing the shear strength test.

ACKNOWLEDGEMENTS

The research was carried out under the support by the Vedecká grantová agentúra VEGA grant agency of the Ministry of Education, Science, Research and Sport of the Slovak Republic, project No. 1/0499/21 and by the Slovak Research and Development Agency under the contract No. APVV-18–0116.

REFERENCES

[1] D. LIUA, K. ZHAO, Y. SONGA, L. ZHANG, X. SONGA, W. LONG: Effect of introducing carbon fiber into AgCuTi filler on interfacial microstructure and mechanical property of C/C-TC4 brazed joints. In Materials Characterization 157 (2019).

[2] Ch. GUOQING, SH. XI, L. JUNPENG, B. ZHANG, Z. BINGGANG, F. JICAI: Electron beam hybrid welding-brazing of WC-Co/40Cr dissimilar materials. In Ceramics International 45 (2019), pp. 7821–7829

[3] E. HODÚLOVÁ, H. LI, M. SAHUL, B. ŠIMEKOVÁ, I. KOVAŘÍKOVÁ: Electron beam brazing of AISI 304 and copper dissimilar materials. In. Welding in the World (2021).

[4] Y. CHANGQUING: Experimental Investigation of Copper/Stainless Steel joints formed by Vacuum Brazing. In. Proc. ICONE18 (2010), pp. 47–55.

[5] S. CHEN, J. HUANG, J. XIA, X. ZHAO, S. LIN: Influence of processing parameters on the characteristics of stainless steel/copper laser welding. In. Journal of Materials Processing Technology (2015) pp. 43–51.

[6] J. ANDRIEUX, O. DEZELLUS, M. BOSSELET, P. SACERDOTE: Details on the formation of Ti2Cu3 in the Ag-Cu-Ti system in the temperature range 790-860 °C. Springer Verlag (2008), pp. 156-162.

[7] J. JIANG, T. B. BRITTON, A.J. WILKINSON: Evolution of dislocation density distributions in copper during tensile deformation. In. Acta Mater (2013), pp. 7227–7239.

A NEW APPROACH TO THE WELDING CURRENT MODULATION IN ELECTRON BEAM WELDING

Ing. Roman Darovec[1]
Ing. František Kolenič, PhD.[2]
Ing. Rastislav Sekerka[3]
Ing. Peter Koršňák[4]
[1]ORCID: 0000-0002-7570-864X, PRVÁ ZVÁRAČSKÁ, a.s, **Slovakia**
[2]ORCID: 0000-0001-9920-2398, PRVÁ ZVÁRAČSKÁ, a.s, **Slovakia**
[3]ORCID: 0000-0001-6968-367X, PRVÁ ZVÁRAČSKÁ, a.s, **Slovakia**
[4]ORCID: 0000-0003-2771-556X, PRVÁ ZVÁRAČSKÁ, a.s, **Slovakia**

Abstract: In modern electron beam welding equipment, the temperature of the thermoemission cathode is controlled by the power of low-energy electrons that fall on the cathode. The power of electrons that bombard the cathode is determined by the multiple of the voltage of the bombarding source U_B and the bombarding current I_b. It has been shown that the ripple of the bombarding source affects the ripple of the welding current. This contribution deals with the issue of designing a solution for the modulation of the welding current I in electron beam welding equipment using the change of the voltage ripple of the bombardment voltage source of the cathode heating. The principle of the presented solution is that we control the modulation of the welding current by changing the voltage ripple of the cathode heating source. Ripple of the cathode bombardment source, which is supplied with mains voltage. has a constant frequency of 100 Hz after rectification, it can be easily controlled by changing the value of its filter capacities. The modulation of the DC component of the welding current in this solution is characterized by the fact that the modulating sinusoidal signal has a constant frequency of 100 Hz and the depth of the modulation is proportional to the value of the filter capacity connected to the cathode bombardment voltage source. It is clear from the control principle that the magnitude of the modulation of the welding current can only be in discrete values, corresponding to the current value of the filter capacity connected to the bombard voltage source. The contribution also presents the method of connecting the filter capacities of the bombardment voltage source and the resulting parameters of the controller for the modulation of the DC component of the welding current by the proposed principle.

Keywords: electron beam welding, thermoemission cathode, modulation of the of the welding current

1 INTRDUCTION

The welding process in electron beam welding is a complex process, the quality and stability of which is influenced by many factors, whether it is the stability of the welding parameters and the performance of the Energoblock itself, the stability of the vacuum during the welding process, and the material of the weldment itself also has an impact. In an ideal welding process, all necessary parameters of the welding process are stable with minimal ripple (e.g., welding voltage UZ, Wehnelt electrode bias UW, Bombard voltage UB, focusing current IF), thus achieving a stable welding current IZ with constant power (Schultz, 2004). In the welding process, it is therefore very important that the energy that we distribute to the material being welded by the electron beam is constant during the welding process and that the electron beam has sufficient sharpness. In this way, we significantly eliminate possible defects in the weld joint, reduce the pores in the weld joint, and ensure the necessary weld depth of the material. During the practice of welding different materials, we came to the knowledge that when welding different types of materials, some materials (e.g. materials based on aluminum alloys) show a higher number of defects in the weld joint during the welding process with stable parameters, which is a consequence of higher gassing of material in the weld bath (Węglowski at all, 2016). Thus, the weld joint shows a higher number of pores, the weld depth is insufficient and the surface of the weld joint is wrinkled. Such materials therefore require a different approach to welding technologies than other materials. Through a long-term study of the technology of welding materials based on aluminum alloys, we found that these materials are best welded if the energy distributed to the weld joint is modulated with a certain frequency, which means that the welding current I (therefore also the electron beam) is modulated with a certain frequency and a certain corrugation (modulation depth), which will be determined by the welding technology itself for the given type of material based on aluminum alloys. With an appropriately chosen frequency and depth of modulation of the welding current I, we can significantly reduce the gassing of these materials (reduction of pores in the weld) and appropriately shape the weld pool. For example, for welding HVH heat exchangers for electric cars (AlMgSiFe alloy), it is suitable if we modulate the welding current IZ with a frequency of 100Hz with a modulation depth of approximately 50% (Schubert, 2021).

2 PRINCIPLES OF WELDING CURRENT MODULATION

The first way to modulate the welding current I_Z is to modulate the desired value of the welding current I_Z so that the desired value will be composed of a direct and alternating component, each of which will be separately adjustable. By combining the settings of these two components, the welding current I_Z can be freely modulated. Desired value of the direct and alternating components of the welding current is input to the welding current regulator I_Z, and the output controls the bias voltage of the Wehnelt electrode U_W so that the real welding

current will copy the modulated desired value I_Z. This method of modulating the welding current I_Z has the advantage that it is universal and thus we can use it to modulate an arbitrarily selected shape of the welding current I_Z (SINUS, TRIANGLE, SQUARE) with 100% modulation depth and an arbitrarily selected frequency of the welding current. Here, however, we encounter to the limits of our control loop (I_Z regulator → Wehnelt Excitation → Wehnelt Rectifier → HV cable → Electron beam gun), while in particular the capacity of the filter capacitors of the Wehnelt Rectifier board and the capacity of the HV cable causes a slow response of the control loop to a rapid change in the desired value of I_Z , the consequence of which is the fact that the control loop does not have time to respond to the desired I_Z value with a frequency higher than 100 Hz by changing the bias voltage on the Wehnelt U_W electrode. As a result, the real course of the welding current I_Z (measured value I) is deformed and the modulation depth is reduced. The disadvantage of this method of modulation, in addition to the speed of the speed of the control loop, is the necessity of using a waveform generator for the modulation of the alternating component of the desired value I_Z. The second way to modulate the welding current I_Z is the principle of modulating the voltage on the Wehnelt electrode U_W by the voltage ripple of the Bombard source U_B, while the voltage change on the Wehnelt U_W electrode directly modulates the welding current I_Z at a constant desired value I_Z. The regulator I_Z tries to counteract the change in the welding current from of the desired value, which remains constant, but due to the slow control loop, the controller I_Z cannot suppress this change in the welding current, but only partially limit it. The ripple of the welding current I_Z thus approximately copies the voltage ripple of Bombard. The principle of modulation of the welding current will be explained in the following figures (Fig. 1 and Fig. 2).

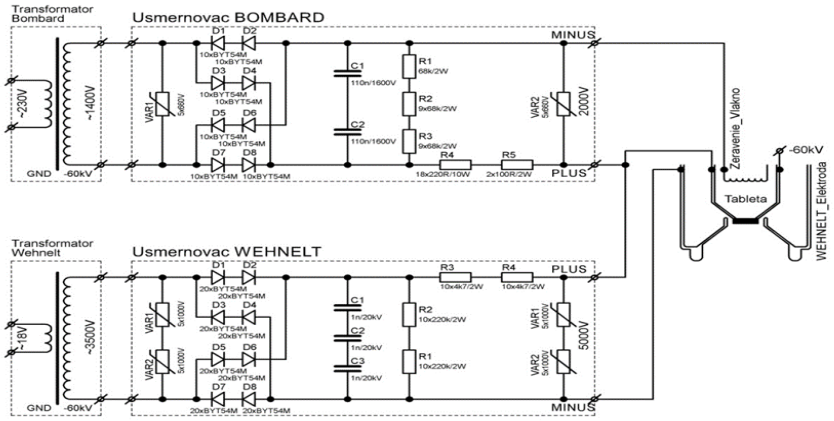

Fig. 1 Connection of bombard and Wehnelt auxiliary sources in a small container of the HV source and electrodes of the electron gun optics

Fig. 1 shows the connection of auxiliary bombard and Wehnelt sources, which are placed in a small container with electrodes of the optics of the electron beam gun. Both auxiliary sources are connected to the HV potential of the -60kV HV source by their positive poles. The negative pole of the bombard source (-2000V) is connected to the cathode holder and the negative pole of the Wehnelt source
(-5000V) is connected to the Wehnelt electrode. The negative pole of the bombard source is thus connected to the Wehnelt source through the resistor divider, formed by resistors R1, R2, R3 and resistors R4, R5. This connection goes through a divider formed by resistors R4, R3 (protective series resistor) and resistors R2, R1 (discharge of filter capacitors C1, C2 and C3), which means that the change in bombardment voltage U_B (ripple) through these resistors will also affect the Wehnelt themselves voltage U_W. In fig. 2 this phenomenon is explained in more detail.

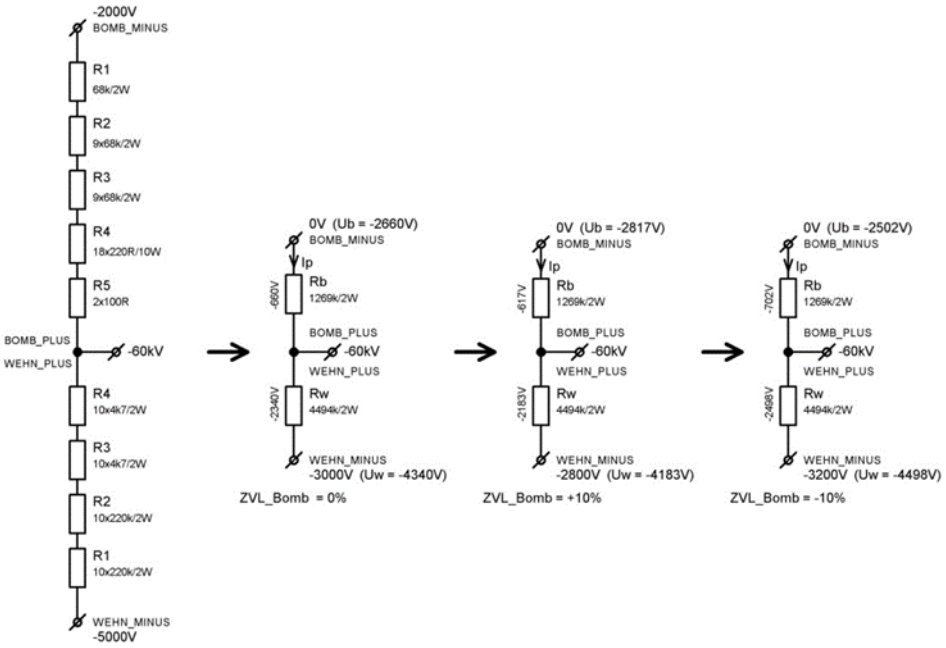

Fig. 2 Distribution of voltages on the resistor dividers of bombard and Wehnelt auxiliary sources according to the ripple of the bombard voltage U_B

As we can see from fig. 2, the Wehnelt source (-5000V) has a 3000V more negative voltage than the bombard source (-2000V), which means that the current Ip flows through resistor dividers Rb and Rw from the positive pole of the bombard source (imagined 0V) to the

negative pole of the Wehnelt source (imagined -3000V) and creates corresponding voltage drops on these resistor dividers, which are then added to the bombardment voltage.
In the first case, the ripple of the Bombard source is 0%, the transverse current Ip, which is induced by a voltage difference of -3000V, causes a voltage drop of -660V on the divider Rb and a voltage drop of -2340V on the divider Rw, which means that the voltage of the Bombard U_B acquires the value - 2660V and the Wehnelt U_W voltage takes on the value -4340V.
In the second case, the ripple of the Bombard source is +10%, the voltage difference in this case will be -2800V and the transverse current Ip will cause a -617V loss on the divider Rb and a loss on the divider Rw -2183V. The Bombard voltage U_B will take the value -2817V and the Wehnelt U_W voltage will take the value -4183V.
In the third case, the ripple of the Bombard source is -10%, the voltage difference in this case will be -3200V and the transverse current Ip will cause a -702V drop on the Rb divider and a -702V drop on the Rw divider -2498V. The Bombard voltage U_B will take the value -2502V and the Wehnelt U_W voltage will take the value -4498V.

Modulation of the welding current Iz by changing the filtering capacity of the bombard source

As we explained in the previous part of the document, we can modulate the welding current I_Z by the ripple of the bombard voltage U_B, because this ripple of the bombard voltage through the resistor dividers modulates the voltage U_W on the Wehnelt electrode. We can influence the ripple of the bombard voltage U_B in basically two ways. By changing the capacity of the filter capacitors of the bombard source or by changing the load of the bombard source by changing the bombard current I_B. The first method of adjusting the ripple of the bombard voltage and thus the modulation of the welding current I_Z by changing the capacity of the filter capacitors is thus more suitable for the needs of electron beam welding in the production or research process.

Remotely controlled switch of the filter capacitors of the bombard source with optical fiber

Our goal was to design a switch that would allow additional filter capacitors to be connected in parallel to the basic filter capacitors and thereby increase the filter capacity of the bomb source. Changing the filtering capacity of the source also changes the value of its voltage ripple. The switch enables the connection of four different filter capacitors to the basic filter capacitor using high-voltage relays. The switching principle is shown on the block diagram of the device fig. 3.

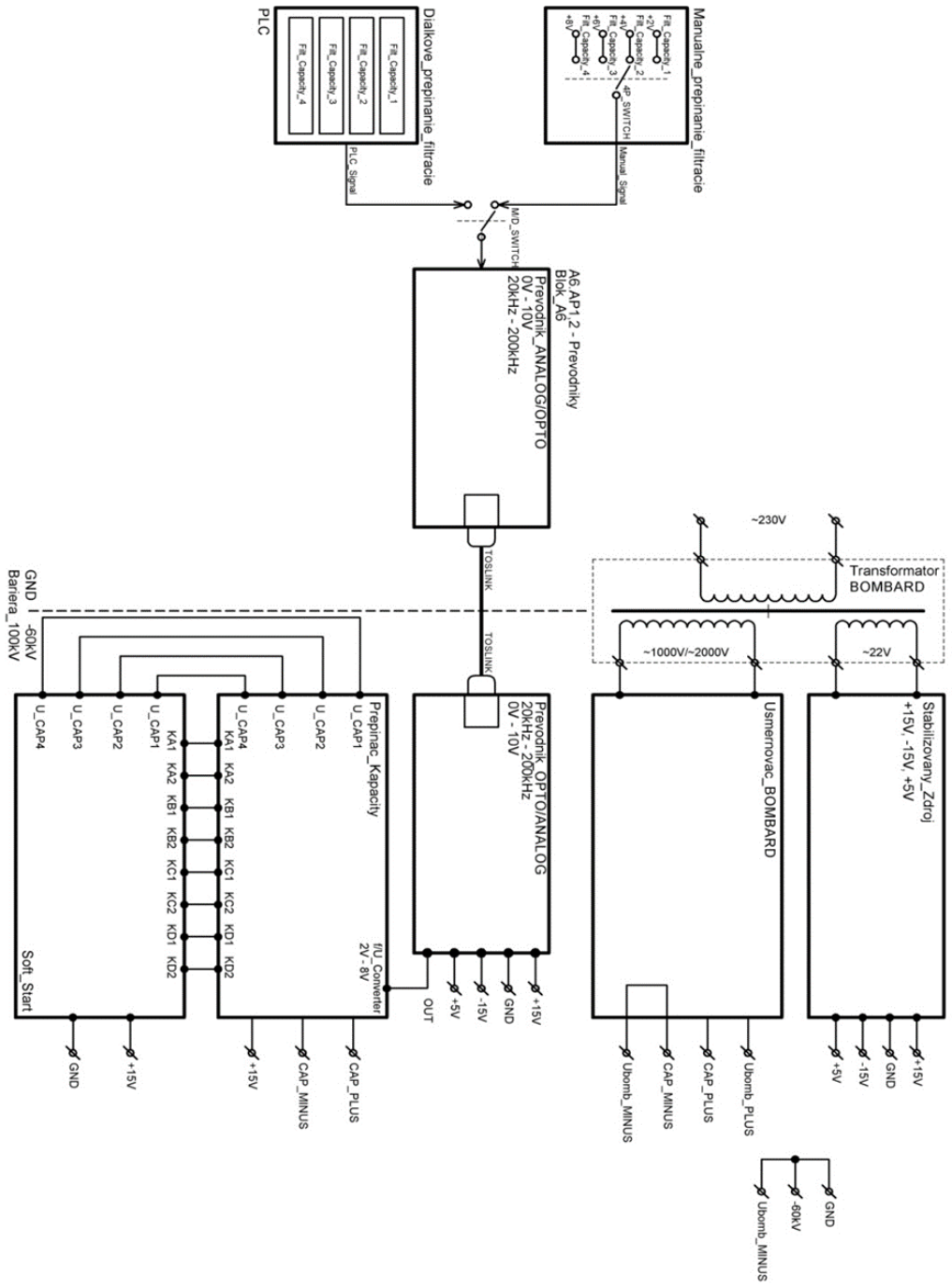

Fig 3 Block diagram of the remote-controlled filter capacitor switch

The operator has two options for switching the relevant filter capacitor manually or remotely. Manual switching of filtration is realized by a four-pole switch and remote switching of filtration by means of a PLC terminal. The switching logic is realized in such a way that each of the four positions of the switch is assigned a different voltage, so that:

- 1st switch position (Capacitor 1) – 2V
- 2nd switch position (Capacitor 2) – 4V
- 3rd switch position (Capacitor 3) – 6V
- 4th Switch position (Capacitor 4) – 8V

It is also implemented in the case of remote filtering switching, where I select the necessary capacitor using the PLC terminal and the PLC module will generate the appropriate voltage according to the table. This analog control signal is then fed through the M/D (manual/remote) switch (M/D_SWITCH) to the input of the optical transmitter, which is realized by a U/f (voltage/frequency) converter (converter_ANALOG/OPTO). Through the TOSLINK optical fiber, the optical signal from the optical transmitter is fed into the small container of the HV source at the input of the optical receiver, which is implemented by the f/U (frequency/voltage) converter (converter_OPTO/ANALOG). Optical transmission provides a 100kV insulation barrier between the electronics of the stand of auxiliary sources (GND potential) and the electronics of the small vessel of the HV source (potential -60kV). From the output of the optical receiver, the analog control signal is fed to the converter_capacity board, which, according to its size, switches the corresponding high-voltage relay, which connects the selected filter capacitor in parallel to the basic filter capacitors. Since the voltage of the bombard source is 1kV to 2kV (optional), it is not possible to directly connect the filter capacitor to the basic filter capacitors, because the current that would flow at the beginning of charging the connected capacitor would acquire too large and short-circuit values. Such a large charging current would have an adverse effect on the life of the filter capacitors and could lead to the failure of the fuse of the primary winding of the bombard transformer. This problem is solved by the Soft_Start board, which is interconnected with the converter_capacity board and ensures the limitation of the charging current of the connected filter capacitor so that the filter capacitor is charged through a power resistor that limits the charging current. The filter capacitor is charged to a certain voltage through this power resistor, which is evaluated by the Soft_Start board and turns on the auxiliary relay, which short-circuits the power resistor with its contacts. The charging current will then be limited by the voltage of the charged filter capacitor itself, and it will be further charged to the full voltage of the Bombard source. The power supply of this system of plates, which together form the filter capacitor switch, is provided by the Stabilized_Source. board in the small container, which provides stabilized supply voltages of +15V, -15V and +5V. The input AC

supply voltage ~22V is supplied to the board from the additional winding of the Bombard transformer.

Boards Switch_ Capacity and Soft_Start

In this part of the document, we will explain more precisely the function of the Switch_capacity and Soft_Start boards, because these boards are a new element in the electronics of the Small Vessel.

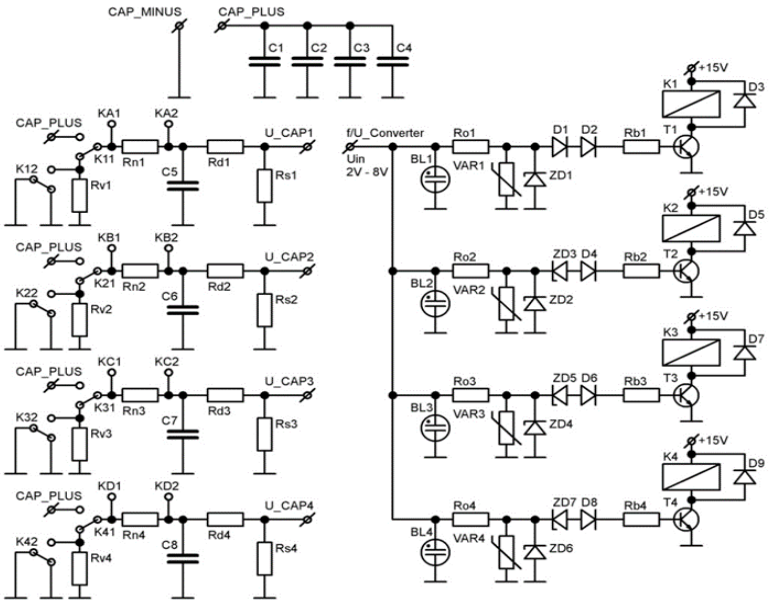

Fig. 4 Electrical diagram of the Switch_Capacity board

Fig. 4 shows the electrical diagram of the Swich_capacity board, which ensures the switching of filter capacitors and thus the change of the total filter capacity. Filter capacitors C1, C2, C3 and C4 are so-called basic (default) capacitors, the total capacity of which determines the smallest possible filtering capacity of the Bombard source. Using four high-voltage, two-pole relays (K1, K2, K3 and K4), we can successively connect four additional filter capacitors C5, C6, C7 and C8 to them. High-voltage relays are switched by the so-called step switch that turns on the corresponding high-voltage relay according to the size of the control voltage UIN. The control voltage from converter_OPTO/ANALOG is graduated in steps of 2V, that means it takes on values of 2V, 4V, 6V and 8V, which corresponds to the switching on of individual high-voltage relays K1, K2, K3 and K4, while the following applies:

• UIN = 2V → K1 ON (C5 ON)

• UIN = 4V → K2 ON (C6 ON)

• UIN = 6V → K3 ON (C7 ON)

• UIN = 8V → K4 ON (C8 ON)

The step switch is implemented using only zener diodes, universal diodes and bipolar transistors, which is why we focused mainly on the device's resistance to voltage discharges. Filter capacitors C1 to C5 are charged through the charging resistor Rnx, which limits the charging current, after being connected to the CAP_PLUS terminal by the Kx1 relay contact. The voltage (U_CAPX) is sensed on the filter capacitors C5 and C8 during charging by the parallel voltage divider Rdx/Rsx. If this voltage exceeds a certain value that is set on the Soft_Start board, the Soft_Start board will automatically bypass the charging resistor Rnx (contacts KAx, KBx, KCx and KDx) and the given filter capacitor will then slowly charge to the Bombard source voltage. On the other hand, when the control voltage UIN decreases, the filter capacitors C5 to C8 are gradually disconnected according to the size of the control voltage, and the filter capacitors are discharged through the discharge resistors Rvx after disconnection.

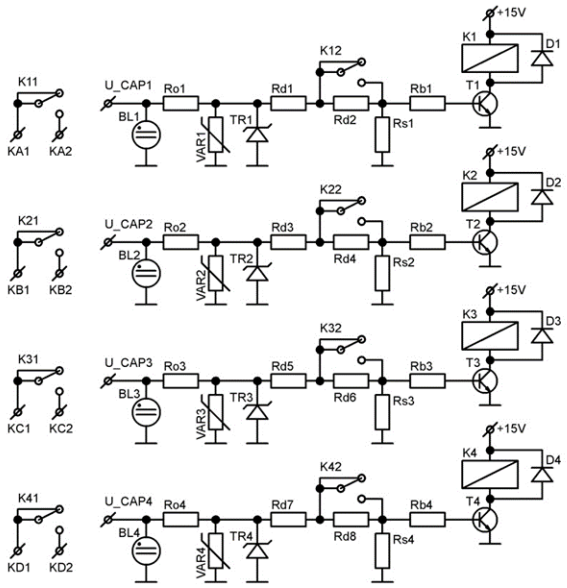

Fig.5 Electrical diagram of the Soft_Start board

In fig. 5 we have the electrical diagram of the Soft_Start board, which ensures, after connecting the filter capacitors C5 to C8 to the Bombard source, their gradual charging with a small charging current through the corresponding charging resistor Rnx. The principle consists in sensing the voltage level on the connected filter capacitor (signal U_CAPx), which

gradually increases during its charging up to the level at which the transistor Tx opens through the resistor divider and the relay Kx switches on. The first pair of contacts Kx1 bridges the corresponding charging resistor Rnx and the second pair of contacts bridges the resistor in the voltage divider Rdx, which ensures that the relay remains closed even with a lower voltage on the filter capacitor. With this function, the Soft_Start board eliminates accidental switching of the relay due to a large voltage ripple on the filter capacitors. If the filter capacitor is disconnected from the Bombard source, the filter capacitor starts to discharge through the discharge resistor Rvx, the voltage on it gradually drops to zero, the relay turns off, and the whole process is repeated later when the filter capacitor is charged.

3 CONCLUSION

The goal of this document was to design a device topology that would allow us to operationally modulate the shape and size of the welding current I during the electron beam welding process, without having to turn off the entire electron beam generation system. The proposed solution brings significant time savings in managing the electrobeam welding process. The proposed system not only meets this condition, but also brings several other advantages. The device is designed exclusively from discrete components and is supplemented with suitable protective elements, which significantly increases its resistance to HV discharges and thereby increases its service life in production operation. The device has a built-in Soft Start function, which protects the filter capacitors from sudden charging current, and last but not least, its operation is simple for the operator of the welding process.

ACKNOWLEDGEMENT

This work was supported by Agency for the Support of Research and Development under Contract No. APVV-20-0100.

REFERENCES

Schultz H.: Electron Beam Welding, Cambridge: Abingdon Publishing, England, 2004, ISBN 1-85573-050 2.

Węglowski M., Błacha S., Phillips A.: Electron beam welding – Techniques and Trends – Review, Vacuum Journal, Volume 130, August 2016, Pages 72-92

G. Schubert: Electron Beam Welding – Process, Applications and Equipment, PTR-Precision Technologies Inc, Enfield, 2021

UNIVERSAL TIME COURSE GENERATOR FOR USE IN ELECTRON BEAM WELDING

Ing. Daniel Kunštek[1]
Ing. Rastislav Sekerka[2]
Ing. Peter Koršňák[3]
Ing. Martin Kopecký[4]
[1] ORCID: 0000-0001-5744-8816, PRVÁ ZVÁRAČSKÁ a.s, Bratislava, **Slovakia**
[2] ORCID: 0000-0001-6968-367X, PRVÁ ZVÁRAČSKÁ a.s, Bratislava, **Slovakia**
[3]ORCID: 0000-0003-2771-556X, PRVÁ ZVÁRAČSKÁ a.s, Bratislava, **Slovakia**
[4] ORCID: 0000-0002-2934-5569, NES Nová Dubnica, **Slovakia**

Abstract: This article deals with the waveform generator for a control (Wehnelt) electrode, by means of which the welding current of an electron beam welding machine is subsequently modulated. The waveform generator consists of two parts. One part uses direct digital synthesis (DDS) to generate the waveform, while the other part adjusts the output characteristics of the generated waveform to the required values.

Keywords: electron beam welding, welding current modulation, waveform generator, direct digital synthesis

1 INTRODUCTION

In electron-beam welding of light aluminum and magnesium alloys, for better degassing of the weld pool and improvement of the formation of the weld joint, it is advantageous to use a welding current with a modulated alternating current on the DC component of the welding current (Węglowski et al., 2016). Older concepts of electron-beam welding equipment used a weakly filtered cathode heating voltage source (also referred to as a bombardment source) for this method. In such a solution, the output voltage from the transformer was rectified by a rectifier bridge and subsequently filtered by a capacitor, which had a smaller capacity than that required for the complete smoothing of the rectified waveform. In this way, the undulation of the bombardment current of the cathode was achieved, and subsequently, with the help of the parasitic capacities of the device, also the undulation of the welding current (Fig. 1).

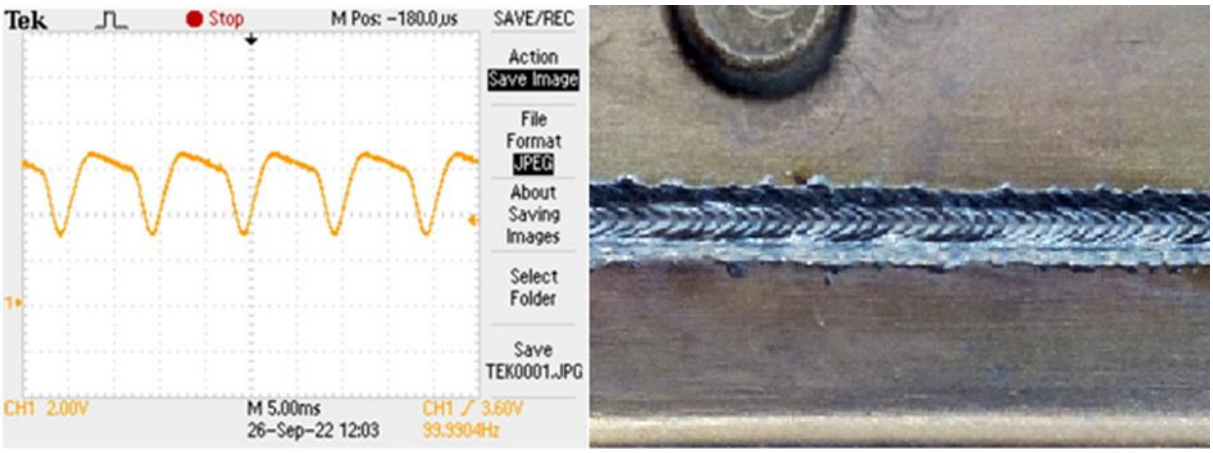

Fig. 1 Weld bead formation with a wavy welding current

In the second generation of modern electron beam welding equipment developed by the company PRVÁ ZVÁRVAČSKÁ, the modulation of the welding current was solved using a switched source. This source indirectly modulated the welding current. In the latest version of the electron-beam welding equipment, the indirect modulation of the welding current is replaced by direct modulation of the control - Wehnelt electrode. This method of modulation can achieve the most faithful modulated welding current with full control of its output parameters.

2 DESCRIPTION OF THE TIME COURSE GENERATOR

The circuit ensuring the generation of input modulation waveforms, which are fed to the input of the switching source, which realizes its own modulation of the control electrode using the applied voltage, is the waveform generator. This ensures the generation of sinusoidal, triangular and rectangular voltage waveforms in the required output parameters such as frequency, amplitude and DC component of the signal, also called offset. The new concept of the source of direct modulation of the welding current requires a new approach to the method of generating the modulation signal. It is no longer enough to use simple analog time course generators, which can only be controlled to a limited extent using analog values from control industrial computers. For full control, it is necessary to use digital generators of time courses.
The proposed circuit solution consists of several parts. The main part is a single-chip generator based on direct digital synthesis from Analog Devices, designated AD9833. Furthermore, it is the circuit that ensures the management of the entire proposed concept. An important part of the design is analog signal processing, where the main circuit consists of a summing amplifier and matching circuits. The last important part is the galvanic isolation of the inputs from the superior industrial computer PLC. The basic circuit of the AD9833

generator works on the principle of direct digital synthesis (DDS), which ensures the creation of an analog signal by generating a time-varying signal in digital form and then converting the thus obtained digital signal to analog in a digital-to-analog converter. The advantage of such a generator over analog ones is that the synthesized signals are repeatable and frequency accurate with fine tuning over a wide range of frequencies. The frequency stability of the output signal of such generators is very high and approaches the stability of the reference oscillator (Analog Devices, 1999). With advances in processor technology, today's DDS generators are very compact and capable of providing the user with a variety of additional functions.

3 TECHNICAL DESCRIPTION OF THE DIGITAL TIME COURSE GENERATOR

The basis of the waveform generator module is the AD9833 circuit, which is capable of generating all three required waveforms, which are: sine, triangular and rectangular waveforms. The manufacturer states that the DDS generator circuit is capable of generating an output signal with a frequency of 12.5 MHz when using a crystal oscillator with a frequency of 25 MHz (Analog Devices, 1999). The circuit is controlled from the parent microcontroller using the SPI (Serial Peripheral Interface) serial interface. The control element of the generator is a microcontroller of the AVR architecture from Atmel. Specifically, the Atmega 16 type is selected for the generator, which provides an operating frequency of 16 MHz, 16 KB Flash memory, 512 B EEPROM and 1 KB SRAM. It also contains eight analog-to-digital (A/D) converters with a resolution of 10 bits, counters, timers and elements for communication via SPI, USART and I2C interfaces (Microchip Technology, 2016). This microcontroller offers the user a number of functions, of which we used the already mentioned SPI communication interface for the needs of the generator, a 3x A/D converter for reading input analog values, a timer, arithmetic-logical operations and a watchdog function for generating a reset of the microcontroller when it is inactive.

The role of the microcontroller is to read the analog voltage values on the potentiometers and the values set using the superior PLC (Fig. 2). The input values for setting the generator are: the output frequency of the generator, the output voltage of the peak-to-peak generator and the value of its DC component - offset. Analog values are fed from the potentiometers or from the superior PLC to the input 10-bit analog-to-digital converters of the microcontroller marked as ADC0-ADC2. After converting the set value of the potentiometer to a digital signal, the microcontroller calculates the value of the relevant parameter. To load the frequency, the ADC value of the conversion is processed and sent to the DDS generator AD9833 using the SPI bus. After processing and recalculation, the output voltage and DC component values are also sent via the SPI bus to the appropriate digital potentiometers, which ensure further processing of the generated signal in the analog part of the generator using circuits with operational amplifiers. In the analog part, the signal from the generator is

first attenuated using a digital potentiometer. The signal adjusted in this way is used to set the size of the output generated signal. The size of the DC component of the generator voltage is set by the second digital potentiometer, using the offset setting of the operational amplifier. Both signals are then added in a summing amplifier. A third digital potentiometer is also used to adjust the signal from the DDS generator AD9833, which serves to weaken the rectangular waveform of the DDS generator, the level of which reaches the values of the supply voltage, compared to the voltage of 0.6 V, which is achieved with sinusoidal and triangular waveforms.

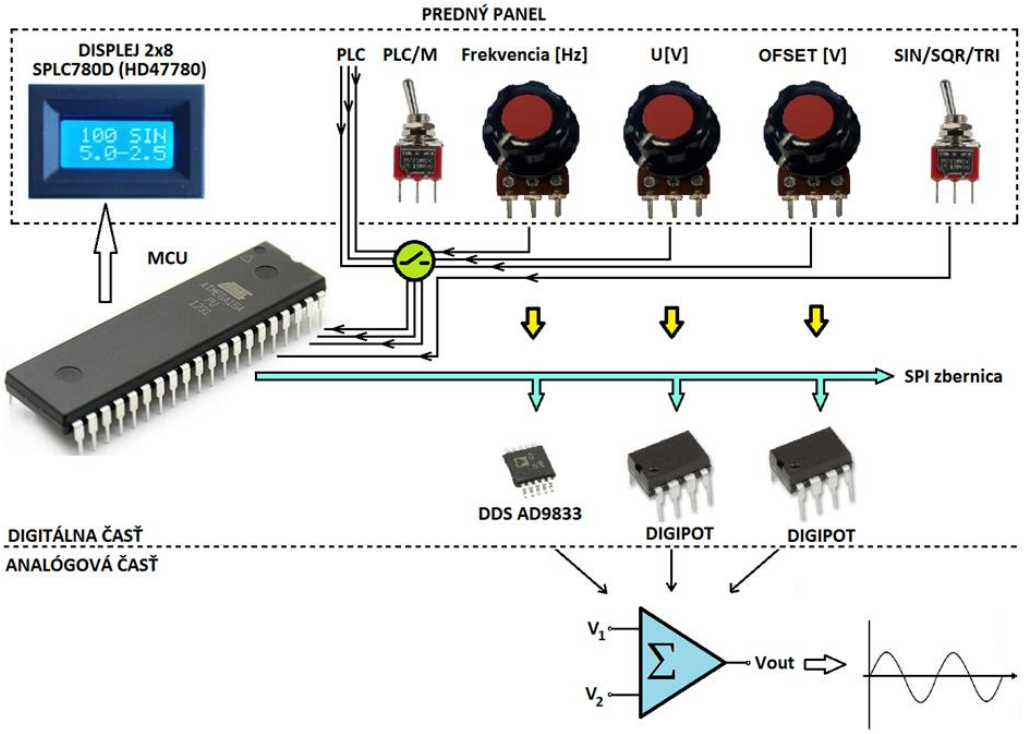

Fig. 2 Principle diagram of the designed DDS generator

Another function of the microcontroller is to display the current set values of the waveform generator on the alphanumeric display. This displays the frequency value in hertz, the magnitude of the output voltage in volts, the magnitude of the DC component of the signal in volts, and the selected waveform type. In order for the display to fit on the front panel of the device, it is 2x8 characters in size. The display uses a Hitachi HD44780 controller clone for its function. I can also use a larger type of display up to the size of 16x4 characters. If it is possible to use such a display due to the size of the front panel, then such a display provides complete data on the set values (Fig. 3).

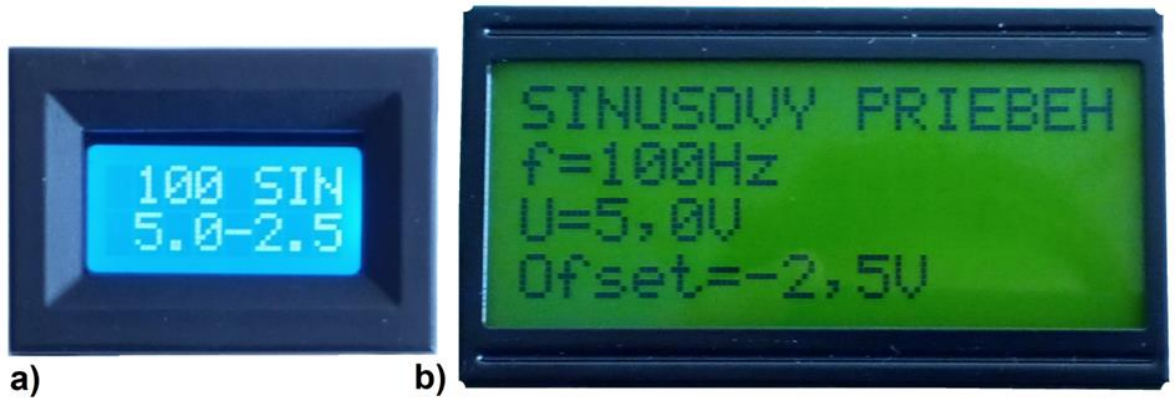

Fig. 3 Display of set parameters a) 2x8 characters b) 16x4 characters

The program for controlling the waveform generator is written in the C programming language. The task of the program is to read the analog value of the desired signal using the input analog-to-digital converters and then convert it to the desired output signal value of the waveform generator. The calculated values are then sent via the SPI bus to three digital potentiometers, the AD9833 signal generator and simultaneously displayed on the display located on the front panel (Fig. 4).

Fig. 4 Front panel of the waveform generator

Figure 5 shows the measured waveforms captured on the oscilloscope. A harmonic signal represented by a sine function, which contains only one fundamental frequency, is displayed without distortion (Fig. 5a) even at a generator frequency of 100 kHz. Signals with a higher number of harmonic frequencies, such as triangular and rectangular waveforms, show shape

distortion at a frequency of 100 kHz due to the smaller width of the transmission bandwidth of the analog part of the generator, represented mainly by the input impedance of the selected digital potentiometers (Fig. 5b). Realistically, the generator will only be used at frequencies up to 1 kHz. At this output frequency, signal distortion does not appear. The designed generator was also tested for resistance to discharges in the emission system of the electron gun. During these long-term tests, a tendency to freeze the program and damage the generator elements appeared. The resulting errors were subsequently analyzed and eliminated by more suitable overvoltage protection of microcontrollers using protective diodes and by inserting a watchdog into the program.

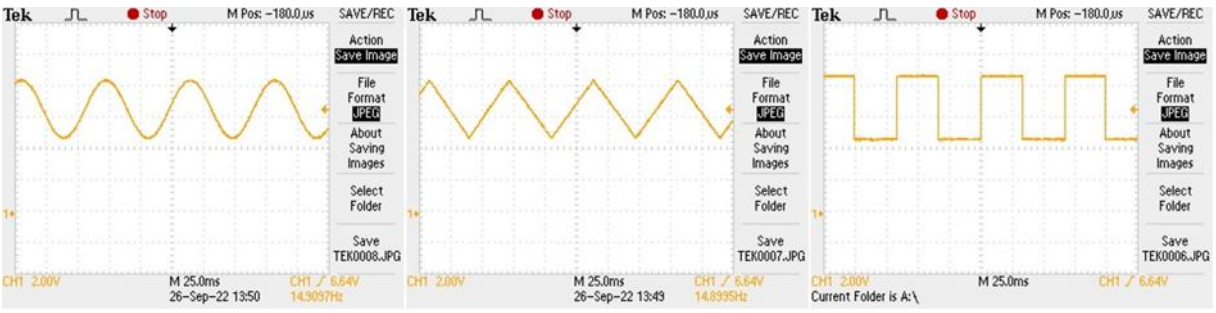

Fig. 5a Measured waveforms of the output signals at a frequency of 1 kHz

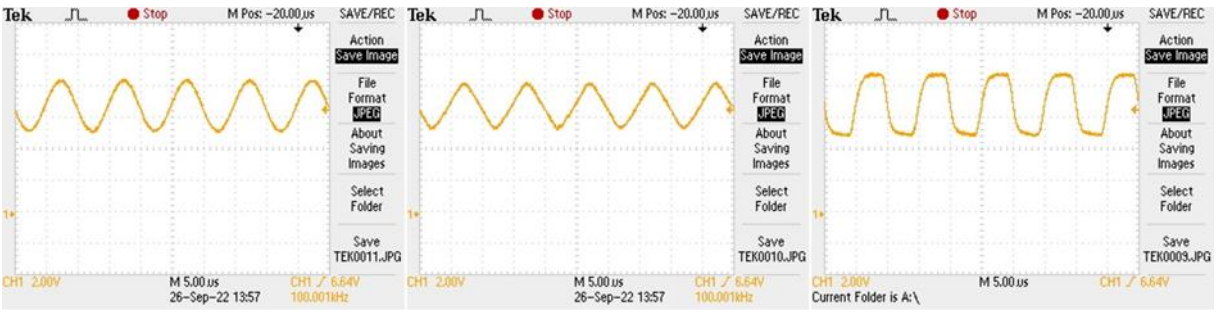

Fig. 5b Measured waveforms of the output signals at a frequency of 100 kHz

4 CONCLUSION

The proposed generator of time courses was integrated into the circuits of direct modulation of the welding current using the course of the voltage on the control electrode of the electron gun. The proposed circuit solution provides new possibilities in the way of influencing the weld pool, which has a positive effect on the quality of the welded joints. The topology of the generator of time courses is based on the integration of modern components of microprocessor technology, which made it possible to achieve higher stability and

reproducibility of the output time courses. The measured time courses of the output signals are practically without distortion up to a frequency of 10 kHz. At a frequency of 100 kHz, we observe a slight distortion, especially of signals with a higher number of harmonics. The parameters of the output values of the generated signals are in full compliance with the requirements placed on welding current waveforms when welding light alloys.

ACKNOWLEDGEMENT

This work was supported by Agency for the Support of Research and Development under Contract No. APVV-18-0402.

REFERENCES

Węglowski M., Błacha S., Phillips A.: Electron beam welding – Techniques and Trends – Review, Vacuum Journal, Volume 130, August 2016, Pages 72-92

Analog Devices, Inc. 1999. A Technical Tutorial on Digital Signal Synthesis. 1999 [cit. 6.11.2023], s. 5.

URL: https://www.analog.com/en/education/education-library/technical-tutorial-dds.html
Analog Devices, Inc. 2019. [online katalógový list]. AD9833. 2019 [cit. 6.11.2023].

URL: https://www.analog.com/media/en/technical-documentation/data-sheets/ad9833.pdf
Microchip Technology Inc. 2016. [online katalógový list]. ATmega16. 2016 [cit. 6.11.2023]. URL: https://ww1.microchip.com/downloads/en/DeviceDoc/doc2466.pdf

MODULAR DESIGN OF UNIVERSAL ELECTRON BEAM DEVICES

Ing. Rastislav Sekerka[1]
Ing. František Kolenič, PhD.[2]
Ing. Peter Koršňák[3]
Ing. Ľuboš Kováč[4]
[1]ORCID: 0000-0001-6968-367X, PRVÁ ZVÁRAČSKÁ, **Slovakia**
[2]ORCID: 0000-0001-9920-2398, PRVÁ ZVÁRAČSKÁ, **Slovakia**
[3]ORCID: 0000-0003-2771-556X, PRVÁ ZVÁRAČSKÁ, **Slovakia**
[4]ORCID: 0000-0003-4308-805X, PRVÁ ZVÁRAČSKÁ, **Slovakia**

Abstract: The paper presents a modern concept for the construction of electron beam welding equipment using mutually compatible equipment modules. The modularity and mutual compatibility of the construction modules of the welding equipment have a significant impact on the production time of the equipment, the reproducibility of its output technical parameters, the speed of service work and, last but not least, have a fundamental impact on the economy of production. The paper focuses attention on the four most important parts of electric beam welding equipment, such as the electron beam generation system, the electron gun, the positioning of the electron gun in vacuum and the modularity of vacuum welding chambers. In the final chapter, an example of the design of an electron beam device of a universal type with two electron guns is presented.

Keywords: electron, beam, welding

1 INTRODUCTION

Electron beam technologies have been used in industrial production for several decades. During their use, they made a huge contribution to the development of practically all industries. They participate in the excellent results that humanity has achieved in the development of scientific knowledge and technical progress over the past 50 years. They play an irreplaceable role in space exploration, the development of air transport and the automotive industry, energy and general engineering (Schultz, 2004). They meet the parameters for inclusion in the group of high-tech technologies. New scientific knowledge and methods, materials and modern computer technology are used in the design of welding complexes. From the point of view of their further development, such factors as their

commercial availability, high reliability, application flexibility and the fact that they are immediately usable for direct industrial applications play an important role.
In the field of development and supply of electro-beam technological complexes, PRVA ZVARACSKA has developed a modular design system (Kolenič, 2014). In this system, structural modules are used as basic building elements, which represent independent functional units. The criteria for the design of functional units or modules are built in such a way that they fulfill the specified function with high reliability, are fully compatible in hardware and software with other modules of the technological complex and enable work in autonomous mode. PRVA ZVARACSKA in the design of structural modules proceeds methodically, by gradual innovation of modules of technological units at the level of current knowledge.

When designing electron beam welding technological complexes, we divide unified modules into basic and additional modules. The basic modules form the core of the technological welding complex, they ensure the primary function of the device - the realization of a welded joint of metal materials in a vacuum. Basic modules include a powerful electron beam generator, which we briefly call an Energoblock, an electron gun, a vacuum welding chamber, modules for creating a vacuum in the welding chamber and in the electron gun, modules for positioning welded parts, CNC control modules, modules for observing and lighting the welding process. Software is an integral part of the technological complex. Additional modules are not a necessary part of the device, but they perform an important function in setting and monitoring process parameters, creating process databases, protecting the weld joint from defects, expanding the technological capabilities of the device, enabling remote diagnostics, prophylaxis and servicing of the device using remote access using web applications. PRVA ZVARACSKA currently has completed the design of several dozen mutually compatible construction modules for the supply of electric beam welding equipment. The modular design concept makes it possible to satisfy practically all technical and technological requirements of customers in the highest quality and within the required time horizon. Some specific customer requirements, especially when supplying highly productive welding equipment, are mostly solved by modifying the design of the selected module using its conceptual solution.

2 SELECTED MODULES OF ELECTRIC BEAM WELDING EQUIPMENT

In the scope of this contribution, it is not possible to present all structural modules that have a clearly defined function in the implementation of the electron beam welding process. . In the following chapters, four important design modules of electron beam welding equipment produced by PZ will be presented.

2.1. ELECTRON BEAM GENERATION MODULE – ENERGOBLOCK

Energoblok is one of the basic design modules and serves to create conditions for the generation of an electron beam and its automatic control (Kolenic and Kovac, 2011). The electron beam itself is created in an electron gun. The PRVA ZVARACSKA manufactures three power levels of electron beam generators with the type designation PZ EB 7.5, PZ EB 15 and PZ EB 30. All power levels have the same external dimensions, they differ in internal equipment. They consist of two unified 19'' Schroff type stands (Fig. 1).

Fig. 1. Energoblock PZ EB 2.5-15

An adjustable and stabilized HV source is located in the first stand, which serves to accelerate the electrons of the electron beam. This source supplies the electrons with kinetic energy, which, when they hit the weld joint, changes into thermal energy and serves to

create the weld joint. In the second stand, there are auxiliary sources that serve to heat the thermo-emission cathode of the electron gun, the control voltage that regulates and stabilizes the welding current, the current source for the magnetic focusing of the beam, the source system for the magnetic deflection of the beam and the PLC logical automaton for manual and automatic operation control energy block. Energoblock type PZ EB 7.5 generates an electron beam with a maximum power of 7.5 kW. At an accelerating voltage of 60 kV, it creates a welding current in the range from 0 to 125 mA. Energoblock type PZ EB 15 generates an electron beam with a maximum power of 15 kW with a welding current from 0 to 250 mA at a voltage of 60 kV. The power block type PZ EB 30 generates an electron beam with a maximum power of 30 kW with a maximum electron beam current of 500 mA at an accelerating voltage of 60 kV. In fig. 1 is presented mechanical construction of energy blocks. The three performance lines of energy blocks are conceptually built on the same basis, they differ in their internal electronic equipment.

The high-voltage source of the accelerating voltage is of the inverter type and consists of the following main parts:

1) Vn transformer with rectifier, filter capacitors and measuring circuits, located in a separate container insulated with transformer oil.
2) Medium-frequency converter with a series-parallel resonant circuit, with a frequency of 20 kHz.
3) Control, regulation, safety and measurement circuits

Excitation of the high-voltage transformer is realized by a medium-frequency inverter. In this solution, the excitation signal is created by alternating switching of transistors T1, T4 and T2, T3 in the bridge, which creates an alternating voltage of a rectangular waveform of constant frequency in the diagonal of the bridge. This voltage is connected to the primary high voltage (HV) winding through a series-parallel resonant LC circuit, which will ensure an almost ideal harmonic course of the excitation voltage and more efficient energy transfer. Voltage stabilization and power regulation of the HV source is solved by changing the switching width of the transistors, which enables regulatory intervention at the level of a few milliseconds. The advantage of this connection is the use of a constant switching frequency of the excitation current, which, when choosing a suitable filtering capacity of the secondary circuit, makes it possible to achieve a very low ripple of the acceleration voltage. With a nominal source power of 30 kW and a switching frequency of 20 kHz is the measured value of the welding voltage ripple at the level of ± 1.0% An optional additional module to the HV source is electronic anti-discharge protection. The electrical diagram of the HV source type PZ EB 30 kW is shown in fig. 2.

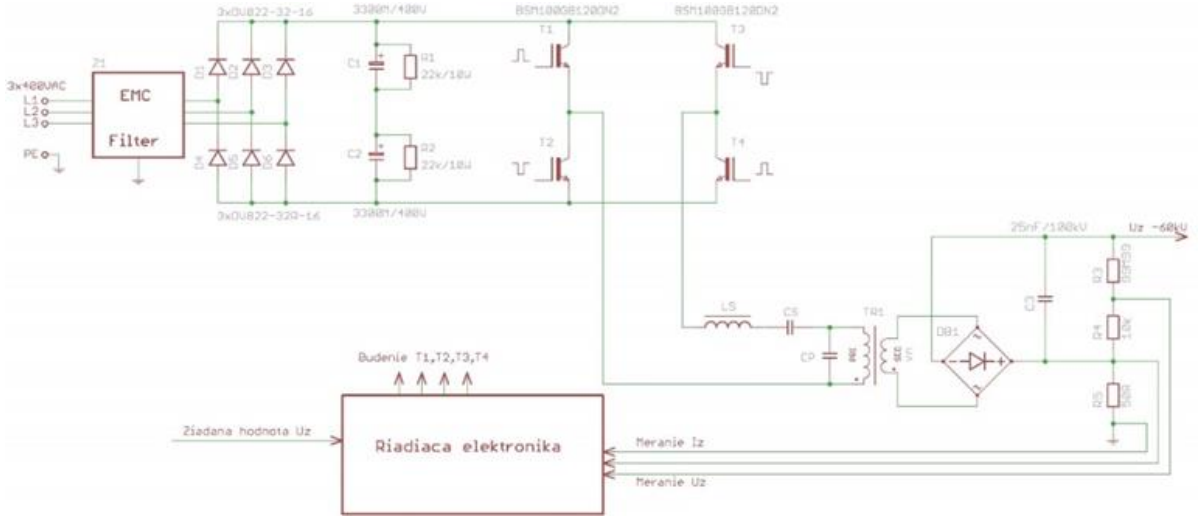

Fig. 2. Electrical diagram of the HV source type PZ EB 30 kW

Auxiliary sources serve to generate the electron beam and set the required welding parameters. They enable manual, automatic and programmatic control of the welding current, focusing current and deflection of the electron beam. The group of auxiliary sources includes filament current source, cathode bombardment current source, control electrode voltage source, focusing current source and deflection source.
Typical technical parameters of the Energoblocks are as follows:

- The magnitude of the accelerating voltage is adjustable from 30 kV to 60 kV.
- The max. power of the electron beam accord. to the type is 7.5, 15, 30 kW.
- Stability of acceleration voltage maximum ± 0.15%.
- Acceleration voltage ripple maximum 1.4%.
- Stability of the welding current maximum ± 0.4% (in the range 5-250mA).
- Ripple of the welding current maximum ± 1.5%.
- Stability of focusing current maximum ± 0.16%.

2.2. ELECTRON GUN MODULE

The electron gun is used to generate, control and adjust a powerful electron beam for the technological operations of welding and surface treatment of metal materials (Kolenic et al., 2016). It is the most important node of the electron beam welding equipment. The energy needed to create the electron beam is supplied from the energy block. The cannon and the energy block must be mutually compatible. We distinguish atmospheric type electron guns and guns intended for use in a vacuum. Atmospheric guns are placed on the wall of the welding chamber, with which they are vacuum-tightly connected. They are mostly connected

statically to the welding chamber, and the weld joint is created in such a way that the welded part moves in relation to the electron beam. Atmospheric electron guns have the same design for all power levels, the difference is the type of cathode and the power of the HV source. An example of the construction of an atmospheric gun is shown in fig. 3.

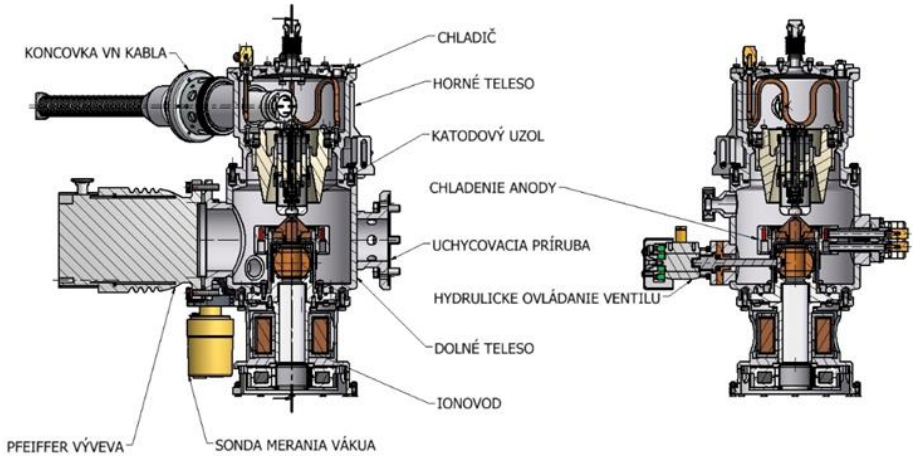

Fig. 3. Atmospheric gun module design

The electron gun cannot properly perform the welding function until it is equipped with additional modules that enable its applicability in welding performance. These are additional modules that allow precise adjustment of the beam to the weld joint. This is realized by a module for observing the welding process using a camera and a module for lighting the weld joint area. These modules, together with the body of the cannon, are attached to a common base and form a separate unit. An example of the configuration of the placement of auxiliary modules on a common base with the cannon is shown in fig. 4.

Fig. 4. Location of auxiliary cannon modules

From a design point of view, the differences between the atmospheric electron gun and the vacuum electron gun are minimal, consisting of minor differences in the sealing of the internal space of the works. Bigger differences are only in the vacuum pumping system of both works. The atmospheric electron gun is pumped by a turbomolecular pump, which is additionally pumped by a rotary pump. The electron gun is pumped into a vacuum only by a turbomolecular pump, while a rotary pump is not necessary, because pumping is ensured by the vacuum system of the welding chamber. The design of the vacuum electron gun is shown in fig. no. 5.

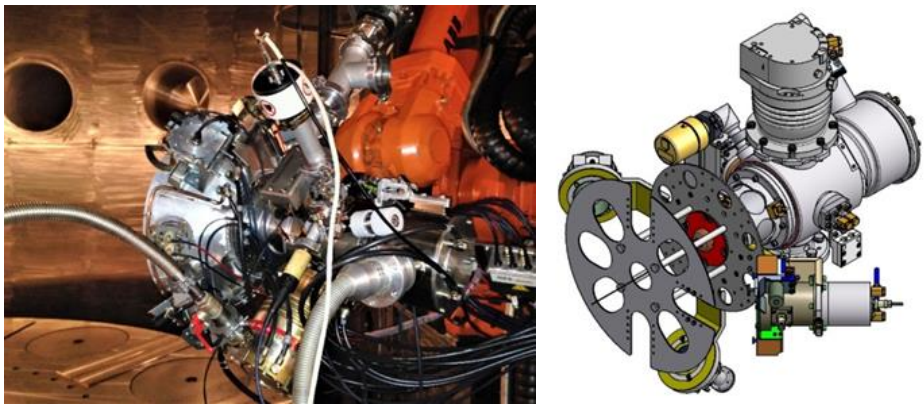

Fig. 5. Design of a vacuum electron gun

Another important condition for the correct operation of this type of electron gun is its positioning in the welding position in the vacuum welding chamber.

2.3 VACUUM ELECTRON GUN POSITIONING MODULE

Two types of vacuum gun positioning modules are solved in PRVA ZVARACSKA. Conceptually, they are different as well as in the way of application. For medium-sized vacuum chambers, a two-axis positioning model in the Cartesian coordinate system with the addition of a manual or fully controlled rotation axis is proposed. The design of a two-axis module with a manual rotation axis is shown in Fig. 6. The x and z axes are fully program-controlled axes that ensure the programmed positioning of the vacuum gun in the x-z plane. The tilting of the gun in the rotation axis is manual. It is used for the realization of linear welds and, in combination with an additional rotary positioner, also for the realization of face and circumferential rotary welds. The presented concept enables the placement of the feeding mechanism for additive manufacturing using additional material in the form of wire. The practical use of this type of positioning system is shown in fig. 7.

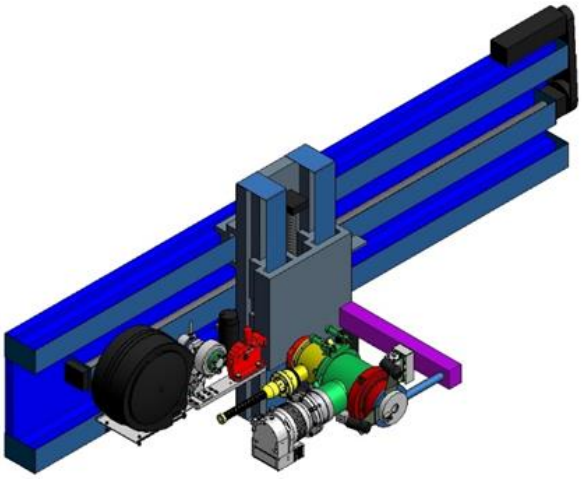

Fig. 6. Design of the vacuum gun positioning module

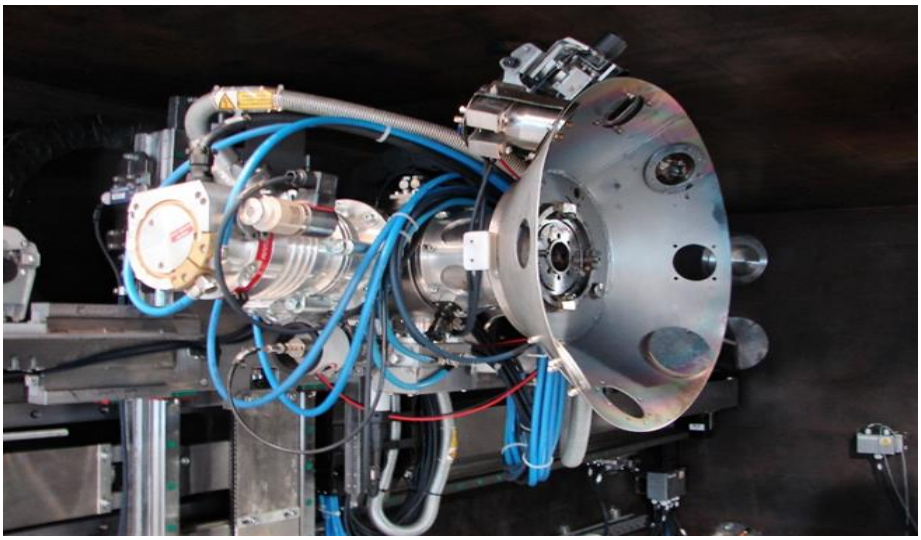

Fig. 7. Practical application of the vacuum gun positioning module

2.4 VACUUM CHAMBER MODULES

In most cases, vacuum chambers are designed using the "fit for purpose" method, i.e. tailor-made for a potential customer. The size and shape of the welding chamber determines the size of the welded parts, the required pumping time to the working vacuum and the electron gun used. The unifying element of welding chamber modules is technological preparation and production technology. Welding chambers must be vacuum-tight, resistant to deformation, they must have a uniform system developed for sealing static flanges and door systems, as well as for sealing moving parts, such as the movement of an atmospheric gun under vacuum. Basically, we divide them into universal and highly productive.
An example of a solution for a universal chamber with a content of 16 m3 is shown in fig. 8.

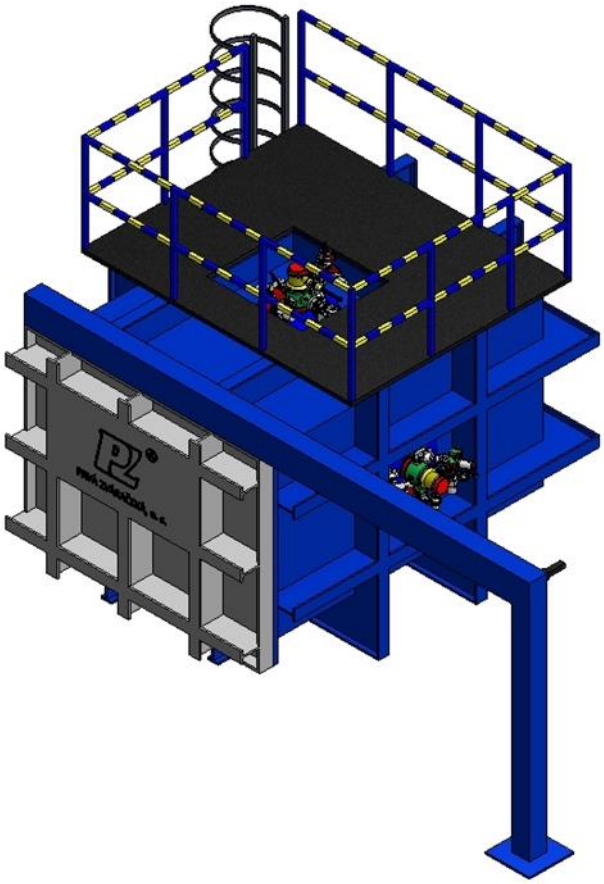

Fig. 8. Example of a universal chamber with a content of 16 m3

Welding chambers designed for highly productive welding must meet the condition of high efficiency. They are intended for welding a large number of identical parts with small dimensional differences. In most cases, they consist of a vacuum welding chamber and one or more auxiliary chambers. Such a design allows the welding chamber to be permanently exhausted to a working vacuum during welding. The auxiliary chambers ensure the function of loading and unloading the weldments as well as the function of aerating and exhausting the auxiliary chamber. During one work shift, the ratio of net welding time to handling and preparation time is at the level of 80%. An example of a modular welding chamber concept for highly productive welding is shown in Fig. 9.

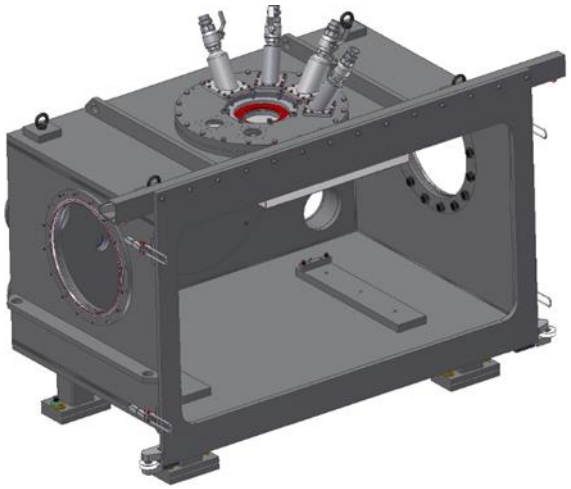

Fig. 9. An example of the design of the welding chamber of a highly productive welding machine

From the presented examples of the design of structural modules of electron beam devices, it is possible to clarify the concept of modular design, which the PRVA ZVARACSKA company uses in the design, construction and production of electron beam devices of various purposes for external customers. This concept proved to be sufficiently flexible, economical and creates conditions for the supply of equipment for external customers in the shortest possible time and in high quality.

2.5 SELECTED EXAMPLES OF THE DESIGN OF ELECTRON BEAM DEVICES

The PZ EZ 30 TWINBEAM welding workplace with a welding chamber volume of 16 m3 is shown as an example of a modular construction. It is intended for welding thin-walled and thick-walled (up to 80 mm) parts in medium vacuum. Construction modules designed for beam power up to 30 kW were used in the construction of the device.

This device, in addition to welding, also enables heat treatment of the surfaces of metal materials and additive manufacturing using additional material in the form of wire. The complex electron beam workplace is equipped with two guns, while it is possible to weld with one gun or two parts at the same time. The time for pumping the vacuum chamber to working vacuum is a maximum of 25 min. To position welds during welding, the vacuum chamber is equipped with an X-Y positioning table, which is integrated with a system for loading and unloading welds into and out of the vacuum chamber, a rotary positioning system, as well as a welding wire feeding system. The overall view of the workplace is shown in fig. 10.

Fig. 10. Welding workplace PZ EZ 30 TWINBEAM

3 CONCLUSION

The aim of the contribution is to present a comprehensive concept of the design and realization of supplies of sophisticated technological equipment and complexes that use modern electron beam technologies with a high degree of automation. Based on the presented results, we can characterize the modular design system as flexible and economically efficient. In this system, unified modules are used as basic building elements, which represent separate functional units that are fully compatible with other modules of the technological complex in terms of hardware and software. The system has the potential to be used on a wider scale in the design and production of universal and single-purpose equipment in the segment of general engineering.

ACKNOWLEDGEMENTS

This work was supported by Agency for the Support of Research and Development under the Contract No. APVV-20-0100.

REFERENCES

Schultz H.: Electron Beam Welding, Cambridge: Abingdon Publishing, England, 2004, ISBN 1-85573-050 2.

Kolenič F.: Large Chamber EBW Machine Using 9 Axes Robotic System for Positioning of Electron Gun and Weldment in Vacuum, 67th IIW International Conference,13th~18th July, 2014, Seoul, Korea.

Kolenič F., Faragula P., Maštalír P.: Modernizácia modulov elektrónového dela umiestneného vo vnútri vákuovej komora, Zvárač XIII/2016, s. 16-19, ISSN 1336-5045.

Kolenič F., Kováč L.: Nová generácia elektrónovolúčových zariadení s výkonom do 30 kW, Zvárač VIII/2/2011, s. 22-24, ISSN 1336-5045.

WELDING CURRENT REGULATOR IN HIGHLY PRODUCTIVE ELECTRON BEAM WELDING SYSTEMS

Ing. Peter Koršňák[1]
Ing. Roman Darovec[2]
Ing. Daniel Kunštek [3]
Ing. Rastislav Sekerka[4]
[1]ORCID: 0000-0003-2771-556X, PRVÁ ZVÁRAČSKÁ, **Slovakia**
[2]ORCID: 0000-0002-7570-864X, PRVÁ ZVÁRAČSKÁ, **Slovakia**
[3]ORCID: 0000-0001-5744-8816, PRVÁ ZVÁRAČSKÁ, **Slovakia**
[4]ORCID: 0000-0001-6968-367X, PRVÁ ZVÁRAČSKÁ, **Slovakia**

Abstract: The paper presents the principle of operation of PID controllers used in industrial automation and the concept of the circuit solution of the welding current controller of electron beam welding equipment. PID controllers are feedback control systems whose goal is to achieve accurate and stable control of a wide range of systems. They consist of three control members proportional, integrative and derivative, which react to the current deviation and generate a response. The paper describes the hardware connection of the welding current regulator using the principle of operation of the PID regulator, which significantly improves the performance and control of the dynamic processes of electron beam welding systems.

Keywords: Regulator, control loop, electron beam welding equipment

1 INTRODUCTION

Electron beam technologies find their application in various industries including aviation, automotive, medical device manufacturing and electronics. Electron beam welding is a highly precise welding technology that is particularly beneficial when joining materials that are difficult to weld using other methods. Its ability to create clean, strong and deep welds has made it an essential technology in a variety of high-tech and high-productivity industries. Due to increasing demands on productivity, reliability and quality in industries, continuous improvement of individual systems of electron beam welding equipment is necessary. It is therefore necessary to design individual systems in such a way that they achieve, control and maintain stable parameters during the entire electron beam welding process. In order to achieve these requirements, different types of regulators are used in the circuit connections of electron beam welding equipment systems, which are designed and adjusted to meet the

requirements of the given application. The greatest demands in terms of dynamic parameters, such as start-up speed, response time to changes and stability, are placed on the welding current controller. To meet these requirements and achieve the desired control performance, a PID controller was designed for welding current control, which is widely used as a feedback control system in engineering and automation. PID controllers are known for their simplicity, efficiency and adaptability to a wide range of control systems.

2 PID REGULATOR

The regulator is generally an input-output circuit widely used in industrial applications for continuous control of a certain process, the input of which is usually a measured and desired signal, or several signals, and the output is a control signal. The controller continuously calculates the error value as the difference between the setpoint and the measured process value and automatically applies an accurate and sensitive correction to the control function. The most used type is the so-called PID controller. PID (proportional integration derivative) controllers use a control loop feedback mechanism to control process variables and are the most accurate and stable controller.

A specific feature of the PID controller is the ability to use the three control elements of the proportional, integration and derivative circuit at the output of the controller to apply precise and optimal control. The block diagram (Fig. 1) shows the principle of how these circuits are connected and how they process individual signals.

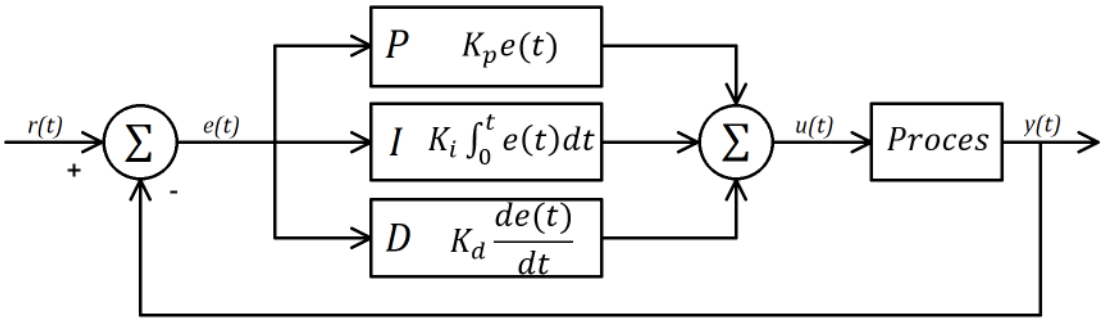

Fig. 1 Block diagram of the PID controller

The PID controller continuously calculates the error value e(t) as the difference between the desired value r(t) and the measured value y(t) and applies a correction based on proportional, integration and derivative terms.

$$e(t) = r(t) – y(t)$$

The controller tries to minimize the error over time by adjusting the control variable u(t).

Overall control function:

$$u(t) = K_p e(t) + K_i \int_0^t e(t)dt + K_d \frac{de(t)}{dt}$$

The term P (proportional component) is proportional to the actual value of the error e(t) and the control output will be proportionally large when using the gain factor Kp.
Term I (integration component) take into account the past values of the error e(t) and integrates them over time. If a residual error occurs after applying proportional control, the integrator tries to eliminate this error by adding a control effect due to the previous cumulative value of the error. When the error is removed, the integration term stops growing.
Term D is an estimate of the future trend of the error e(t) based on its current rate of change. It tries to reduce the effect of the error e(t) by applying the control influence generated by the rate of change of the error. The larger the error, the larger the control effect (Araki, 2009). When the error is changing rapidly, the derivative component generates a larger correction signal that dampens the oscillations and reduces overshoot. It is particularly useful in systems where it is necessary to react to rapid changes in the error signal. However, the derivative term can cause noise and instability in some systems, for example if there is high frequency noise in the system. Therefore, the derivative term should be set to suit the specific characteristics of the controlled system to avoid overcompensation and instability.
A balance of the effects of these members is achieved by tuning the loop to produce the optimum control function. Tuning the control loop means adjusting its control parameters to optimal values for the required control response. The tuning constants K must be derived for each control application because they depend on the response characteristics of the entire external controller loop. These are dependent on the behaviour of the measuring sensor, the final control element, possible delays of the control signal and the process itself. Approximate values of the constants can usually be specified initially knowing the type of application, but are usually refined or tuned by introducing the desired changes in the values of the constant K during the process and observing the response of the system. A balance of the effects of these members is achieved by tuning the loop to produce the optimum control function. Tuning the control loop means adjusting its control parameters to optimal values for the required control response. The tuning constants K must be derived for each control application because they depend on the response characteristics of the entire external controller loop. These are dependent on the behaviour of the measuring sensor, the final control element, possible delays of the control signal and the process itself. Approximate values of the constants can usually be specified initially knowing the type of application, but

are usually refined or tuned by introducing the desired changes in the values of the constant K during the process and observing the response of the system.
Optimal behaviour when changing a process or changing a setpoint varies by application. The two basic requirements for a controller are staying at a given setpoint (regulation) and tracking commands (implementation of setpoint changes). Specific criteria for tracking orders include rise time and settling time. Some processes must not allow the process variable to exceed the set value if, for example, it would be unsafe (Lipták, 2003).
Although a PID controller has three control members, some applications only need one or two members to provide adequate control. This is achieved by setting the unused parameters to zero and in the absence of other control members it is called a PI, PD, P or I controller. PI controllers are quite common in applications where the action of the derivative component would be sensitive to measurement noise, but the integration term is necessary for the system to reach its target value (Tan et al., 1999).

3 WELDING CURRENT REGULATOR IN ELECTRON BEAM WELDING SYSTEMS

Electron beam welding devices contain several regulators of different types, e.g., acceleration voltage regulator, welding current regulator, bombarding current regulator, etc. Different requirements are placed on them. In terms of dynamic parameters such as start-up speed, speed of response to value changes, stability and minimization of the level of overregulation, the welding current regulator must meet the highest demands. By setting its control variable u(t) at the output, it must ensure the most accurate course of the welding current according to the required course for the given application. In the ideal case, this means ensuring the generation of the welding current without a delay compared to the desired value, without over-regulation and with an immediate change of value according to the desired course of the given process. In real conditions, it is impossible to achieve such a state. The response time to a change does not depend only on the speed of the regulator, but on the entire system for controlling the size of the welding current, that is, also on the response speed of the voltage source for the control electrode.
With the previous version of the welding current regulator, it was necessary to adjust its response speed to suit the given application. In welding processes, where the fastest possible rise of the welding current to the desired value or a sudden change in the value of the welding current is necessary, it was necessary to set a fast response of the regulator, which resulted in a certain exceeding of the desired value of the welding current - overregulation. In such cases, it is necessary to consider to what extent it is permissible to exceed the value of the welding current in the given process, so that errors do not occur in the weld joint. If exceeding the desired value of the welding current during start-up or a step change was unacceptable, the response of the controller was slowed down and thus there was a greater delay in the response of the entire system for controlling the size of the

welding current. In such cases, it was necessary to take into account the size of the delay when planning the welding processes and movements. If the given application allows it, a suitable solution to these shortcomings of the controller is the use of the so-called the slope of the welding current, when the welding current rises smoothly from zero value to the required value in a certain time, this defines the steepness of the start-up. With such a gradual start-up of the welding current, it is possible to speed up the response of the controller, thereby reducing the delay time and reducing the amount of overregulation during the start-up of the welding current. However, not every application allows using a long enough time to ramp the welding current to the required value, and if the steepness of the ramp is too large, the problem of over-regulation above the required value occurs again. Therefore, a new topology of the welding current regulator with higher control dynamics was proposed, which eliminates the above-mentioned shortcomings, minimizes the size of the exceedance of the desired value during start-up and shortens the response delay time. When designing the controller with higher control dynamics, emphasis was placed on backward compatibility with devices in which the previous version of the controller was used, and therefore it is possible to replace them without interfering with the connection of existing devices.

Fig 2 shows the circuit diagram of the welding current PID controller with higher control dynamics.

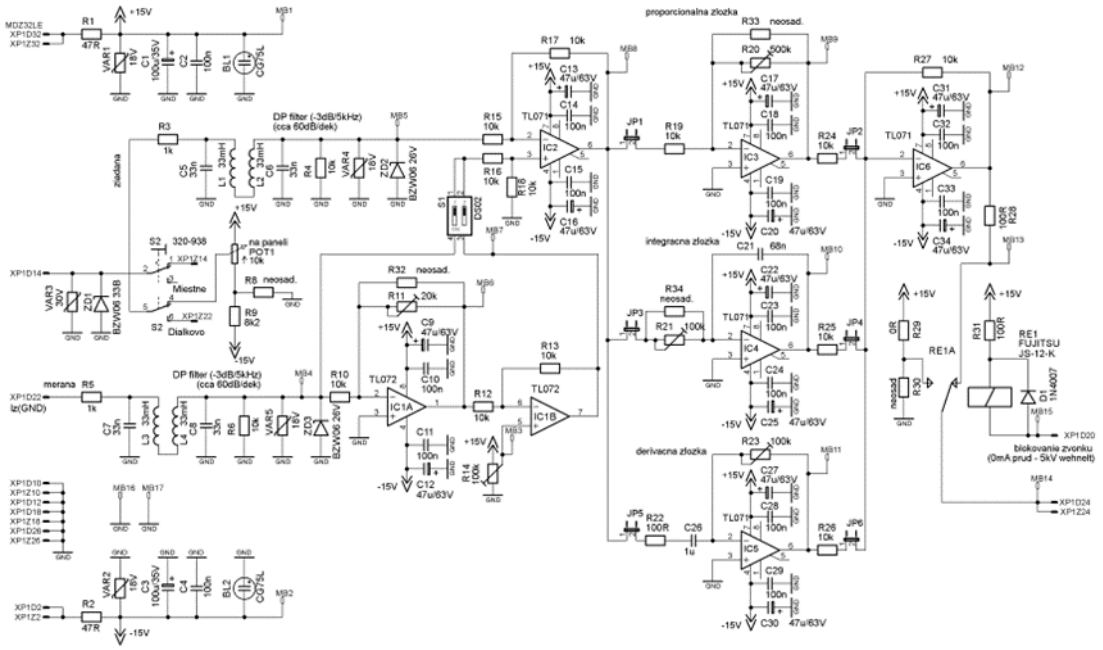

Fig. 2 Circuit diagram of the connection of the PID controller

The controller includes low-pass filtering for the setpoint and measured value to remove high-frequency noise components and thus prevent unwanted changes in the output. The calculation of the difference between the desired and the measured value of the welding current is realized using the operational amplifier IC2 TL071 connected as a differential amplifier, which amplifies the difference between the two input voltages. The amount of amplification is given by the ratio of pairs of resistors R17/R15 and R18/R16. The calculated difference (error value e(t)) is fed to the individual inputs of the PID controller members, where their response is generated according to the size of the set constants Kp, Ki and Kd. Operational amplifier IC6 TL071, connected as a summing amplifier, performs the algebraic sum of the output voltages of the individual members of the PID controller. This means that the output voltage of the summing amplifier is proportional to the sum of the voltages at its input. This output voltage represents the control variable u(t).

Controller tuning involves selecting appropriate values for the proportional, integral, and derivative gain constants (Kp, Ki, and Kd) to achieve the desired control performance. The tuning process is often iterative and experimentation may be necessary in tuning to ensure a balance between speed of response, stability and minimization of oscillations.

In fig. 3 shows the waveforms of the measured (yellow waveform) and desired (blue waveform) value of the welding current Iz when ramping up to a value of 50mA. The delay between the onset of the desired value and the onset of the measured value is caused by the response of the entire control loop. The size of the response depends on the speed of the controller's response and on the speed of the final control element, in this case on the speed of change of the voltage on the control electrode.

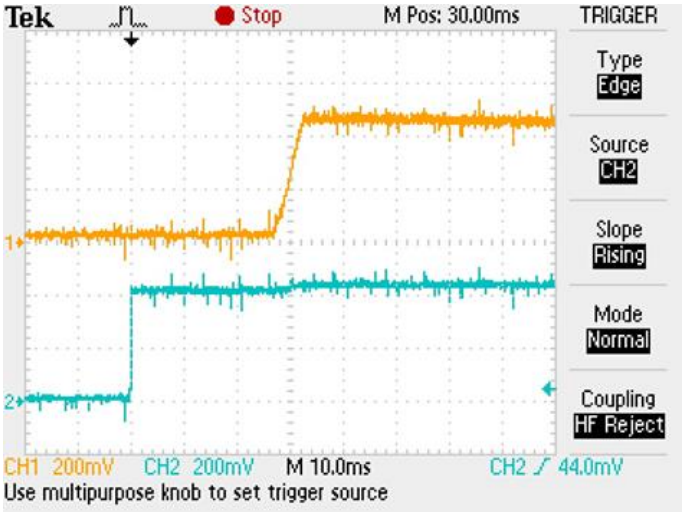

Fig. 3 Starting welding current Iz = 50mA, course of measured and desired value

Fig. 4 shows the course of the output of the regulator (blue) and the course of the rise of the welding current Iz (yellow) to the value of 50mA. The proportional component of the controller reacts the fastest to the change in input parameters (change in the desired value), which is represented by a step change in the voltage at the output of the controller from positive saturation to a value of 0V. At the same time, the influence of the integration component of the regulator begins to be applied, which manifests itself as a smooth drop in voltage up to the value of negative saturation of the regulator output. The size of the step change of the proportional component and the steepness of the decline of the integration component is given by the set coefficients Kp and Ki. The entire process of transition of the regulator output from positive saturation to negative saturation takes 22 ms. During this time, the voltage on the control electrode starts to drop, which controls the flow of electrons emitting from the LaB6 cathode and thus the size of the welding current Iz. Another 6 ms takes until the filter capacities on the voltage source for the control electrode are discharged and the voltage on it drops to such a level that electrons start to be emitted and the size of the welding current and thus the size of the measured value entering the controller circuit starts to rise. The controller reacts to this change in the measured value by changing the output voltage to such a level that a stable desired value of the welding current is ensured during the entire process. It takes another 6 ms to reach the required value of the welding current. The entire process of starting the welding current is therefore delayed by 34 ms.

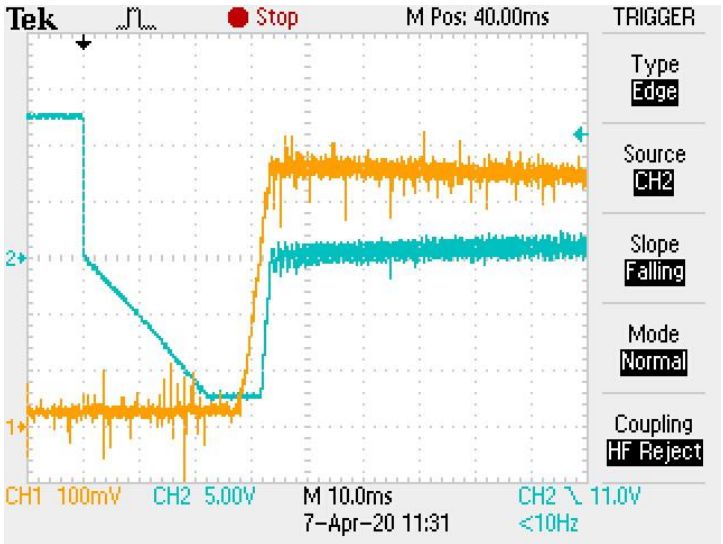

Fig. 4 Start of the welding current Iz = 50mA, the course of the measured value and the output voltage of the regulator with higher control dynamics

For comparison, fig. 5 shows the start-up of the welding current of the original controller, in which only the integration component was applied at the output. The steepness of the change of this component is defined by the size of the set coefficient Ki and the size of the voltage difference between the measured and desired value of the welding current amplified by the proportional component connected in series before the integration element. The entire start-up process from the beginning of the voltage changes at the regulator output to the stabilization of the welding current value at Iz = 50mA takes approximately 54 ms, which is 20 ms more than with a regulator with higher control dynamics. In percentage terms, the regulator with higher control dynamics has a 37% faster ramp-up of the welding current to the required value compared to the original regulator.

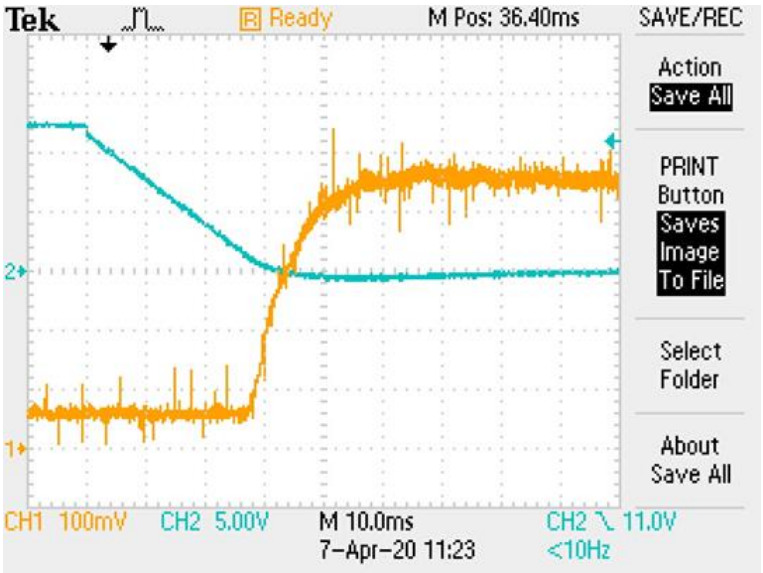

Fig. 5 Start of the welding current Iz = 50mA, the course of the measured value and the output voltage of the original regulator

Another advantage of the regulator with higher control dynamics compared to the original regulator is the minimum exceeding of the required value of the welding current. In fig. 6 on the left is the course of the measured value of the welding current (yellow course) and the output voltage (blue course) of the original regulator. When the welding current rises to the value of Iz = 80 mA, the original controller does not react quickly enough to the sharp increase in the measured value, resulting in the welding current being exceeded up to the value of 140 mA, and the time for the welding current to settle to the required value was extended to 58 ms. Such overregulation is a frequent cause of defects in the weld joint. The curves in fig. 6 on the right show the onset of the welding current Iz = 80mA with a regulator

with higher control dynamics. In this case, there is only a minimal overregulation to a value of approximately 82mA.

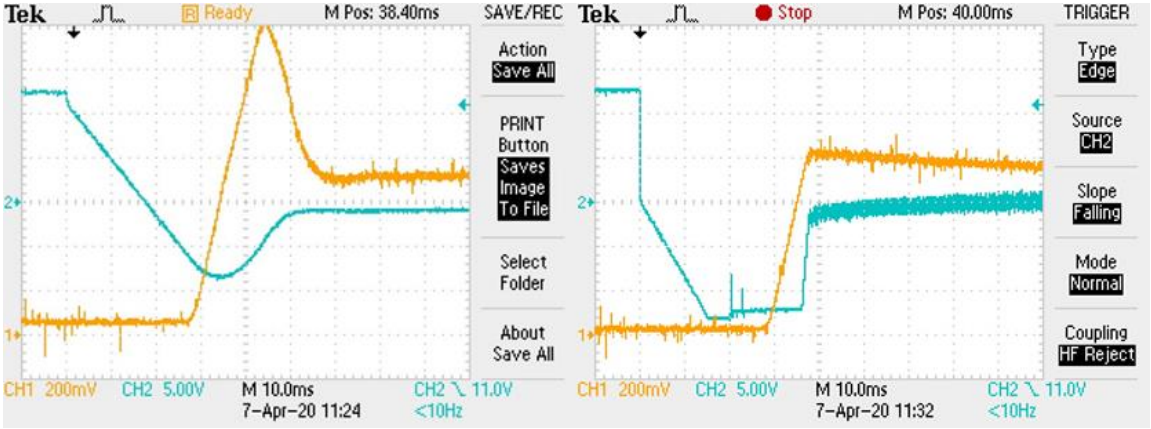

Fig. 6 Comparison of the starting welding current Iz = 80mA of the original controller (left) and the controller with higher control dynamics (right), the course of the measured value and the output voltage of the controller

The disadvantage of the original welding current regulator is also the different stabilization time of the welding current at different desired values. A regulator with higher control dynamics has only minimal time differences in the rise of the welding current for different required values. For a better comparison of both controllers, the coefficient of the integration component was set to such a value that the ramp-up of the integration component of both controllers was the same. The ramp-up time is approximately the same for both controllers for the desired value of the welding current Iz = 50mA, but as the desired value of the welding current increases, the time required to reach a stable desired value increases with the original controller and the amount of overregulation above the desired value increases. Thanks to its fast response, the regulator with higher control dynamics eliminates the occurrence of overregulation.

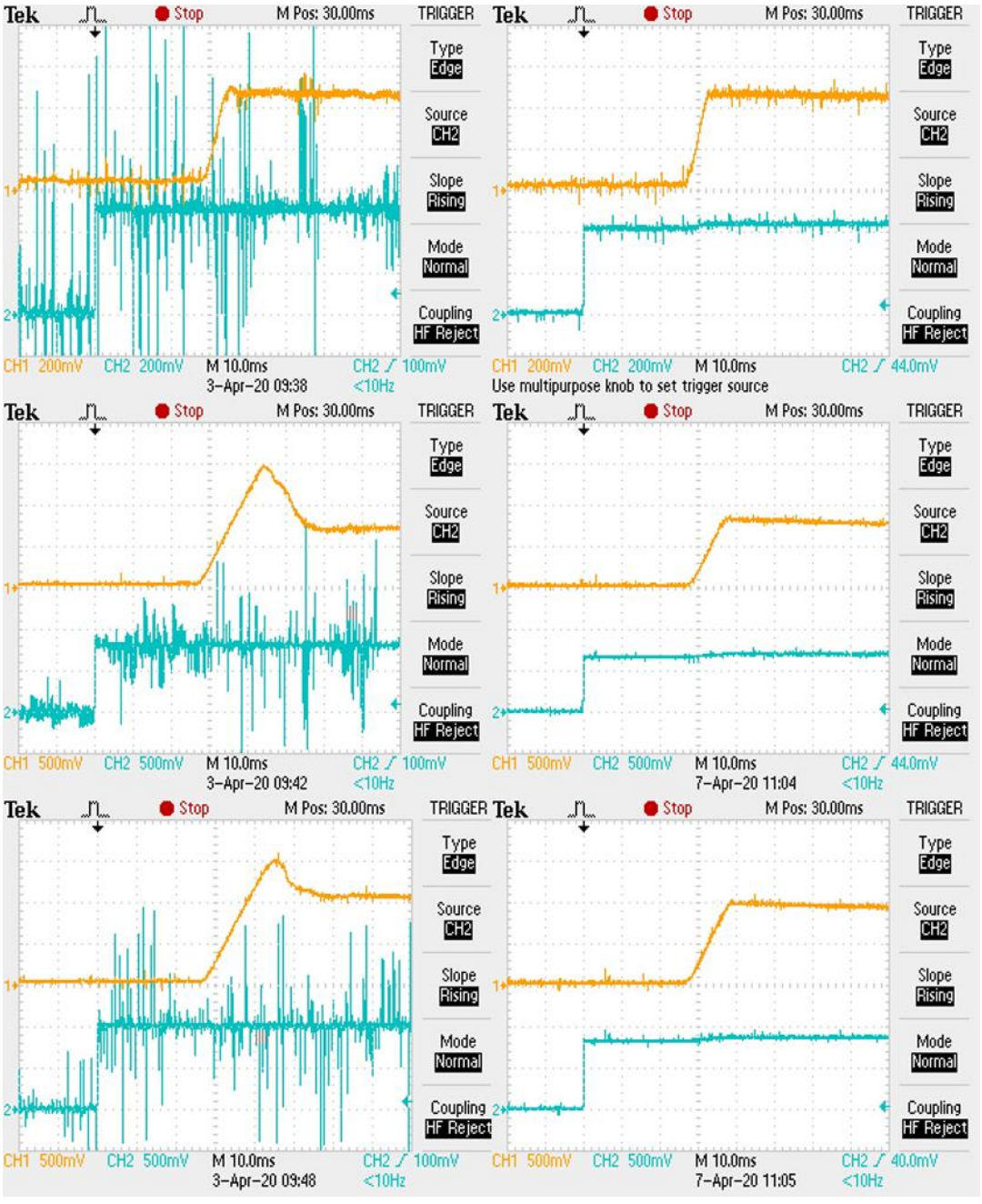

Fig. 7 Comparison of welding current surges of the original controller (left) and a controller with higher control dynamics (right)

Table 1 Comparison of welding current rise times for the original controller and a controller with higher control dynamics

Desired value of the welding current Iz	50mA	80mA	100mA
Start-up time - original regulator	36 ms	56 ms	60 ms
Start-up time - regulator with higher control dynamics	34 ms	36 ms	38 ms

The electronics of the Iz controller with higher control dynamics is implemented on a printed circuit board in a modular design with the control brought out on the front panel. The board is made in the standard for insertion into a 19" module, the size of the module is 100x160mm.

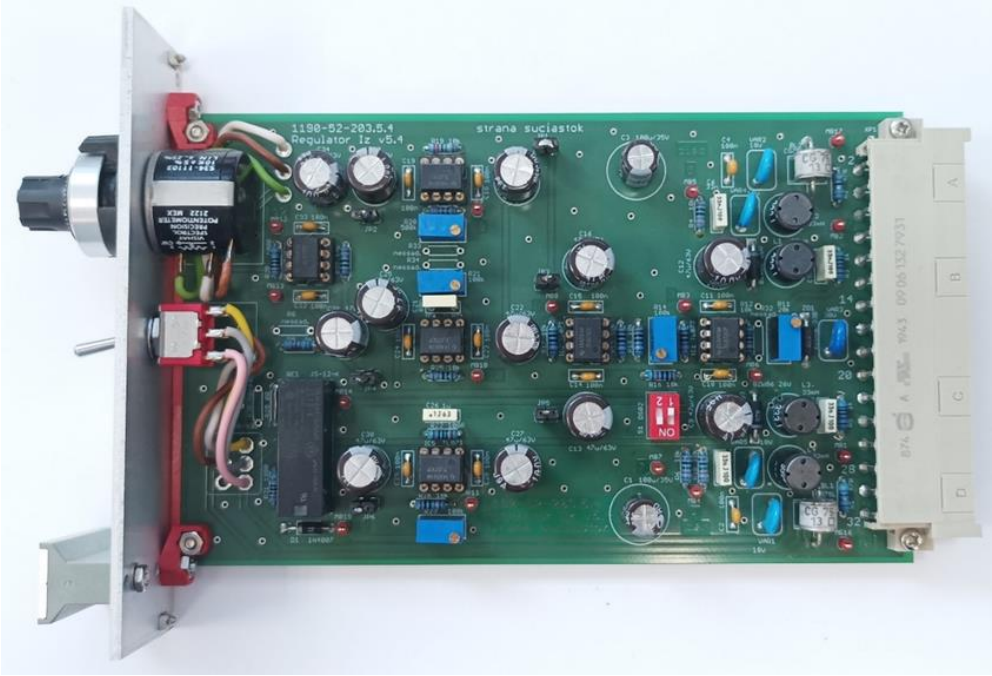

Fig. 8 Circuit board of the welding current regulator with higher control dynamics

4 CONCLUSION

A significant improvement in the dynamic parameters of electron beam welding equipment was achieved with the new concept of the circuit connection of the welding current regulator. By appropriately setting the individual gain coefficients of the PID controller, a higher control dynamic was achieved compared to the previous solution of the welding current controller. However, from the experiments and measured waveforms, it follows the necessity of

improving the dynamic parameters of the next node of the electron beam control and generation system, namely the Wehnelt voltage source. This source generates voltage for the control electrode, which controls the flow of electrons from the electron gun, and represents another important circuit determining the dynamic parameters of electron beam welding systems.

ACKNOWLEDGEMENTS

This work was supported by Agency for the Support of Research and Development under the Contract No. APVV-18-0402.

REFERENCES

Araki, M. (2009). "CONTROL SYSTEMS, ROBOTICS AND AUTOMATION – Volume VII - PID Control" (PDF). Japan: Kyoto University.

Lipták, Béla G. (2003). Instrument Engineers' Handbook: Process control and optimization (4th ed.). CRC Press. p. 108. ISBN 0-8493-1081-4.

Tan, Kok Kiong; Wang Qing-Guo; Hang Chang Chieh (1999). Advances in PID Control. London, UK: Springer-Verlag. ISBN 978-1-85233-138-2.

STRUCTURAL ANALYSIS AND CORROSION PROPERTIES OF MATERIALS USED FOR CONSTRUCTIONS

Ing. Lukáš Válek[1]
Prof. Ing. Mária Dománková, PhD.[2]
Assoc. prof. Ing. Jozef Bárta, PhD.[3]
[1]ORCID: Slovak University of Technology, Faculty of Materials Science and Technology in Trnava, **Slovakia**
[2]0000-0002-0595-1943: Slovak University of Technology, Faculty of Materials Science and Technology in Trnava, **Slovakia**
[3]0000-0003-0607-4433: Slovak University of Technology, Faculty of Materials Science and Technology in Trnava, **Slovakia**

Abstract: Semi-finished products made of austenitic stainless steel are commonly used today, primarily in the food industry. These materials are often exposed to extreme corrosive environments. The article focuses on the structural analysis and corrosion resistance of these semi-finished products. Six samples were analyzed - macrostructure and microstructure analysis of weld joints on profiles were performed using optical microscopy, as well as corrosion testing according to ASTM A262 Method A. Based on the material analysis, it can be observed that defects such as lack of fusion, cracks, or root penetration were observed on the samples. Samples 1, 3, and 5 were susceptible to intergranular corrosion. Samples 2, 4, and 6 exhibited a structure that is not susceptible to intergranular corrosion. In the case of some samples, the corrosion test revealed an inappropriate microstructure that did not correspond to the state after solution annealing.

Keywords: Stainless steel, welding, corrosion test ASTM A262 method A, intergranular corrosion, secondary phases

1 INTRODUCTION

Owing to their excellent mechanical properties and corrosion resistance, austenitic stainless steels have been extensively used in vessels, as well as in the petrochemical, aerospace, nuclear, and chemical industries [1–8]. The relatively high chromium (Cr) and molybdenum (Mo) contents of these steels provide high corrosion resistance. Nowadays, various welding methods are used to join corrosion resistant steels. Most of the arc welding technologies as

well as beam technologies were successfully applied to weld these materials. Biggest difference in application potential of these technologies is in heat input. Most common technologies used to weld stainless steels are TIG welding or laser beam welding. TIG welding is mainly applied in hand workshops whereas the Laser beam welding is applied in industrial applications that require high productivity.
Weld joints produced by laser beam welding exhibit better corrosion resistance [9,10] with a narrow weld width and low residual stresses [11]. However, pore formation and thermal cracking generally occur during laser welding because of rapid cooling [12,13], leading to inhomogeneity in the weld microstructure and properties [10].
Welding process may cause austenite to be unstable in temperature range from 873 to 1173 K due to formation of Cr-rich carbides and intermetallic phases, such as the sigma phase and chi phase at grain boundaries [14–22]. Intergranular corrosion (IGC) of austenitic stainless steel is a conventional and serious problem as sensitization can occur with welding, heat treatment (e.g. post weld, stress relief) [23]. Cr-rich carbides precipitate adjacent to grain boundaries, and the corresponding Cr-depleted zone is susceptible to attacks in a corrosive medium, thereby resulting in IGC.

2 METHODOLOGY OF RESEARCH

Material analysis involved the submission of 6 samples of various semi-finished products made of austenitic stainless steel AISI 316 (X6CrNiMo) with the specified chemical composition as shown in Table 1. Table 2 provides the dimensions of all analyzed products with their respective labels.

Table 1 Typical chemical composition of AISI 316 steel [24]

Chemical composition of AISI 316 steel [wt.%]								
C	**Mn**	**Si**	**Cr**	**Ni**	**Mo**	**S**	**P**	**Fe**
max. 0.07	max. 2.00	max. 1.00	16,5 - 18.5	10,5 - 13.5	2,0 - 2.5	max. 0.03	max. 0.045	bal

Table 2 Dimensions of Analyzed Semi-finished Products

Sample number	**Type of semi-finished product**
1	Profile 80 x 80 x 4
2	Profile 80 x 140 x 4
3	Profile 80 x 160 x 4
4	Profile 80 x 40 x 4
5	Profile Ø 60 x 3,5
6	Profile Ø 76.1 x 3.6

The material analysis was focused on the evaluation of structural analysis of weld joints, corrosion resistance (according to ASTM A262 method A) on the surface and in cross-sections of samples.

Sample preparation was carried out using standard metallographic procedures. Cooling fluid was applied to the cutting wheel to prevent material overheating, which could potentially alter the structural properties at the cut location. After sample extraction, heat mounting was performed using a Buehler SimpliMet 1000 instrument. The mounted samples were wet-grinded using Buehler AutoMet 300 equipment with SiC abrasive discs of different grit sizes (240, 600, and 1200). Subsequently, the ground samples were polished on the same device. The samples were first polished using 9 μm diamond suspension with the simultaneous addition of lubricant. The same procedure was used with 3 μm diamond suspension. The final step was electrochemical polishing using a Buehler Vibromet 2 instrument with 0.05 μm MasterPrep polishing suspension for 15 minutes. After polishing, the samples were rinsed under running water using cotton, cleaned with ethanol, and dried with hot air.

After thorough rinsing and drying, the samples underwent electrolytic etching, which also served as a corrosion test. Etching was carried out in 10% sulfuric acid. The sample was connected to the positive pole, while the negative pole was immersed freely in the electrolyte. Etching was performed for 90 seconds at a voltage of 10 V and a current density of 1 A/cm². The resulting "etched" sample facilitates the evaluation and classification of the degree of attack after visualization using a light microscope. The continuity of etched grain boundaries is observed, typically at a magnification of 250 times. According to ASTM A262 method A [25], the attack is evaluated as shown in Figure 1.

- Step Structure – in case of the absence of chromium-rich carbides at the grain boundaries; different dissolution rates of differently oriented grains of the material result only in the formation of steps between individual grains,
- Dual Structure – with some pits at grain boundaries, without pits surrounding the entire grain, indicating partial precipitation at the boundaries,
- Ditch structure - when the grain boundary contains such a quantity of chromium carbides that the pits after the test merge into a continuous groove enclosing at least one grain.

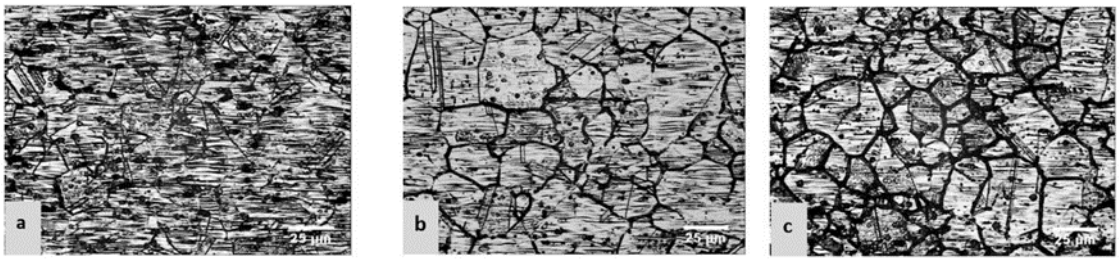

Fig. 1 Examples of microstructures after the application of the corrosion test in austenitic stainless steel: a) step, b) dual, c) ditch

Materials with microstructures classified as step or dual can be recommended for operation according to ASTM A262 method A standard. The evaluation of microstructure character after the corrosion test was performed using a Neophot 32 optical microscope.

3 RESULTS

Description of macrostructure: In the case of sample 1 (Figure 2a), a lack of fusion was observed in the central part of the weld joint and a crack in the root section. Such crack formation can create conditions for crevice corrosion in operation and also act as stress concentrators while loaded. In the case of samples 2 (Figure 2b), 4 (Figure 3a), and 5 (Figure 3b), an overflow of the weld joint root or the formation of sharp transitions were identified, which can serve as stress concentrators.

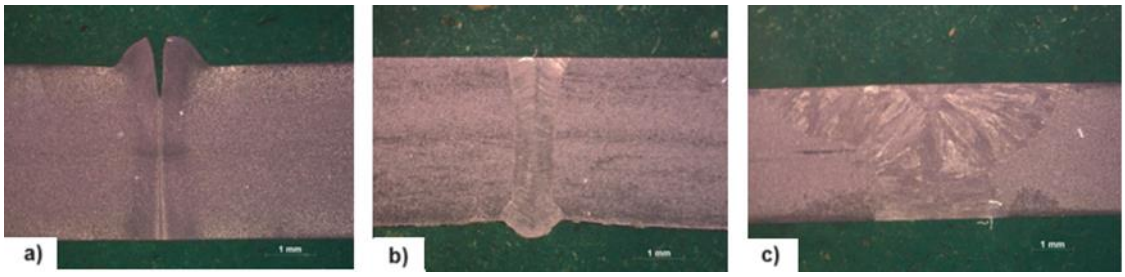

Fig.2 Macrostructural analysis results of samples:
a) Sample 1, b) Sample 2, c) Sample 3

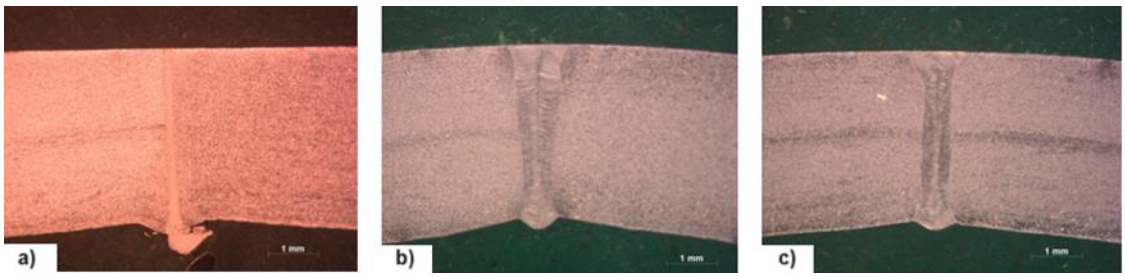

Fig. 3 Macrostructural analysis results of samples:
Sample 4, b) Sample 5, c) Sample 6

In the case of sample 1, the microstructure consists of austenite with a polyhedral morphology. As observed from the cross-section (Figure 4a), in the surface region up to a

depth of about 50 µm, the grain boundaries were clean without the presence of secondary phases. However, in the remaining part of the sample, the microstructure exhibits characteristics classified as ditch structure according to corrosion test standards (Figure 4b). The steel is therefore susceptible to intergranular corrosion. The observed microstructure does not correspond to the state after solution annealing. The weld metal (Figure 4c) has a dendritic morphology and is composed of austenite, which is typical for the austenitic steel microstructure after welding process.

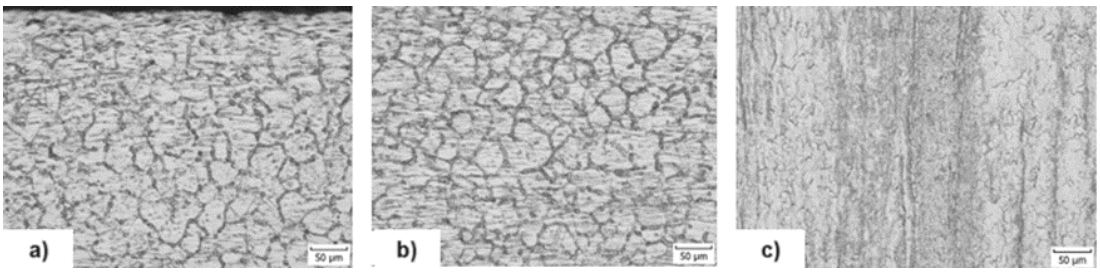

Fig. 4 Microstructure of Sample 1:
a) surface of the base material, b) middle part of the base material, c) weld metal of the joint

The microstructure of Sample 2 is composed of austenite with a polyhedral morphology. Grain boundaries are clean without the presence of secondary phases. Based on the corrosion test, the microstructure is classified as step structure, it is not susceptible to intergranular corrosion, and steel with such a microstructure exhibits good corrosion resistance. The microstructure characteristics correspond to the state after solution annealing, as documented in Figure 5.

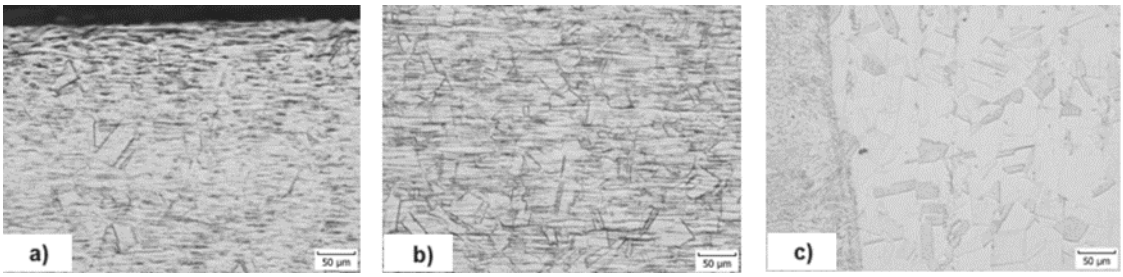

Fig. 5 Microstructure of sample 2:
a) surface of the base material, b) middle part of the base material, c) weld metal of the joint

The character of the microstructure in sample 3 is very similar to that of sample 1. The microstructure is composed of austenite with a polyhedral morphology. As observed from the cross-section (Figure 6a), in the surface region up to a depth of approximately 100 μm, the grain boundaries are clean without the presence of secondary phases. In the subsequent part, the microstructure exhibits characteristics classified as ditch structure based on the corrosion test (Figure 6b). The steel is susceptible to intergranular corrosion. The microstructure does not correspond to the state after solution annealing. The microstructure in the weld joint area can be observed in Fig. 6c.

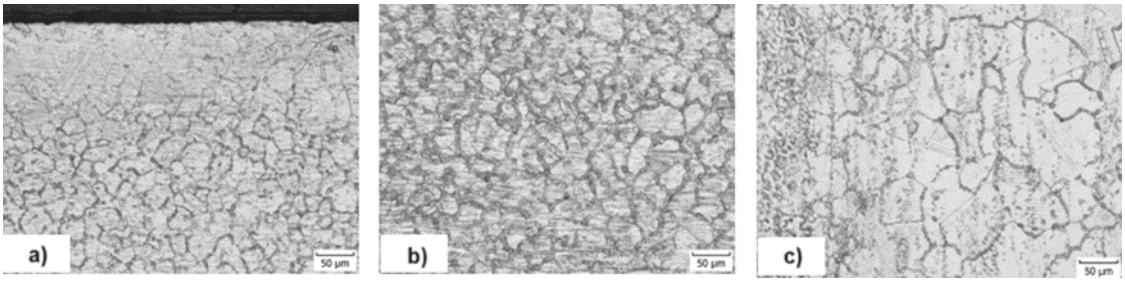

Fig. 6 Microstructure of Sample 3:
a) surface of the base material, b) middle part of the base material, c) weld metal of the joint

The microstructure of Sample 4 is composed of austenite, with occasional individual particles of secondary phases observed along some grain boundaries (Figure 7a, b). Based on the corrosion test, the microstructure is classified as dual structure. The steel is not susceptible to intergranular corrosion. The microstructure characteristics correspond to the state after solution annealing, although the duration of solution annealing should have been longer. In the central line of the weld metal, porosity can be observed (Figure 7c).

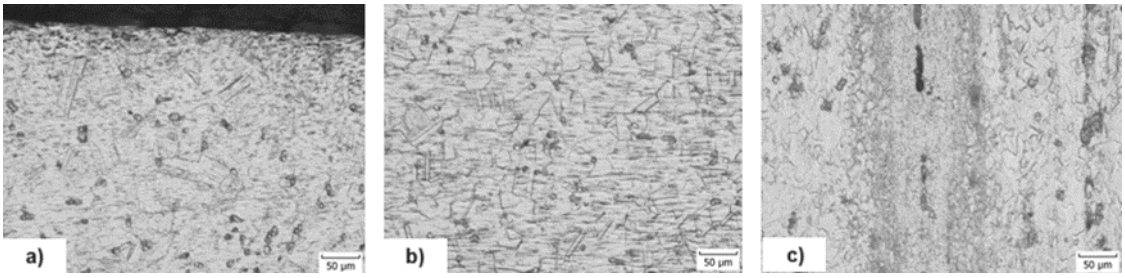

Fig.7 Microstructure of Sample 4:
edge of the sample, b) middle part of the sample, c) weld joint area – voids can be observed in the central line of the weld metal

The microstructure of Sample 5 is again very similar to that of Samples 1 and 3. The microstructure is composed of austenite with a polyhedral morphology. Throughout the sample cross-section (Figure 8a, b, c), secondary phases are precipitated along grain boundaries. Based on the corrosion test, the microstructure is classified as ditch structure. The steel is susceptible to intergranular corrosion. The microstructure does not correspond to the state after solution annealing. In the heat-affected zone (Figure 8c), partial dissolution of secondary phases occurred.

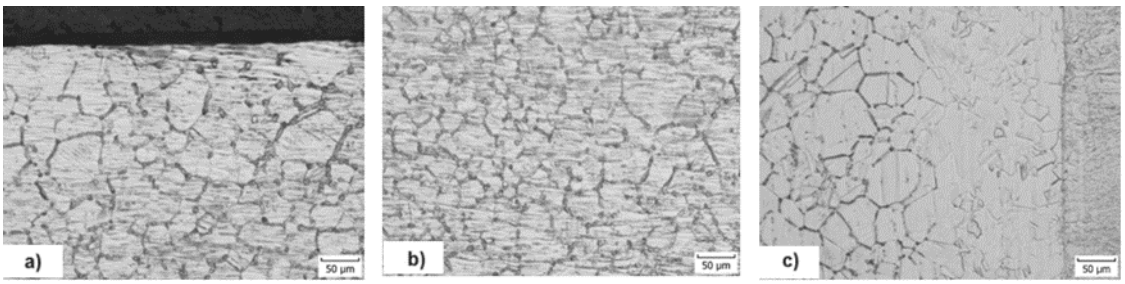

Fig. 8 Microstructure of Sample 5:
a) surface of the base material, b) middle part of the base material, c) weld metal of the joint

The microstructure of Sample 6 is very similar to that of Samples 2 and 4. The microstructure of the sample is composed of austenite with polyhedral morphology. Grain boundaries are clean without the presence of secondary phases (Figure 9a, b, c). Based on the corrosion test, the microstructure is classified as step structure. It is not susceptible to intergranular corrosion, and steel with such a microstructure exhibits good corrosion resistance. The microstructure characteristics correspond to the state after solution annealing.

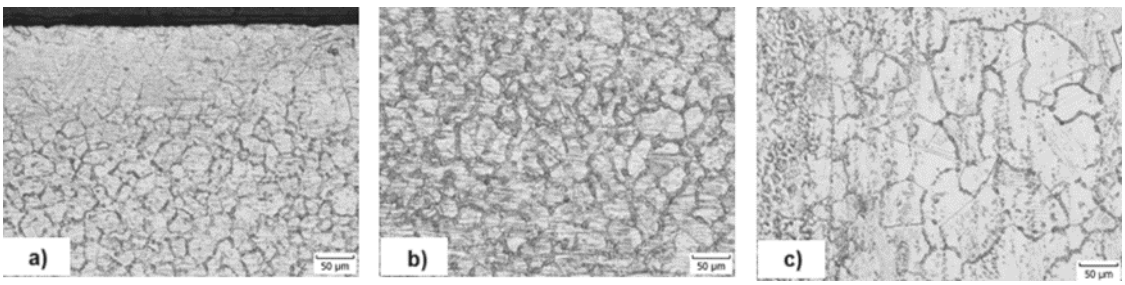

Fig. 9 Microstructure of Sample 6:
a) surface of the base material, b) middle of the base material, c) weld metal of the joint

4 CONCLUSION

Based on the material analysis, the following conclusions can be drawn:

- From the macroscopic analysis of weld joints, it can be concluded that in the case of Sample 1, a lack of fusion was observed in the central part of the weld joint. For Samples 1, 2, 4, and 5, an overflow of the weld joint root was identified.
- All the analyzed samples exhibited an austenitic matrix with polyhedral morphology, while the weld metal had a dendritic morphology. In the interdendritic space, the existence of a low proportion of δ-ferrite can be expected. In the case of Sample 4, porosity was observed in the weld metal, likely caused by the keyhole collapse during solidification of the molten pool.
- In the case of some samples, the corrosion test revealed an inappropriate microstructure that did not correspond to the state after solution annealing. Secondary phases were present at grain boundaries, causing the steel to become susceptible to intergranular corrosion.

Table 3 The classification of microstructure after the application of the corrosion test ASTM A262 method A

Sample number	Type of Semi-finished product	Microstructure classification	Corrosion resistance
1	Profile 80 x 80 x 4	Ditch structure	Susceptible to corrosion
2	Profile 80 x 140 x 4	Step structure	Not susceptible to corrosion
3	Profile 80 x 160 x 4	Ditch structure	Susceptible to corrosion
4	Profile 80 x 40 x 4	Dual structure	Not susceptible to corrosion
5	Profile Φ 60 x 3.5	Ditch structure	Susceptible to corrosion
6	Profile Φ 76.1 x 3.6	Step structure	Not susceptible to corrosion

REFERENCES

[1] M. Ghosh, S. Chatterjee, Effect of interface microstructure on the bond strength of the diffusion welded joints between titanium and stainless steel, Mater. Charact. 54 (2005) 327–337.

[2] S.X. Li, L. Li, S.R. Yu, Investigation of intergranular corrosion of 316L stainless steel diffusion bonded joint by electrochemical potentiokinetic reactivation, Corros. Sci. 53 (2011) 99–104.

[3] F. Delaunois, A. Tshimombo, V. Stanciu, Monitoring of chloride stress corrosion cracking of austenitic stainless steel: identification of the phases of the corrosion process and use of a modified accelerated test, Corros. Sci. 110 (2016) 273–283.

[4] H. Takahashi, Y. Shindo, H. Kinoshita, Mechanical properties and damage behavior of non-magnetic high manganese austenitic steels, J. Nucl. Mater. 258–263 (1998) 1644–1650.

[5] C. Fang, Y.T. Song, J. Wei, Microstructural characteristics of the laser welded joint of ITER correction coil sub case, Fusion Eng. Des. 98–99 (2015) 1960–1963.

[6] J.J. Xin, C. Fang, Y.T. Song, Effect of post weld heat treatment on the microstructure and mechanical properties of ITER-grade 316LN austenitic stainless steel weldments, Cryogenics 83 (2017) 1–7.

[7] G.H. Aydogdu, M.K. Aydinol, Determination of susceptibility to intergranular corrosion and electrochemical reactivation behaviour of AISI 316L type stainless steel, Corros. Sci. 48 (2006) 3565–3583.

[8] J. Xu, X.Q. Wu, E.H. Han, Acoustic emission response of sensitized 304 stainless steel during intergranular corrosion and stress corrosion cracking, Corros. Sci. 73 (2013) 262–273.

[9] Qian M, DuPont JN. Microsegregation-related pitting corrosion characteristics of AL-6XN superaustenitic stainless steel laser welds. Corrosion Sci 2010;52:3548e53. https://doi.org/10.1016/j.corsci.2010.07.007.

[10] Bal KS, Dutta Majumdar J, Roy Choudhury A. Study of intergranular corrosion mechanism of fiber laser welded 3- mm-thick Hastelloy C-276 sheet. Corrosion Sci 2019;157:406e19. https://doi.org/10.1016/j.corsci.2019.06.015.

[11] Zhang D-Q, Jin X, Gao L-X, Joo HG, Lee KY. Effect of laserearc hybrid welding on fracture and corrosion behaviour of AA6061-T6 alloy. Mater Sci Eng, A 2011;528:2748e54. https://doi.org/10.1016/j.msea.2010.12.021.

[12] Xiao R, Zhang X. Problems and issues in laser beam welding of aluminumelithium alloys. J Manuf Process 2014;16:166e75. https://doi.org/10.1016/j.jmapro.2013.10.005.

[13] Molian PA. Solidification behaviour of laser welded stainless steel. J Mater Sci Lett 1985;4:281e3. https://doi.org/10.1007/BF00719791.

[14] G.R. Garcésa, J.L. Cozeb, J.L. Garin, σ-phase precipitation in two heat-resistant steelsinfluence of carbides and microstructure, Scripta Mater. 50 (2004) 651–654.
[15] M. Schwind, J. Källqvist, J. Nilsson, σ-phase precipitation in stabilized austenitic stainless steels, Acta Mater. 48 (2000) 2473–2481.
[16] H. Sahlaoui, H. Sidhom, J. Philibert, Prediction of chromium depleted-zone evolution during aging of Ni–Cr–Fe alloys, Acta Mater. 50 (2002) 1383–1392.
[17] A.F. Padilha, D.M. Escriba, E.M. Morris, Precipitation in AISI 316L(N) during creep tests at 550 and 600 °C up to 10 years, J. Nucl. Mater. 362 (2007) 132–138.
[18] Y.H. Kim, D.J. Lee, J.C. Byun, The effect of sigma phases formation depending on Cr/Ni equivalent ratio in AISI 316L weldments, Mater. Des. 32 (2011) 330–336.
[19] K. Chandra, V. Kain, R. Tewari, Microstructural and electrochemical characterisation of heat-treated 347 stainless steel with different phases, Corros. Sci. 67 (2013) 118–129.
[20] A. Pardo, M.C. Merino, A.E. Coy, Influence of Ti, C and N concentration on the intergranular corrosion behaviour of AISI 316Ti and 321 stainless steels, Acta Mater. 55 (2007) 2239–2251.
[21] K. Kaneko, T. Fukunaga, K. Yamada, Formation of M23C6-type precipitates and chromium depleted zones in austenite stainless steel, Scripta Mater. 65 (2011) 509–512.
[22] S.X. Li, Y.N. He, S.R. Yu, Evaluation of the effect of grain size on chromium carbide precipitation and intergranular corrosion of 316L stainless steel, Corros. Sci. 66 (2013) 211–216.
[23] Y. Zhou, K.T. Aust, U. Erb, Effects of grain boundary structure on carbide precipitation in 304L stainless steel, Scripta Mater. 45 (2001) 49–54.
[24] Available on the internet: [cit. 2023-09-25] <https://virgamet.com/1-4404-1-4401-aisi-316-316l-s31603-s31600-stainless-steel>.
[25] ASTM A262: Standard practices for Detecting Susceptibility to Intergranular Attack in Austenitic Stainless Steel, USA, 2015.

THE INFLUENCE OF THE WORKING POSITION OF THE WELDER IN ASSESSING WELDING RISKS

Ing. Petra Marková, PhD.[1]
Ing. Vanessa Prajová, PhD.[2]
Ing. Mária Homokyová, PhD.[3]
Ing. Martina Horváthová, PhD.[4]
[1]ORCID: 0000-0001-8636-1293, Slovak University of Technology in Bratislava, Faculty of Materials Science and Technology in Trnava, **Slovakia**
[2]ORCID: 0000-0002-1260-4675, Slovak University of Technology in Bratislava, Faculty of Materials Science and Technology in Trnava, **Slovakia**
[3]0000-0001-9263-6206, Slovak University of Technology in Bratislava, Faculty of Materials Science and Technology in Trnava, **Slovakia**
[4]ORCID: 0009-0003-0062-9394, Slovak University of Technology in Bratislava, Faculty of Materials Science and Technology in Trnava, **Slovakia**

Abstrakt: In practice, every occupation involves working in a variety of work positions and using a diverse number of work items or tools in a wide range of work activities. In the case of the position of welder, it is necessary to understand that such an employee performs welding work by a variety of methods, e.g., shielded atmosphere welding, electric arc welding, gas welding, and the like. The welding itself is also related to other work activities that are carried out before or after the welding itself - preheating, heating, visual inspection of welds, soldering, cutting, cleaning of welded surfaces, as well as finishing of welded surfaces to the final form. Each of these activities may involve working positions which may not always be optimal and may affect both work performance and the ability to perform the job in the long term. It is therefore important to assess the risks arising from the work and the working environment of a particular employee in order to prevent risks. And not only those that have an immediate effect, but also those risks that are cumulative-pathogenic and need a longer period of exposure to have a negative impact on the employee. The subject of interest in the article are working positions during welding, which can potentially increase the risk of development of musculoskeletal disorders of the welder, depending on the frequency of their occurrence during welding. The aim of the article is to identify unacceptable working positions in welding from an ergonomic perspective.

Keywords: work posture, welder, musculoskeletal disorders, ergonomic risk

1 INTRODUCTION

Welding

Welding (Žiaková, 2023) creates a number of potential hazards that can cause damage to health. The welder comes into contact with harmful fumes produced during welding (dust, optical radiation). There is also the increased noise level, often combined with the effects of vibration on the body. Dangers can arise from contact with hot materials and surfaces, flammable substances in the welding area or from failure to follow the working procedure when working with lasers. As the welder's workplace may not always be indoors, it is necessary to consider not only the heat load but also the cold load in the context of unsuitable climatic conditions. In addition to the aforementioned hazards, inappropriate working position or prolonged unilateral loading of the welder's small muscle groups should clearly be counted among them.

Who is a welder?

Nowadays, welding is very often used in various industries, so it is necessary to identify the skills that a welder must possess. Modern welding involves many different technologies that a welder needs to master and needs to know the H&S and fire safety regulations; legal regulations, maintenance rules (Kurso.com, 2023).

The welder is required to pass the working tests, which are verification tests of the welder's skills before starting welding work on equipment subject to Decree No. 508/2009. Welders must have the working tests if the employer wishes to use them for scheduled overhauls, overhauls, process stoppages, short-term shutdowns or routine maintenance. The exception when a welder is not required to have a working test is an unexpected accident when an immediate intervention is required and a welder with a valid test is not available at the time. Welders' work tests are also not required when welding non-pressure parts not subject to Decree No. 508/2009, the welder then works under the supervision of a competent welding technologist/engineer who vouches for the welder's skills (Gardian, 2020).

Working positions when welding

The efficiency of working positions and movements depends not only on the working method but also on the level of workplace organization, the level of design of machines, tools and equipment (Sablik, 1990).

Forced position represents permanent work in a certain position. From the ergonomic point of view, this is a very unfavourable phenomenon. Forced positions are the cause of various diseases and ailments, such as swollen feet, the development of varicose veins. The way to avoid these postures is to increase the interval of work breaks to allow a change of position (Marek and Skřehot, 2009).

The working position is greatly influenced by the nature, type of work performed, dimensions and layout of the employee's workstation. The workstation layout must be designed in such a way that a physiologically unacceptable working position is not adopted in any case. It must allow work activities to be carried out in the basic sitting or standing postures, with the possibility of alternating between these postures. Body balance and orientation in space are determined by a complex system of reflexes which, via the central nervous system, adapt muscle tone to a particular position. This includes uprighting reflexes, tonic reflexes and also stabilizing reflexes (Ulbrichová, 2023).
Depending on which of the working postures is predominant at work, it is also appropriate to design the working environment. The working environment for sedentary work should be designed so that all necessary components are within reach of the employee and no higher than 15 cm above the work surface. Individual components or work tools with which the employee comes into contact when seated should not weigh more than 4.5 kg. On the other hand, standing work is preferred in workplaces where frequent movement between workstations or handling of heavier loads is required. Also, the performance of standing work is characterized by the frequent occurrence of work operations where bending or stretching is necessary (Lusetic, 2018).
There are three basic body positions envisaged by the Slovak legislation in Annex 4 of Decree No. 542/2007 Coll., namely (Ulbrichová, 2023):

- acceptable position - sitting or standing, or alternating between sitting and standing;
- unacceptable position - the total time spent working in an 8-hour shift in each unacceptable working position must not exceed 30 min;
- conditionally acceptable position - the total time spent working in an 8-hour shift in each conditionally acceptable working position must not exceed 160 min and the duration of each working position must not exceed 1 min - 8 min, depending on the type of position and the frequency of movements.

Conditionally acceptable + unacceptable work position: the total time worked in conditionally acceptable and unacceptable work positions shall not be more than half of an 8-hour shift.
Job evaluation in terms of work positions is most relevant in stable work locations (e.g., belt manufacturing and other jobs) where the employee is at the same location for more than half of the 8-hour shift and performing the same work activity. In doing so, the work position cannot be chosen by the employee, but the work position is directly dependent on the design of the machine, the layout of the workplace, the spatial parameters of the workplace and so on. The work position is always assessed only in the context of the activity performed, that is, if it is a structural part of the work activity and not a random activity (Ulbrichová, 2023).
If the work activity requires precision and concentration, the sitting position is preferable. In contrast to seated work, standing work exhibits increased static load, greater energy expenditure and less opportunity to perform precise and coordinated movements.

The advantage of standing work is that it allows for a greater range of movements, the development of greater forces, and more frequent alternation of working positions. The ideal upright posture requires the least muscular activity (Ulbrichová, 2023). The best solution is a job in which the employee has the opportunity to alternate working positions, which ideally allows for perfect ergonomic variability of his or her workstation.

Risks related to the performance of the welder's work

If the hazards associated with welding are ignored, the result can be damage to the welder's health, ultimately causing a decline in work performance or poor workmanship. Of the health impairments most commonly associated with welding are visual impairments, harmful effects on the respiratory system, skin, increased hearing stress, heat stress, harmful effects of non-ionising radiation, accidents, burns, and injuries to small muscles in the upper limbs. It may also be fire, explosion or danger to other persons. And last but not least, just in connection with inappropriate working postures and diseases of the support and musculoskeletal system due to static load (Žiaková, 2023).

The main purpose of work categorization is to determine the level of risk in the work performed in terms of protecting the health of employees at work. In addition, also taking the necessary measures to reduce the level of risk, i.e. eliminating or reducing the riskiness of work (the occurrence of occupational diseases and damage to health) mainly by technical and organizational measures to the lowest possible level.

The criteria of the above categorization are (Pohorelá, 2019):

- the level and nature of individual work and work environment factors that may affect the health of employees;
- health risk assessment (evaluation) and assessment of changes in the health status of employees.

The classification of particular types of work (e.g. construction worker, bus driver, chemist, welder) into a specific category in terms of health risks is nowhere precisely established. It is up to each employer, in cooperation with the occupational health service, to ensure the categorisation of the work carried out in the workplace. Its role is, among other things, to provide professional and advisory activities to the employer to fulfill its obligations under the law of protection, promotion and development of public health (Pohorelá, 2019).

Act No. 355/2007 Coll. on the Protection, Promotion and Development of Public Health (Section 31) provides for the categorization of employees' work. According to the level and nature of work and work environment factors that may affect the health of employees, the assessment of health risks, and based on changes in the health status of employees, work is classified into four categories (sometimes referred to as risk categories).

The most serious risk is the development of an occupational disease in an employee. Carpal tunnel syndrome is one of the most commonly reported occupational diseases. The second most common disease is vibration sickness and the third most common disease is noise-induced hearing impairment (MG Business Services, 2023).
According to Hatiar (2018), modifiable risk factors are the most common consequence of the occurrence of musculoskeletal disorders and diseases. Among the given risk factors that affect a person most negatively in the work process, we rank the following factors:

- extreme or unnatural joint positions;
- insufficient rest and lack of time to recover after work;
- monotony of work, i.e. high frequency and repetition of the same movements over and over again;
- static load on the muscles at work;
- unsuitable temperature;
- individual factors, such as various diseases such as diabetes or endocrinological diseases or pregnancy;
- local mechanical loads;
- noise and vibration;
- lighting;
- excessive force;
- other risk factors such as lack of freedom of initiative by employees, shift work and similar factors (Sinay et al., 2017).

2 METHODOLOGY

The article is based on the results of EUROSTAT surveys, EU-OSHA analyses, the Statistical Office of the Government of the Slovak Republic, and the Ministry of Health of the Slovak Republic. In the preparation of the article we also used materials collected in industrial enterprises in Slovakia. In addition, the research material was obtained through diploma and dissertation theses of students of the Faculty of Materials Technology in the study programme "Industrial Management". The obtained data were processed by epidemiological methods of retrospective cohort study. Published research results of foreign authors were also an important source for the evaluation of outcomes. In the preparation of the thesis, basic thought processes such as analysis, synthesis, abstraction, concretization, deduction, analogy, comparison, etc. were used. The interpretation of the data was processed through descriptive and quantitative statistical methods.

3 RESULTS

Europe's largest occupational health survey reports that the most common work-related health problems are back pain, affecting 46% of employees, and neck, shoulder and upper limb pain, affecting 43% of employees. Between 2007 and 2013, the percentage of workers reporting musculoskeletal disorders increased from 59% to 62%. The occurrence of such conditions often cannot be reduced to a single cause and prevention can only be successful if the occupational aspect of the cause is reduced. For work-related health problems, it is estimated that the number of days lost due to illness is 1.6 to 2.2 times higher than the number of days of temporary disability caused by the injury. One tentative explanation is that these disorders develop gradually over time. Longer-term impairments and chronic diseases increase with age. Given demographic changes, especially in developed countries, the importance of topics such as occupational health and safety for labour market policy will increase significantly in the future (Rusu, Constantinescu, & Marinescu, 2021).

Statistical data on hazardous work or related occupational diseases of the Slovak Republic are collected by the National Centre of Health Information and presented by the Office of Public Health. On the basis of the last report of 2022 addressing the situation regarding occupational health for 2021, the following findings can be stated.

In the Slovak environment, 525 occupational diseases were identified in 2022 (Figure 1). In 2022, the rate of newly recognized occupational diseases was 20.2 cases per 100,000 workers in that year. Compared to 2021 (16.5 cases per 100,000 workers), the rate of newly recognized occupational diseases increased by 22.0%. Comparing 2001 (27.2 cases per 100 000 workers) with 2022, the rate of newly recognised occupational diseases fell by 25.8%. In the current year, newly diagnosed occupational diseases were higher among women, with 329 cases of CVD (62.7% of total cases; 26.9 cases per 100,000 working women). Compared to 2021 (267 female CVDs), the number of new cases of occupational diseases in women increased by 23.2%. For men, there were 196 cases of CVD (37.3%; 14.2 cases per 100,000 working men). Year-on-year (2021; 156 cases), the number of new cases of occupational diseases in men increased by 25.6% (NCZI, 2023).

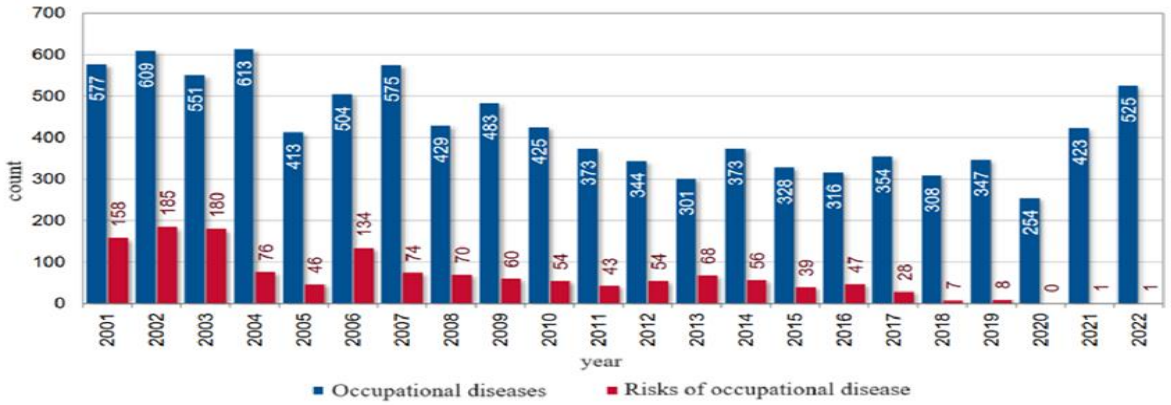

Fig.1 Evolution of the number of occupational diseases and risks of occupational diseases, 2001-2022 (NCZI, 2023)

Their most common types (Figure 2) and classification by sector (Figure 3) are shown in the following charts. In addition, it can be seen from these statistics that occupational diseases were most frequently recorded among employees aged 55 to 59. However, this was a year-on-year decrease to 22% of cases.

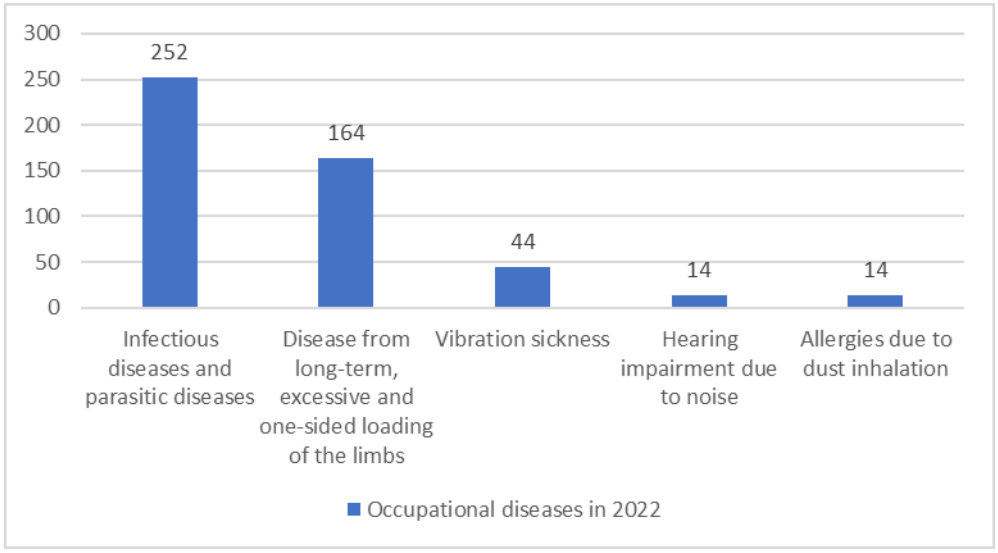

Fig.2 The most common occupational diseases in the Slovak Republic by type in 2022 (Own processing according to NCZI, 2023)

In 2022, COVID-19 was still a significant influence on the most frequently reported occupational diseases, as evidenced by the values in terms of type of disease but also in relation to the classification of economic activities where the disease was reported, for a total of 233 persons. All of the following types of occupational diseases replicate the main risk factors reported for the welding profession. The statistical results document that diseases related to prolonged, excessive and unilateral loading of the limbs, which are diseases of the bones, joints, tendons and nerves of the limbs, are the second most numerous group of occupational diseases and are also closely related to working postures; therefore, the working postures, the dimensional design and the layout of the workplace must be given adequate attention.

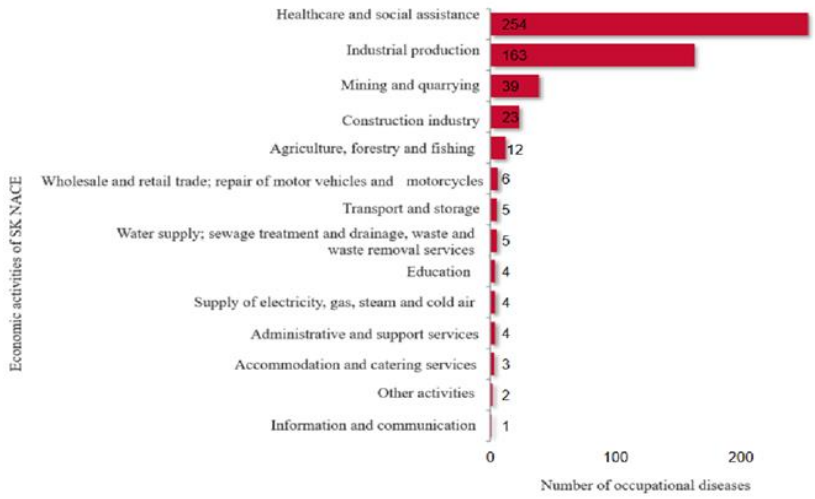

Fig.3 Economic activities with the highest number of newly recognised occupational diseases, 2022 (NCZI, 2023)

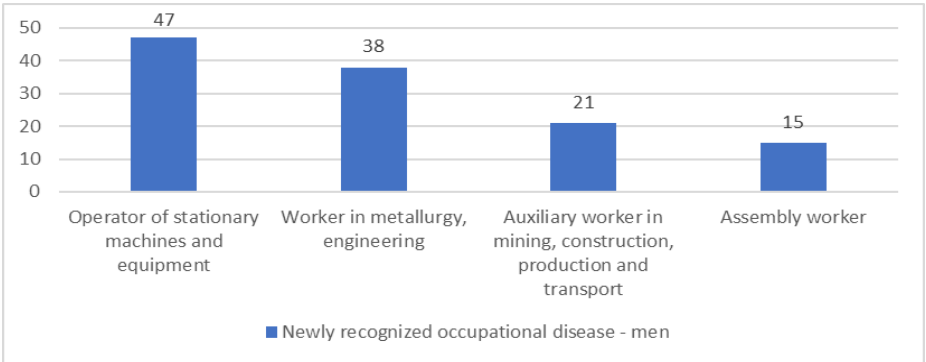

Fig.4 Newly diagnosed occupational disease in 2022 by sex (own elaboration according to NCZI, 2023)

Looking at the incidence of diseases from a gender perspective, given that the welding job is predominantly performed by men, we present statistics for men only (Figure 4).

When looking at the incidence of occupational diseases in the Slovak Republic over the last twenty years (Figure 1), there was a significant decline in 2013, which could not be sustained or was again achieved, while in the previous year we see an increase in the incidence, which represents a negative trend. It is important to note that employees with an occupational disease represent a comparable loss to the employer as in the case of a fatality, as they are unable to work in their original job. Ultimately, the employee must be compensated, which will incur additional costs.
Specifically, most cases of the impact of the work environment and the work performed on an employee's health are in the area of musculoskeletal disorders (MSDs). These are injuries to nerves, muscles, tendons, cartilage or joints, which are generally caused by the performance of the work or the working environment, and these two aspects are the main reasons for a long-lasting impairment of health. We can mention a few specific injuries that fall into this category: arthritis, back pain, sprains or strains and carpal tunnel syndrome. Arthritis can be defined as a rheumatic disease affecting the joints and tissues surrounding the joints of the human body. (Work-Related Musculoskeletal, 2020).

The most common ergonomic injuries that arise from non-ergonomic solutions at work are (recursosdeautoayuda.com, 2022):

- carpal tunnel syndrome (caused by pressure on the meridian nerve, which runs from the shoulder to the hands). Carpal tunnel syndrome can be described as compression of the median nerve at the wrist, which can result in tingling, impaired sensation or weakness in the hand and fingers. Between 300 and 500 thousand operations related to this diagnosis are performed worldwide each year;
- ganglion cysts (the sign is a lump under the skin usually on the wrist often caused by overuse of the joint, leading to inflammation);
- Raynaud's disease (a sign is numbness in certain areas of the body due to restricted blood supply);
- tendonitis (a sign is pain or swelling in the joints due to repetitive and uncomfortable positions);
- problems in the lower back (the consequence may be prolonged sitting in uncomfortable positions, lifting, bending and twisting);
- other musculoskeletal disorders (MSDs).

4 DISCUSSION

To eliminate the danger of inappropriate working positions, it is necessary to alternate working positions, choose appropriate work breaks. Provide suitable work mats or take time for compensatory exercises. The design of an ergonomically suitable workplace, based on

principles that take into account the adaptation of the workplace for each worker and for each work task, plays an important role in preventing the development of unsuitable working postures.

Workstation parameters correspond to hand and leg mobility in all directions and reach capabilities (MG Business Services, 2023):

- strength requirements do not exceed the physical capabilities of the workers,
- the efficiency of the movements is achieved by appropriate auxiliary technical equipment,
- the movements of the limbs and the body are balanced to avoid unilateral movement loads,
- working movements which place high demands on precision, strength or speed are concentrated within the optimum reach of both hands,

Ergonomic principles in the design of workplaces and work environments aim to create the best conditions for the employee within the work process. A well-designed workplace according to ergonomic requirements should be (Očkajová et al., 2013):

- clear, providing optimum optical conditions, adapted for quick and easy visual orientation and providing an adequate viewing distance,
- convenient, providing a comfortable working position for the worker, with appropriate spatial dimensions,
- arranged so that annunciators, controls, handling equipment, tools and work aids are optimally positioned for comfortable work performance,
- hygienic, with optimum lighting, acoustic and microclimatic conditions, with provision for the protection of the worker against harmful substances, radiation and vibration, and with sufficient opportunity for keeping the workplace clean and tidy,
- safe, there must be protection for the worker at the workplace against the occurrence of accidents, there must be safe access to the workplace and exit from the workplace must be easy in the event of an accident,
- aesthetically pleasing and evoking favourable aesthetic feelings conducive to improving work performance.

5 CONCLUSION

We subscribe to the findings of Macdonald and Oakman (2022) that workplace risk management practices focus mainly on biomechanical risks, as do the risk assessment methods used by ergonomists. Translating research evidence into more effective workplace practices requires a more comprehensive risk management framework that incorporates both types of hazards, i.e. not only risks of supporting-motor difficulties but also psychosocial risks. In this context, we assess the validity of different MSD risk assessment methods for

different purposes, focusing in particular on the requirements for routine workplace risk management. These include selecting assessment methods that are fit for purpose, prioritising hazards that most affect risk, and control measures as high up the risk control hierarchy as possible. Occupationalists could facilitate more effective workplace risk management by promoting: awareness of the need for change; improved guidance from OSH regulatory bodies; research into issues related to workplace management of MSDs; and professional development programmes on the topic for occupational therapists and other OSH professionals.

ACKNOWLEDGEMENTS

The paper is a part of project KEGA No. 027STU-4/2022 “Integration of the requirements of practice in the automotive industry with the teaching of subjects within the study programs Process Automation and Informatization in Industry and Industrial Management”. The paper is a part of project KEGA of the Ministry of Education of the Slovak Republic No. 018TUKE-4/2022 "Creation of new study materials including an interactive multimedia university textbook for the field of computer support of engineering activities".

REFERENCES

Gardian, J. (2020). Evidencia a pracovné skúšky zváračov. [online] Available at: https://slovnaft.sk/images/slovnaft/pdf/o_nas/centrum_dodavatelov/sd_hse_poziadavky_pre_kontraktorov/conf/evidencia_a_pracovne_skusky_zvaracov.pdf [Accessed 18 Oct. 2020].

Hatiar, K. (2018). Základy ergonómie. In Šulcová, M., Krutý, F., Moricová, S.: Pracovné lekárstvo.

KURSO.com, (2023). Práca zvárača. [online] Available at: https://kurso.com.pl/sk/kurzy-a-skolenia/zvaranie/praca-zvarac/ [Accessed 18 Oct. 2023].

Lušetić, T., Trstenjak, M., Ćosić, P. (2018). Ergonomic design of workplace. [online]. Available at: https://www.researchgate.net/publication/327542735_ERGONOMIC_DESIGN_OF_WORKPLACE [Accessed 18 Oct. 2020].

Macdonald, W., Oakman J. (2022). The problem with “ergonomics injuries”: What can ergonomists do? In Applied Ergonomics [online]. 2022, Roč. 103, s. 103774. ISSN 00036870.]. Available at: doi:10.1016/j.apergo.2022.103774 [Accessed 18 Oct. 2023].

Marek, J., Skřehot, P. (2009). Základy aplikované ergonomie. Bezpečný podnik. Praha: VÚBP. ISBN 978-80-86973-58-6

MG Business Services (2023). Pracovná zdravotná služba (PZS), 8 kľúčových informácií pre zamestnávateľa. [online] Available at: https://www.mg-service.sk/pracovna-zdravotna-sluzba-pzs-8-klucovych-informacii-pre-zamestnavatela/ [Accessed 18 Oct. 2023].

NCZI, (2023). Choroby z povolania alebo ohrozenia chorobou z povolania v SR 2022. [online] Available at: https://data.nczisk.sk/statisticke_vystupy/choroby_povolania/Choroby_z_povolania_2022_Sprava_k_publikovanym_vystupom.pdf [Accessed 18 Oct. 2023].

Očkajová, A, a kol. (2013). Pracovné prostredie a ergonómia. Banská Bystrica: UMB FPV, 402 s. ISBN 978-80-557-0617-7

Pohorelá, P. (2019). Kategorizácia (zaraďovanie) prác podľa zdravotných rizík. [online] podnikajte.sk. Available at: https://www.podnikajte.sk/zakonne-povinnosti-podnikatela/kategorizacia-prac-zdravotne-rizika [Accessed 18 Oct. 2023].

Recursosdeautoayuda. (2022). Čo je to ergonómia: vlastnosti a typy. [online]. Available at: https://www.recursosdeautoayuda.com/sk/ergonomia/ [Accessed 18 Oct. 2023].

Rusu, C., Constantinescu C., Marinescu S. (2021). A generic hybrid Human/Exoskeleton Digital Model towards Digital Transformation of Exoskeletons-integrated workplaces. Procedia CIRP [online]. Roč. 104, s. 1787–1790. ISSN 22128271. Available at: doi:10.1016/j.procir.2021.11.301 [Accessed 18 Oct. 2023].

Sablik, J. (1990). Ergonómia. Bratislava: SVŠT. ISBN 80-227-0299-4

Sinay, J., Balážiková, M., Hovanec, M. (2017). Bezpečné pracovné prostredie. Košice: TUKE, Strojnícka fakulta, 84 p. ISBN 978-80-553-3139-3

Ulbrichová, R. (2023). Vybrané kapitoly z preventívneho pracovného lekárstva I. Martin: Univerzita Komenského v Bratislave. Jesseniova Lekárska Fakulta v Martine. Ústav verejného zdravotníctva. 89 s. ISBN 978-80-8187-141-2

Work-Related Musculoskeletal Disorders & Ergonomics | Workplace Health Strategies by Condition | Workplace Health Promotion/CDC. (2021). [online] Available at: https://www.cdc.gov/workplacehealthpromotion/health-strategies/musculoskeletal-disorders/index.html [Accessed 18 Oct. 2023].

Žiaková, M. (2023). Hodnotenie nebezpečenstiev a posúdenie rizika pre pracovné zaradenie ZVÁRAČ – vzor. [online] epi.sk. Available at: https://www.epi.sk/vzor/hodnotenie-nebezpecenstiev-a-posudenie-rizika-pre-pracovne-zaradenie-zvarac-vzor.htm [Accessed 18 Oct. 2023].

ALGORITHM AS A TOOL IN PROGRAMMING AND IMPLEMENTATION OF AUTOMATED PROCESSES

Ing. Miriam Matúšová, PhD.[1]
[1]ORCID: 0000-0002-2128-3041, Faculty of Materials Science and Technology in Trnava, Slovak University of Technology, **Slovakia**

Abstract: The constant changes in automation and robotization surprise with new trends and solutions that a person not interested in the subject has no idea about. Robotic solutions in industrial enterprises are quite complex and complicated. Sometimes robotics or automation is suitable for a given activity or workplace, sometimes not. Thus, the question of implementing automated processes is directly dependent on the requirements, technical, spatial and financial capabilities of the enterprise. However, if companies want to move forward and be continuously competitive, the issue of automation and robotization must not be alien to them. Thus, if the primary task of manufacturing companies is to produce products as quickly and efficiently as possible, in the required quality and at the lowest possible cost - automation and robotization is a necessity, or companies should make progress in this area compared to their competitors.

Keywords: process, innovation, automation, robotic, flow diagram

1 INTRODUCTION

When considering the introduction of automation or robotics into practice, it is necessary to focus on defining the theoretical knowledge in the field of automation, robotics, end-effectors, vision systems and manufacturing processes in industry. It is important in the reflection part to discuss general concepts in the field of automation, its benefits and current trends in the world, which are also used in enterprises. Knowledge in the field of robotics, types of currently used industrial robots, their control, types of feasible robotic work processes and the main advantages determine the possibilities of use in practice and determine the eventual applicability for the enterprise.

2 LITERATURE REVIEW

Currently, programmable automation is used as a device tailored to a specific class of product change requirements. Individual operations and processes, such as material

processing or assembly work, can therefore be changed by modifying the control program. It is primarily implemented for so-called batch production, or the production of a product in medium-sized batches at regular intervals. An example of this type of automation is, for example, a CNC lathe producing a specific product in a specific product class based on a specified program. This can be represented, for example, by numerically controlled machines or industrial robots. The primary advantages of programmable automation may be flexibility in dealing with variations or product changes, or low cost for large batch production. In the case of disadvantages, the primary one is of course the long reprogramming time for a new product (Gupta, et al., 2016).

The issue of robotics covers many different fields. Stand-alone robots are practically unusable their effective use occurs only when they are used in collaboration with other devices or production machines. They are generally embedded in a system that is designed as a whole to perform certain tasks or complex operations (Gupta, et al., 2016)

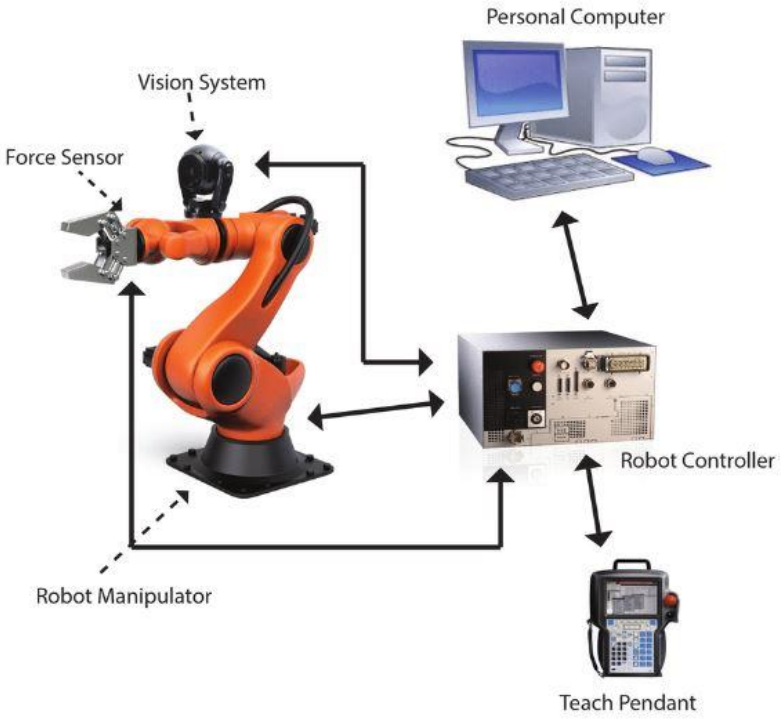

Fig. 1 Robot operation control (jteryu.top)

Robotic movements are controlled through a controller under the supervision of a computer running some type of program (fig.1). Therefore, if the program is changed, the robot's actions will change accordingly. Thus, the primary purpose in introducing a robot into production is to have a device that can perform various activities without the need for rework (Niku, 2010).

3 ROBOTICS AND THEIR STRENGTHS AND WEAKNESSES

Robotic systems must meet technical, economic and social requirements and factors before they can be implemented in industrial practice in order to achieve the desired outcome. Thus, if implemented correctly, industrial robots can improve the quality of life by freeing workers from dirty, boring, dangerous and strenuous work.

A long-term study on the use of robotics and automation highlights the advantages/benefits of robots and their implementation:

1. Robots sharply increase overall productivity, workplace safety, efficiency, and production quality
2. Robots do not need the environmental comforts of humans - lighting, fresh air, ventilation, and sound protection.
3. Robots can easily work in hazardous environments and with hazardous substances.
4. Robots can work continuously without feeling tired, bored, and do not need health insurance or vacations.
5. If the robots are not damaged or nothing happens to them they have constant repetitive precision.
6. Robots are considerably more accurate than humans.

In the same way that the advantages and benefits of robotics are described, it is necessary to point out the disadvantages:

1. Robotization causes economic and social problems due to the displacement of some workers from their jobs.
2. In the event of an unforeseen, exceptional situation that is not included in the relevant programme, robots are not able to react adequately. As a consequence, it is therefore necessary to ensure sufficient workplace safety.
3. Robotization represents an excessively high initial cost for the acquisition and deployment of robots and the costs associated with training and programming. (Harmoko, et al.,2022)

The overall concept of smart industrial robot control follows the principle of “see-think-act”. Even though this principle originally has been addressed in the field of mobile robotics (Siegwart, et al., 2011), it is also becoming more relevant in the context of smart

manufacturing. The diagram illustrated in Figure 2 is built upon this principle and integrates such core functionalities of smart industrial robots as:

- Perception;
- High-level instruction and context-aware task execution;
- Knowledge acquisition and generalization;
- Adaptive planning. (Arents, et al.,2022)

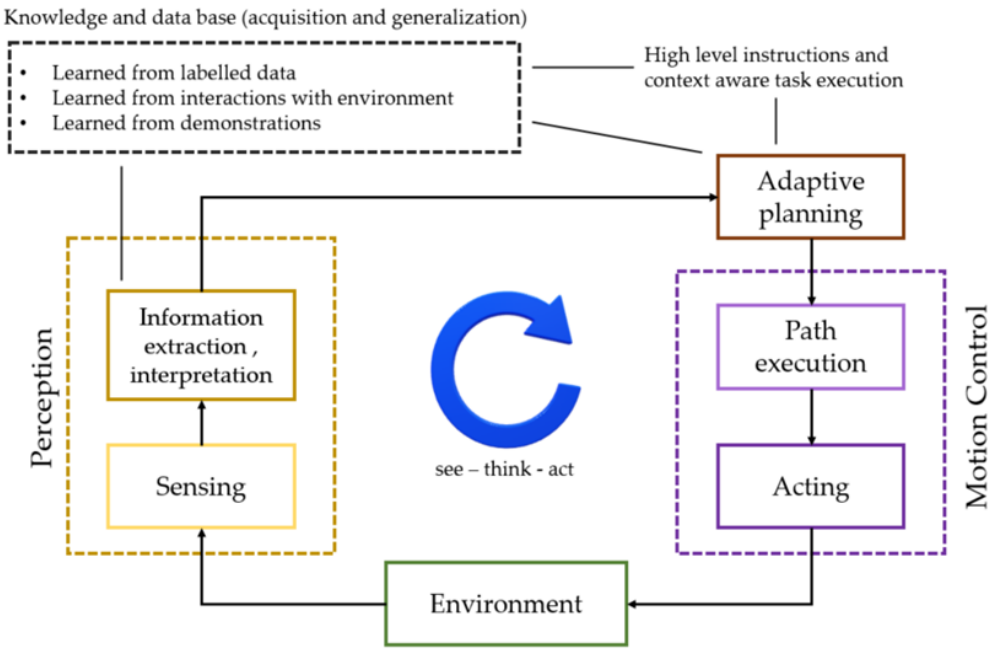

Fig. 2 Smart industrial robot concept (Arents, et al.,2022)

4 MAPPING TOOL FOR PROCESS MANAGEMENT

The new industrial revolution is being described as the era of digitization, in which industries are being transformed by intelligent machines, data collection processes and artificial intelligence that enable them to make autonomous decisions in real time.

The impact of such developments in manufacturing and assembly technology around the world is leading to an increasing focus by companies on flexible automation. Such systems include process workstations, which in many cases are fully automated handling systems, conveying systems, warehouse systems, control systems and other auxiliary equipment. In recent decades, it has become commonplace to automate assembly work, which is often linked to production technologies within a single flexible manufacturing and assembly system. The functionality of the entire production-assembly system needs to be designed,

process-tracked and set up for efficient production. Component wear and tear or unreliability can cause losses that need to be monitored and subsequently eliminated. (Jung, 2004)

4.1 MAPPING OF PRODUCTION PROCESSES

When designing production in manufacturing and assembly processes, it is important to have a clear idea of the process by which a given production line will be implemented.
A process is defined as a logical sequence of activities and steps that are designed and implemented to achieve a specific output or result. A process in an enterprise has a clearly defined beginning, course and end, with linkages to other processes. It is important to analyse the outputs of a process and ensure that the inputs and outputs between processes are identical. Each process has a 'process card' which provides detailed information on the process name, process operator, inputs, outputs, upstream processes, downstream processes, resources, etc. Setting the objective and measurable indicators of the process are key to its successful implementation and monitoring of results. The resources required for the implementation of the processes should be used optimally in order to maximize the efficiency of the processes (Papulova 2014).
Process mapping is an important element for better understanding and significant improvement of processes.

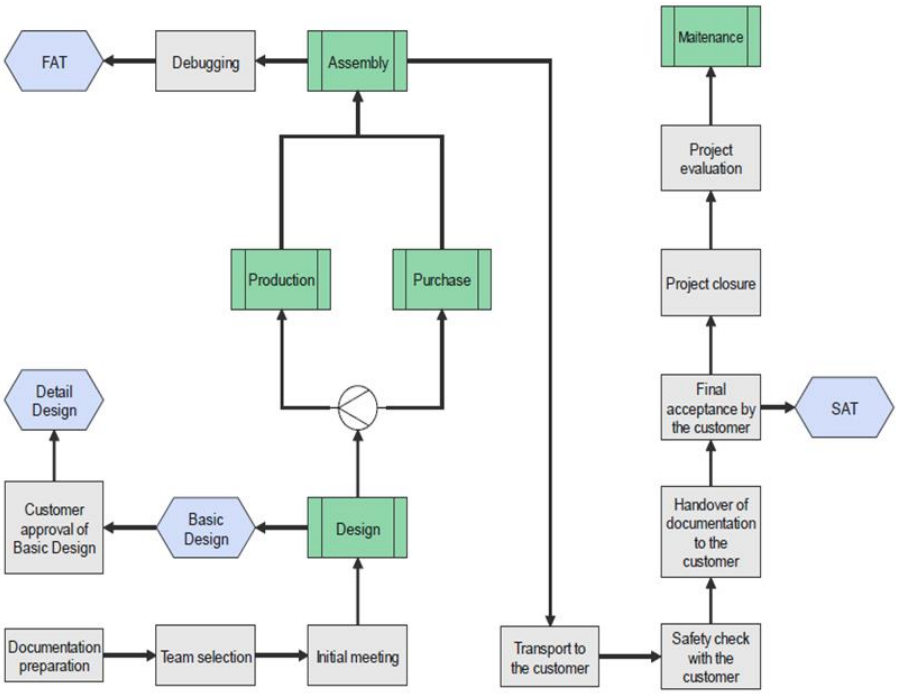

Fig. 3 Flow diagram of processes and steps

Process mapping is a proven analytical and communication tool designed to optimize current processes and to introduce a new process-oriented company structure. A process map (fig.3), also known as a flow diagram, is a tool that allows to visualize processes and their individual steps. A process map starts by identifying the inputs and outputs of a process. Inputs may include raw materials, labor, financial resources, and so on, while outputs may be finished products, semi-finished products, or other output products of the process. It then maps the sequence of steps that are required to achieve the process objectives. These steps include the individual workstations and machines that are part of the production process. The process map includes information about the time requirements that are associated with each step of the process and also information about the responsibilities for each step.

5 ALGORITHM OF ROBOT WORK WITH PRODUCT HANDLING

For an easier overview of the workflow, Figure 4 shows the environment on which the algorithm of the manipulation process was developed.
Since with the increasing number of tasks and processes, it is often lost track of how the individual process steps are interconnected and how they influence each other, it is necessary to draw up a conceptual flowchart representing the processes and all the factors that the proposed automation contains. The produced conceptual flow diagram, shown in Figure 5, serves as a visual tool to show the progression and interconnection of the process

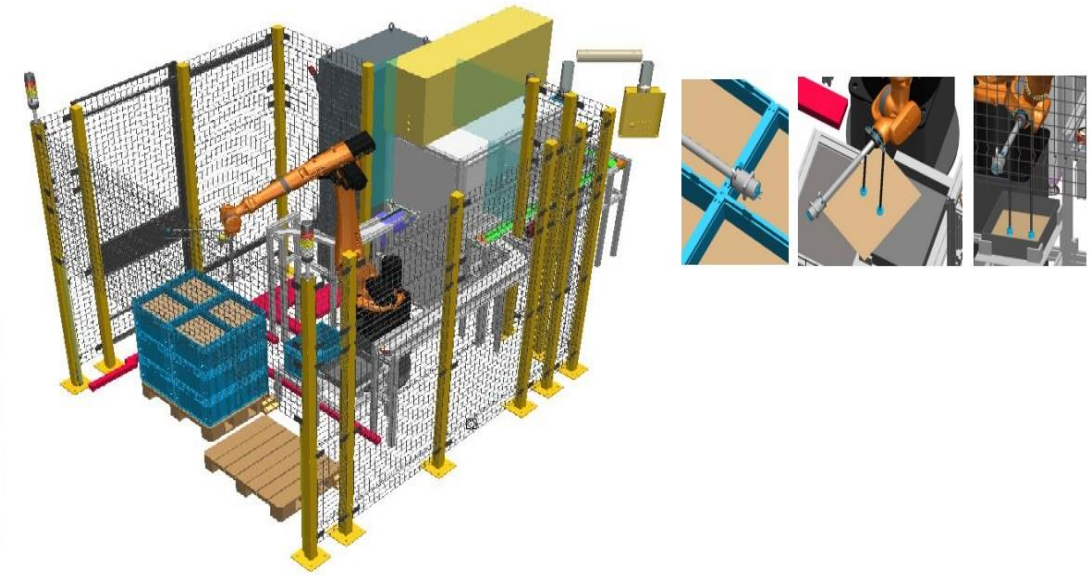

steps. This tool primarily assists in the final programming and implementation of the automated processes in practice.

In Figure 5, the input process/information is the arrival of pallet Q2 with the currently produced type size Q1. The first process is to check the start of the program of the brought in typo dimension Q1. This program can be pre-prepared for the time range remotely from a PC, selected manually by a worker on the machine control panel, or started automatically when a QR code is read on the pallet. The following steps have been designed for safety. These include checking that the safety door is closed and that the light gate at the pallet entry area is interrupted. If one of these safety conditions is violated for more than approximately 5 minutes (these 5 minutes are used to assemble the pallet entrance at the workplace), a signal is sent to the responsible worker who will come to the workplace and check if the safety door is closed or locked properly and what is the reason for the interruption of the signal. Once the security conditions have been verified, it is the turn of the Photoneo 3D scanner or camera scanning, depending on the proposed automation version, to check that the entry pallet is in place.

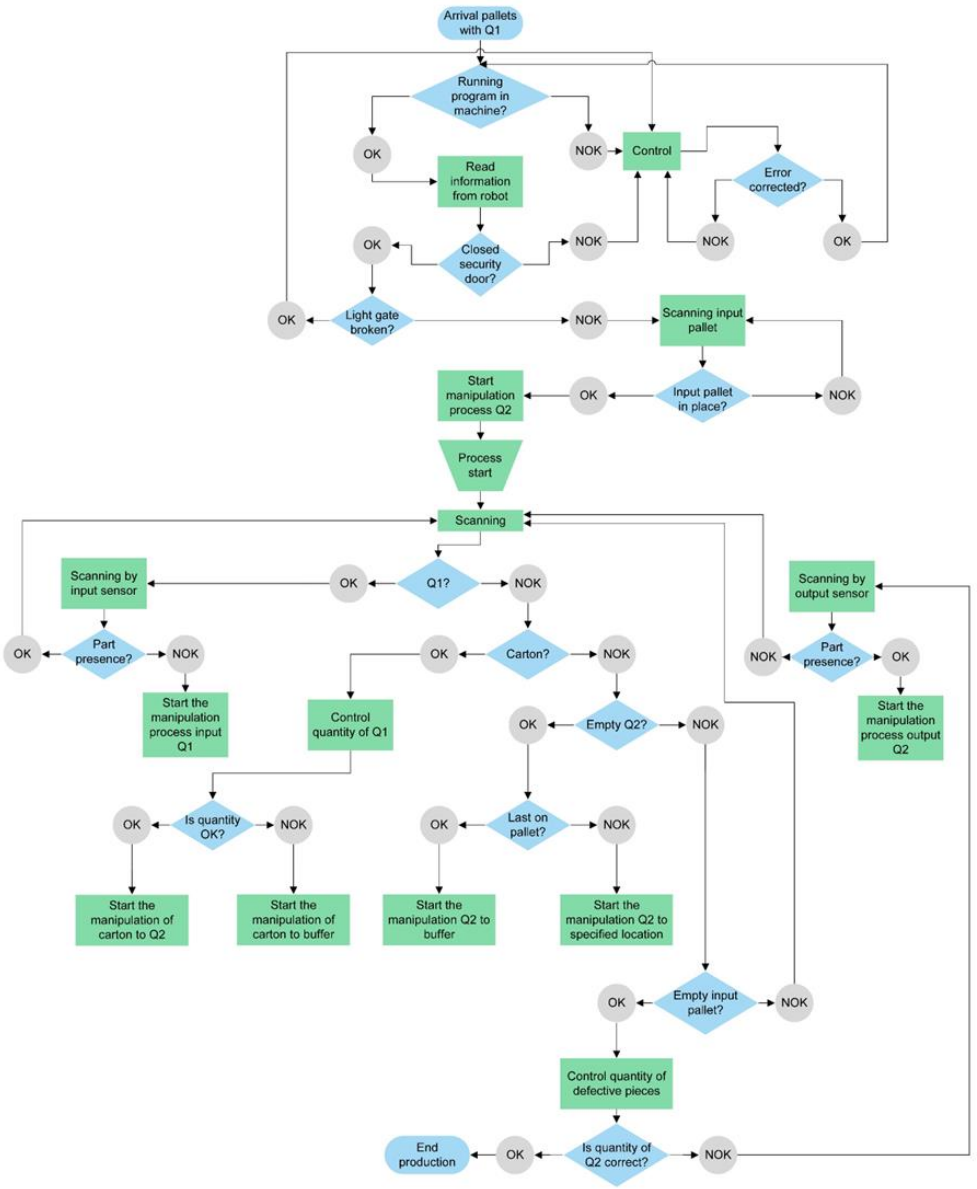

Fig. 5 Flow diagram of work process handling

If it is, the robot automatically grabs the first Q2, which always stores itself in the same place in the tray after the previous production is completed, and transfers it to the pre-programmed exact location on the output pallet. After the first handling action is performed, there is an imaginary switching on of the repetitive robotic stroke, where the robot scanner/camera successively senses the input pallet and performs handling actions according to the type of part detected (Q1, carton, empty Q2) and the output information from the capacitive sensors.

When part Q1 is sensed, information is sent from the input capacitive sensor via the PLC about the presence/absence of the part on the input conveyor. If the part of the conveyor sensed by the capacitive sensor is empty, the robot transfers the part from Q2 to the conveyor. Otherwise, the robot waits for further information from the scanner/camera or PLC for further actions. If a carton (located between the layers Q1 in Q2) is scanned, the PLC checks the number of finished pieces taken from the output conveyor to the output Q2. When the number of finished output pieces is correct, or if the number of pieces loaded in Q2 corresponds to one so-called tier, the robot grabs the carton and places it in the output Q2 on the output pallet, thus creating space for the next tier. Otherwise, the robot transfers the carton to the tray. If an empty Q2 is captured, the PLC sends a signal to the robot if it is the last Q2 on the input pallet. If Q2 is the last one, it is transferred by the robot to the tray. If it is not the last one, it is translated to a precisely programmed location on the output pallet. If the situation occurs that the scanner does not scan either Q1, the carton, or Q2 there can be two consequences. The first is a mis-scan, in which case the scan is repeated. The second consequence is that there is nothing more on the input pallet. In this case, the PLC checks the number of defective pieces produced in the machine and recalculates whether the number of correctly produced parts equals the number of output parts handled, or the number of scans taken by the output capacitive encoder. If the result does not agree, the robot and PLC wait for the last signal from the output capacitive sensor. If the result agrees, the PLC shuts down the program in the machine, shuts down and locks the robot, releases the entry through the safety door, and enables the interrupt light gate for removal of finished parts.(Dujka,2023)

6 CONCLUSION

Process maps provide a better explanation of processes than words, allowing you to see the process clearly and identify "waste" and areas for improvement. Process modelling allows understanding of the context and links to other processes. Disadvantages of process maps include distraction, i.e. the modelling itself is more important than the goal, i.e. models are not intended for process participants but are only used by specialists involved in modelling, miscommunication - models are not a means of communication. Disadvantages arise only when process modelling methods and tools are used incorrectly, so that, if the established rules and procedures are followed, these undesirable effects should not occur.
Process mapping is used to find bottlenecks or weak points where little or no value is added to the outputs of business processes. Problems in mapping arise, for example, if top management exhausts itself by studying details at lower levels instead of focusing on changes identified during periods of process elimination or simplification, or if employees prefer to direct the process analyst's attention to vendors, external customers, or businesses that do not directly threaten their own positions in the enterprise. These artificial barriers that

limit process mapping should be avoided in process improvement efforts. The aim of process re-engineering analysis is to adapt business processes to customer requirements as much as possible, to eliminate everything unnecessary from business processes and to maximize the added value of business processes.
By elaborating the basic process procedures, it is possible to create an idea flow chart representing the processes and all the factors that the proposed automation contains. The flowchart must satisfy Complexity, i.e. express in maps all types of processes and their hierarchical structures, thus creating interdependencies. Modularity must be ensured, breaking down large processes into smaller and clearer ones so that complex problems can be refined step by step. For clarity of map creation and use, maps should be manageable by both map creators and map users, and each hierarchical level should use the same process map creation tools.

ACKNOWLEDGEMENT

The paper was written in the framework of project KEGA 001STU-4/2022 entitled "Support of distance learning in the form of online access for selected subjects of computer-assisted study programmes".

REFERENCES

Arents, J., Greitans, M. Smart industrial robot control trends, challenges and opportunities within manufacturing. Applied Sciences, 2022, 12.2: 937

Dujka, S. Design of automation concept for loading and unloading of components at the belt tensioner lubrication workplace,2023 MSc. STU Trnava

Gupta, A. K., Arora, S. K., Westcott, J. R. Industrial Automation and Robotics: An Introduction. Mercury Learning & Information,2016. ISBN 978-1-938-54930-4

Harmoko, H., et al. Identifying the Socio-Human Inputs and Implications in Robotic Process Automation (RPA): A Systematic Mapping Study. In: International Conference on Business Process Management. Cham: Springer International Publishing, 2022. p. 185-199

Jung, J. Mapping of Business Process Models to Workflow Schemata–An Example Using MEMO-OrgML and XPDL. Arbeitsberichte des Instituts für Wirtschaftsinformatik, Universität Koblenz-Landau, 2004, 47

Niku, S. B. Introduction to Robotics: Analysis, Control, Applications. JOHN WILEY & SONS, 2010, INC. ISBN 978-0-470-60446-5

Papulová, Z. Procesný manažment, Kartprint ,2014, 234p, ISBN: 9788089553235
Siegwart, R., Nourbakhsh, I.R.; Scaramuzza, D. Introduction to Autonomous Mobile Robots; MIT Press: Cambridge, MA, USA, 2011.
https://www.jteryu.top/products.aspx?cname=main+types+of+robots&cid=93

USING THE SHEWHART CONTROL CHARTS BY TURNING PROCESS EVALUATION

Ing. Katarína Lestyánszka Škůrková, PhD.[1]
Ing. Filip Praj[2]
[1]ORCID: 0000-0003-0088-5454, Faculty of Materials Science and Technology in Trnava, Slovak University of Technology, **Slovakia**
[2]ORCID: 0000-0003-2303-5532, Faculty of Materials Science and Technology in Trnava, Slovak University of Technology, **Slovakia**

Abstract: This article has been handled of statistical evaluation of capability process of turning by screws production in RIBE Slovakia, k.s. In technical practice, the important group of statistic methods is formed by analyze of qualification of measures, production equipment and qualification of process. By the term „process qualification“ we mean ability of the process to observe technical parameters required by required value and tolerance limits. Finding of process capability we can isolate in estimate process capability (before starting the production) and permanent process capability. Also we had finished the reguest for capability of process, where the index of capability process Cp and Cpk are bigger than the determinated value on 1.33 point.

Keywords: process, Shewhart control charts, normality, quality

1 INTRODUCTION

In technical practice, the important group of statistic methods is formed by analyze of qualification of measures, production equipment and qualification of process. From statistic methods mentioned above is the most used one examination of process qualification. . By the term „process qualification“ we mean ability of the process to observe technical parameters required by required value and tolerance limits. Finding of process capability we can isolate in estimate process capability (before starting the production) and permanent process capability. The main distinction is in time span, in quantity of obtained values and in the form of obtaining. These information presents the fact for the customer about expected fulfilment his requirements.

We can say that the process is capable if Cp a Cpk are bigger than 1.33.
Between input data belong:

- definitive conditions series production
- convenient and able measuring accuracy equipment
- able production facilities
- statistically encompassment process through the quality control charts
- test on assumed division
- technical a others specification correctly expressive customer's request

2 METHODOLOGY OF RESEARCH

Description of the process:
Operating step: Turning by production order WZ 12 860 B RIBE ISR – axial screw
Mark: slot width
Rating value: 1.62 +0.08 mm
Lower Specification limit (LSL): 1.62 mm
Upper Specification limit (USL): 1.70 mm
Check centre: profiloprojector Mitutoyo with precision 0.001 mm.
Production device: turning machine TRAUB TB 30
Volume of subgroup: N = 250 screws
Measure of subgroup: n = 5 screws
Interval of taking: every 30 minutes
Number of subgroups: k = 50

Criteria for valuation competence are indexes Cp and Cpk. From look specification products as critical sign we consider screw´s slot width 1.62 +0.08 mm. We measure the slot width by profiloprojector with precision 0.001 mm and with capability of measuring device. We suppose normal division of the process and suitability of applications partitions we appreciate through the medium likelihood networks. By regulation of the turning process we shall use regulating schema control chart for average and span(,R). In the turning process as production machine we use turning machine TRAUB TB 30.

Calculation of specification limits
average range in subgroups

$$\overline{X_i} = \frac{1}{n}\sum_{j=1}^{n} X_{ij} \qquad (1)$$

i = 1, 2 ....k and j = 1, 2 ...n,

X_{ij} *– measured value in i- subgroups*

j –serial number of measured values in i- subgroups

k –number of subgroups

n –file size

span in subgroups

$$R_i = MAX(X_{ij}) - MIN(X_{ij}) \quad (2)$$

i = 1, 2 ... k and j = 1, 2 ...n

MAX (X_{ij}) and MIN(X_{ij}) is maximum and minimum value in i-th subgroup.

***average of process*:**

$$\overline{\overline{X}} = \frac{1}{k}\sum_{i=1}^{k}\overline{X_i} \quad (3)$$

$\overline{X_i}$ *- average of j – th subgroup*

Average of span:

$$\overline{R} = \frac{1}{k}\sum_{i=1}^{k}R_i \quad (4)$$

R_iX_i are spans and averages in *i*-th subgroups (*i*=1, 2, ...*k*). $\overline{R}$ and $\overline{\overline{X}}$ in quality control charts are central lines (*CL*).

Calculation of specification limits:

$UCL_R = D_4 . \overline{R}$ (5)

$LCL_R = D_3 . \overline{R}$ (6)

$$UCL_{\bar{X}} = \overline{\overline{X}} + A_2 . \overline{R} \quad (7)$$

$$LCL_{\bar{X}} = \overline{\overline{X}} - A_2 . \overline{R} \quad (8)$$

D_4 ,D_3 and A_2 are constants moving in dependence on volume of subgroups *n* in our case n = 5: $D_3 = 0.000$, $D_4 = 2.114$, $A_2 = 0.577$.

Qualification of turning process

$$C_p = \frac{USL - LSL}{6.\hat{\sigma}} = \frac{T}{6.\hat{\sigma}} \quad (9)$$

$$C_{PK} = \frac{USL - \overline{\overline{X}}}{3.\hat{\sigma}} \quad (10)$$

$$C_{PK} = \frac{\overline{\overline{X}} - LSL}{3.\hat{\sigma}} \quad (11)$$

USL – Upper Specification limit

LSL – Lower Specification limit

3 RESULTS

In turning process of screw RIBE we obtained values for 50 subgroups. Characteristics $\overline{X}$ and *R* are applied in quality control charts. Than we added to quality control charts regulation bounds and central lines.

For quality control chart ($\overline{X}, R$) are actual these regulation bounds:

UCL_X = 1.6758 mm

UCL_R = 0.04525 mm

LCL_X = 1.6448 mm

The process is mastered well, no regulating limit was overloaded and no trend or violation about middle period was shown. The process is in a mastered situation and no systematic influences do impact. General average $\bar{x}$ = 1.66016 mm, average span R = 0.054 mm. The process can by after attestation of qualification treated as qualitatively qualified, indicators of qualification C_p and C_{pk} are higher than 1.33. **Cp = 1.45 Cpk = 1.44**

Consequently we figure our values to quality control chart (fig. 1), where on the top is the control chart for $\overline{X}$ and the low is for *R.*

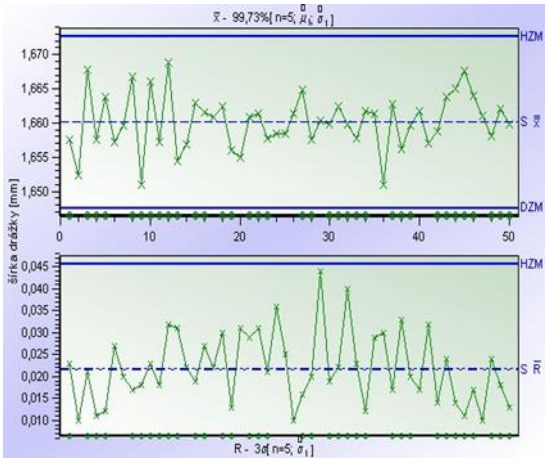

Fig. 1 Quality control chart

4 CONCLUSION

The capability of turning process in RIBE Slovakia showed, that the process provides products, which satisfy claimed quality criteria's. Values of a potential process capability Cp = 1.45 and a real process Cpk = 1.41. These values are higher than a rate 1.33 and the process is able to provide products in compliance with tolerance zones.

ACKNOWLEDGEMENTS

This paper was written as a part of this project: KEGA 027STU-4/2022 "Integration of the requirements of practise in the automotive industry with the teaching of subjects within the study programs Process Automation and Informatization in Industry and Industrial Management" and a part of project KEGA of the Ministry of Education of the Slovak Republic No. 018TUKE-4/2022 "Creation of new study materials including an interactive multimedia university textbook for the field of computer support of engineering activities".

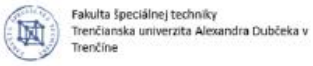

REFERENCES

HRUBEC J. 2001: Riadenie kvality. ES SPU Nitra, s.203. ISBN 80-7137-849-6

KONSTANCIAK M. 2012. Analysis of technological strategies on the example of the production of the tramway wheels. In: Archives of Materials Science and Engineering Vol.57 Iss.2 s. pp. 69-743.

AIKENS C. H. *Quality inspired management. The key to sustainability.* New Jersey: Pearson Education, Inc., publishing as Prentice Hall., 2011, p. 623.

ANDRÁSSYOVÁ, Z. – PAULÍČEK, T. – PICHŇA, P. – KOTUS, M.: Improving quality of statistical process by dealing with non-normal data in automotive indurstry. In *Management systems in production engineering.* No. 3 (2012), s. 26--30. ISSN 2299-0461.

ANDRÁSSYOVÁ, Z., Hrubec, J., Kotus, M. Assembly process capability of automotive seats. *Acta technologica agriculture*. Nitra: SPU, 2011, 14, 3, 74-78.

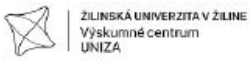

ISBN 978-80-8096-298-2

EAN 9788080962982